





**LIBRARY**  
**Michigan State**  
**University**

This is to certify that the

dissertation entitled


"Investigation of Low-Lying Excited Electronic States  
of Perylene; Two-Photon Excitation Spectroscopy of  
Perylene in Solution and in Supersonic Jet"

presented by

Jeonga Yu

has been accepted towards fulfillment  
of the requirements for

Ph.D. degree in Chemistry

  
Major professor

Date March 19, 1990

**PLACE IN RETURN BOX** to remove this checkout from your record.  
**TO AVOID FINES** return on or before date due.

DATE DUE	DATE DUE	DATE DUE
_____	_____	_____
_____	_____	_____
_____	_____	_____
_____	_____	_____
_____	_____	_____
_____	_____	_____
_____	_____	_____

**MSU Is An Affirmative Action/Equal Opportunity Institution**

c:\cinc\datedue.pm3-p.

INVESTIGATION OF LOW-LYING EXCITED ELECTRONIC STATES OF  
PERYLENE; TWO-PHOTON EXCITATION SPECTROSCOPY OF  
PERYLENE IN SOLUTION AND IN A SUPERSONIC JET

BY

JEONGA YU

A DISSERTATION

Submitted to  
Michigan State University  
in partial fulfillment of the requirements  
for the degree of

DOCTOR OF PHILOSOPHY

Department of Chemistry

1990



00603553

ABSTRACT

INVESTIGATION OF LOW-LYING EXCITED ELECTRONIC STATES OF  
PERYLENE; TWO-PHOTON EXCITATION SPECTROSCOPY OF  
PERYLENE IN SOLUTION AND IN A SUPERSONIC JET

BY  
Jeonga Yu

Two-photon excitation spectroscopy has been utilized to study the low-lying excited electronic states of perylene. The fluorescence from the two-photon induced electronic excited states of perylene in *n*-hexane solution at room temperature has been measured using two-photons from the same excitation laser under both linear and circular polarization conditions over the incident dye laser wavelength spectral region 560 – 840 nm (two-photon energy 35,700 – 23,800 cm<sup>-1</sup>); a portion of the two-photon excitation (TPE) spectrum, over the region 650 - 840 nm (two-photon energy 30,770 – 23,800 cm<sup>-1</sup>), was also obtained from a 77 K isopentane glass. From the observed peaks and the ratio of the two-photon cross sections for circularly and linearly polarized incident excitation beams ( $\Omega = \delta_{\text{cir}} / \delta_{\text{lin}}$ ), low-lying  $\pi\pi^*$  electronic states of gerade parity in the 23,800 – 35,700 cm<sup>-1</sup> range, as well as a dipole-forbidden  $B_{3u}^-$  state below 26,500 cm<sup>-1</sup>, have been located and characterized. The results are compared with values of perylene excited state origins predicted by calculations, or observed by various alternative experimental methods.

In order to provide more definitive assignments and more direct comparison to theory, two-photon excitation of perylene in a supersonic jet was attempted. To characterize and optimize a home-built supersonic jet system, the one-photon spectra of perylene over the spectral region 410 – 420 nm, of iodine in the  $X(^1\Sigma) \rightarrow B(^3\Pi)$  transition region (578 – 596 nm), and of [2,2]paracyclophane ( $\lambda (S_0 \rightarrow S_1) = 280 - 320$  nm) were obtained under various conditions. The preliminary results of the two-photon excitation of supersonic jet-cooled perylene, over the region 576.8 – 577.8 nm (two-photon energy 34,670 – 34610  $\text{cm}^{-1}$ ), is reported.

## ACKNOWLEDGMENTS

I would like to thank professors G. E. Leroi and D. G. Nocera for their help and advice throughout my graduate work, and professors G. T. Babcock and S. R. Cruoch for serving on my guidance committee.

I am also grateful for the opportunity to get to know many special people during the past years at Michigan State University. Their concern and friendship have made this experience pleasant.

More importantly, I want to thank my parents and family. Without them this all would have not been possible.

Financial support from Michigan State University and National Science Foundation is also gratefully acknowledged.

## TABLE OF CONTENTS

	Page
LIST OF TABLES. . . . .	vi
LIST OF FIGURES . . . . .	vii
CHAPTER I      INTRODUCTION . . . . .	1
I.   Linear Spectroscopy . . . . .	2
II. Nonlinear Spectroscopy . . . . .	5
A. Two-Photon Absorption . . . . .	7
B. Characteristic Properties of Two-photon Transitions . . . . .	11
1. Intensity Dependence . . . . .	11
2. Polarization Dependence . . . . .	12
3. Resonance Effect . . . . .	16
C. Experimental Techniques . . . . .	22
1. Fluorescence Measurement . . . . .	24
2. Detection of TP Absorption by MPI of Molecules . . . . .	25
III. Motivation . . . . .	26
CHAPTER II    TWO-PHOTON SPECTROSCOPY OF PERYLENE IN SOLUTION . . . . .	35
I.   Experimental . . . . .	36
A. Materials . . . . .	36
B. Absorption and Emission Spectra . . . . .	36

C. Two-photon Excitation Spectra . . . .	37
1. General Considerations . . . . .	37
2. Polarization Measurement Procedure . . . . .	57
3. Dye Laser Wavelength Scan . . . .	60
II. Results and Discussion . . . . .	63

CHAPTER III	TWO-PHOTON SPECTROSCOPY IN A SUPERSONIC JET . . . . .	93
I.	Introduction . . . . .	94
II.	Supersonic Expansion . . . . .	95
	A. Translational Cooling . . . . .	101
	B. Vibrational and Rotational Cooling . . .	105
	C. Condensation and Complex Formation . . . . .	109
III.	Spectroscopy in Supersonic Jets . . . . .	111
	A. The Number of Excited Molecules . . .	112
	B. Detection . . . . .	114
IV.	Limitations of Supersonic Jet Spectroscopy . . . . .	119
	A. Vaporization . . . . .	119
	B. Sensitivity . . . . .	122
V.	Experimental. . . . .	123
	A. Jet Generating System . . . . .	123
	B. Excitation Source . . . . .	131
	C. Detection . . . . .	132

VI. Results and Discussion . . . . .	135
A. Pressure Effect . . . . .	136
1. Chamber Pressure . . . . .	136
2. Carrier Gas Pressure . . . . .	139
B. Distance Effect . . . . .	142
C. Nozzle Size Effect . . . . .	145
D. Sensitivity . . . . .	145
E. TPE of perylene . . . . .	148
REFERENCES . . . . .	157

## LIST OF TABLES

Tables	Page
1-1	Examples of Four-Wave Mixing . . . . . 6
1-2	Values of the Polarization Variables F, G, and H for Two-Photon Transitions. . . . . 15
1-3	Examples of the Two-Photon Tensor Patterns for Groups . . . . . 17
2-1	Observed and Calculated In-Plane Vibrational Frequencies ( $\text{cm}^{-1}$ ) of Perylene . . . . . 81
2-2	Comparison of Experimental and Calculated Values of Transition Energies to Low-Lying Symmetry-Forbidden Excited States of Perylene . . . 90

## LIST OF FIGURES

Figures		Page
1-1	Various multiphoton absorption processes . . . . .	8
1-2	The two-photon absorption processes of a molecule . . .	20
1-3	UV-visible electronic absorption spectrum of perylene ( $10^{-4}$ M) in <i>n</i> -hexane solution . . . . .	27
1-4	The nine Kekule structures of perylene classified according to symmetry . . . . .	30
1-5	Bond lengths (Å) in the ground and excited state of perylene . . . . .	32
2-1	Two-photon transition processes . . . . .	38
2-2	A schematic diagram of the two-photon excitation of fluorescence measurement . . . . .	41
2-3	The florescence measurement sample chamber for two-photon excitation . . . . .	43
2-4	Dispersed fluorescence spectra: (a) $\lambda_{\text{ex}} = 365$ nm: (b) $\lambda_{\text{ex}} = 584$ nm . . . . .	46
2-5	Power dependence of the two-photon induced fluorescence of perylene ( $\sim 10^{-4}$ M in <i>n</i> -hexane) at different initial laser wavelengths . . . . .	48
2-6	The tuning range and relative output power of dyes used in the TPE of perylene . . . . .	51
2-7	The spectral response of the photodiode . . . . .	53



2-8	Liquid nitrogen dewar and high-vacuum cell for 77 K TPE measurement . . . . .	55
2-9	The alignment of the polarization changing optics . . .	58
2-10	Representation of the electric field vector in space . . .	61
2-11	The electronic circuit diagram of the stepping motor interface . . . . .	64
2-12	The symmetries of the $\pi$ -electron cloud of the ground state and the electronic excited states of perylene . . .	67
2-13	One-photon UV-visible absorption and two-photon excitation spectra of perylene in <i>n</i> -hexane solution . . .	69
2-14	TPE of perylene in <i>n</i> -hexane solution ( $\sim 10^{-4}$ M) and polarization ratio, $\Omega$ , plotted as a function of the incident dye laser wavelength . . . . .	71
2-15	TPE spectrum of perylene in isopentane at 77 K . . . .	73
2-16	Observed and calculated energy level diagram of the excited electronic states of perylene near the peak at $26,500\text{ cm}^{-1}$ . . . . .	77
2-17	Two-photon transitions to various vibrational levels of a $B_{3u}^-$ electronic symmetry state . . . . .	83
2-18	Energy diagram of the lower excited electronic states of perylene . . . . .	88
3-1	Velocity distribution in an effusive and in a supersonic beam . . . . .	97
3-2	Shock structure surrounding the expanding gas of a free jet. . . . .	99
3-3	The geometric cooling of the translational degrees of freedom in relation to the expansion axis . .	102
3-4	Vibrational and rotational cooling <i>via</i> collisions in a jet . . . . .	106
3-5	Various two-beam double resonance spectroscopies . . .	117

3-6	The experimental set-up of a time of flight mass spectrometer coupled with laser desorption into a supersonic jet followed by laser MPI . . . . .	120
3-7	Schematic block diagram of the supersonic jet experiment . . . . .	124
3-8	Schematic diagram of the chamber employed for supersonic expansion experiments . . . . .	126
3-9	A side-view cross section of the sample compartment .	128
3-10	Schematic diagram of the detection system . . . . .	133
3-11	The LIF spectra of jet-cooled iodine molecules at different chamber background pressure . . . . .	137
3-12	The LIF spectra of perylene in a jet as a function of the carrier gas pressure . . . . .	140
3-13	The LIF spectra of perylene in a jet at different distances from the nozzle to the laser intersection . .	143
3-14	The effect of nozzle size on the internal temperature cooling . . . . .	146
3-15	The LIF from [2,2]paracyclophane expanded through a supersonic jet . . . . .	149
3-16	TPE spectrum of perylene in a supersonic jet . . . . .	151
3-17	The relaxation processes following two-photon excitation in solution and in a jet . . . . .	154

## **CHAPTER I**

### **INTRODUCTION**

## I. LINEAR SPECTROSCOPY

When Maxwell formulated the electromagnetic theory of light, he made the approximation that the dielectric susceptibility ( $\chi$ ) and magnetic permeability ( $\eta$ ) to the medium were independent of the strengths of the applied fields, and thus the dielectric polarization ( $P$ ) and magnetization ( $M$ ) were linearly proportional to the field amplitudes ( $E, H$ )[1],

$$\mathbf{P} = \epsilon_0 \chi \cdot \mathbf{E} ; \mathbf{M} = (\eta - 1) \cdot \mathbf{H} \quad (1-1)$$

where  $\epsilon_0$  is the permittivity of free space. The susceptibilities ( $\chi$ ), in which the resonant structure of the spectra are contained, must be regarded as complex numbers in order to describe the behavior at all frequencies; then the optical frequency fields need to be written in complex notation

$$\mathbf{E}(\mathbf{r}, t) = \frac{1}{2} \{ \mathbf{E}(\mathbf{r}) e^{-i(\omega t - \mathbf{k} \cdot \mathbf{r})} + \mathbf{E}^*(\mathbf{r}) e^{i(\omega t - \mathbf{k} \cdot \mathbf{r})} \}, \quad (1-2)$$

where  $\mathbf{k}$  is the wave vector and  $\omega$  is the frequency of the wave. Thus, the wave equation becomes

$$\nabla^2 \mathbf{E} - \frac{1}{c^2} \frac{\partial^2 \mathbf{E}}{\partial t^2} = \frac{4\pi}{c^2} \frac{\partial^2 \mathbf{P}}{\partial t^2}, \quad (1-3)$$

which relates the wave vector,  $\mathbf{k}$ , to the susceptibility,  $\chi$ . The disparate optical behavior of linear media is contained in the relative magnitudes of

the various constitutive coefficients and in their behavior as a function of frequency.

In transparent dielectrics (or at frequencies far removed from a transition resonance),  $\mathbf{E}$  and  $\mathbf{H}$  are in phase but the ratio of amplitudes is changed from free space. The resultant relationship between  $\mathbf{P}$  and  $\mathbf{E}$  contains a phase lag which is experimentally observed as the refractive index ( $n = k/k_0$ ), where  $n^2 = 1 + \text{Re}\chi$  ( $\text{Re}\chi$  means the real part of  $\chi$ ) and  $k_0$  is the wave vector in vacuum. The observable intensity of the wave is defined as

$$I = \frac{nc}{8\pi} |\mathbf{E}(\mathbf{r})|^2, \quad (1-4)$$

where  $c$  is the speed of the light in the vacuum.

At frequencies near resonance, the electric field is absorbed to an extent determined by the extinction coefficient  $K$ , where  $2nK = \text{Im}\chi$  (imaginary part of  $\chi$ ); the imaginary term in the wave vector introduces an attenuation factor  $\exp(-\chi k_0 r)$  on the electromagnetic wave. The attenuation (extinction coefficient) in absorbing media obeys the Beer-Lambert law

$$(\mathbf{k} \cdot \nabla)I = -2KI. \quad (1-5)$$

Early workers in quantum mechanics recognized that variations of the index of refraction and attenuation coefficient contained crucial information about the energy levels of the medium. Bohr related the attenuation coefficient to the probability of a transition between energy levels separated by the energy of a quantum of light,  $E = h\nu$ . Fermi expressed the transition probability per unit time,  $\Gamma_{ij}$ , in terms of the

matrix element of the dipole moment operator  $\mu = er$  which connected the two levels

$$\Gamma_{ij} = \frac{\pi}{2\hbar} [ \langle i | \mu \cdot \mathbf{E}(\mathbf{r}) | j \rangle ]^2 \rho(E_i - E_j - \hbar\nu), \quad (1-6)$$

where the factor  $\rho(E)$  is a density-of-states function that reflects the observed lineshape and  $e$  is the electronic charge. If the refractive index of the medium is different from one, the dipole moment operator needs to be corrected for the local field,  $\mu \rightarrow ((n^2+2)/3) er$ . Einstein calculated the probability for spontaneous light emission per unit time

$$A_{ba} = \frac{4n |\langle b | \mu | a \rangle|^2}{3\hbar^4 c^3} (E_b - E_a)^3 \quad (1-7)$$

and pointed out that the transition rate in the Fermi equation applies equally to absorption and stimulated emission processes. Kramers and Kronig showed that the variation of the index of refraction was related to the absorption. Thus, the quantum mechanics of the classical methods of spectroscopy - emission, absorption, and dispersion - was well understood early in the twentieth century[2-5]. The fourth method of linear spectroscopy - light scattering - required more complicated methods and was explained by using a vibrating model[6,7].

These classical phenomena of linear spectroscopy contributed immeasurably to the growth of quantum mechanics and our understanding of atoms and molecules. The experimental limitations, however, that resulted from the unfavorable selection rules, Doppler broadening and other complicating phenomena, were recognized as intrinsic to linear spectroscopy.

## II. NONLINEAR SPECTROSCOPY

The term nonlinear spectroscopy refers to those phenomena involving light where the induced polarization,  $P$ , of an atomic or molecular electron cloud is not at the same frequency as that of the driving electric field,  $E$ . For centrosymmetric molecules,  $P$  is related to  $E$  by the expression

$$P = \epsilon_0 E (\chi_1 + \chi_3 E^2 + \dots) \quad (1-8)$$

where  $\epsilon_0$  is the permittivity of free space and  $\chi_i$  are the susceptibility tensors of  $i$  with rank  $(i+1)$ [8].

Linear spectroscopy occurs when the susceptibilities are space and time independent, and when  $\chi_1 \gg \chi_3$ . Therefore,

$$P(\omega) = \epsilon_0 E(\omega) \chi_1, \quad (1-9)$$

where  $\omega$  is the frequency of the driving radiation. In systems with inversion symmetry, the lowest-order nonvanishing nonlinear susceptibility is of third order,  $\chi_3$ . The third-order polarization can be expanded into the form:

$$P_3(\omega_1) = \chi_3(\omega_1, \omega_j, \omega_k, \omega_1) E(j) E(k) E(1), \quad (1-10)$$

where four waves are being mixed by  $\chi_3$ . Several common combinations of frequencies are shown in Table 1-1. Like the first order polarization, the

**Table 1-1. Examples of Four-Wave Mixing.**

Resultant Frequency	Mixed Frequencies	Resonance Frequency	Phenomenon
$3\omega_1$	$\omega_1, \omega_1, \omega_1$	---	Frequency tripling
$\omega_1$	$\omega_1, \omega_1^*, \omega_1$	---	Self-focusing
		$\omega_1 = \omega_e$	Self-induced transparency
$\omega_2$	$\omega_1, \omega_1^*, \omega_2$	---	Intensity-dependent refractive index
		$\omega_1 + \omega_2 = \omega_e$	Two-photon absorption
		$\omega_1 - \omega_2 = \omega_v$	Stimulated Raman emission
		$\omega_2 - \omega_1 = \omega_v$	Inverse Raman absorption
$2\omega_1 - \omega_2$	$\omega_1, \omega_1, \omega_2^*$	---	Four wave mixing
		$\omega_1 - \omega_2 = \omega_v$	CARS

\* = the complex conjugate of the electric field strength.

$\omega_e$  = an electronic transition.

$\omega_v$  = a vibrational transition.



third order (nonlinear effect) can be used to obtain structural information[9-11].

The possibility of observing optical frequency nonlinear phenomena requires high field strength. An upper bound for the field strength can be estimated by the field,  $E_0$ , binding an electron to the nuclei, and leads to the approximate rule that  $\chi_1/\chi_3 \sim E_0$ [12]. A typical value for  $E_0$  would be  $3 \times 10^8 \text{ V cm}^{-1}$  which corresponds to an intensity of  $\sim 10^{15} \text{ W cm}^{-2}$ . The experimental dilemma was alleviated when the first laser was designed by T. Maiman[13]. After that, nonlinear optical effects (resulting from the higher order terms) including stimulated Raman gain[14], multiphoton absorption[15], second harmonic generation[16], sum and difference frequency generation[17], saturated absorption[18], etc., were discovered and verified.

### A. Two-Photon Absorption

Multiphoton absorption, one of the nonlinear effects, basically consists of the excitation of molecules by two or more photons. The upper state of the transition decays like any excited state, either nonradiatively to the ground state, or to a fluorescing state and then to the ground state. Alternatively, it may undergo photochemical change. New vibronic and electronically excited states, which are not accessible *via* one-photon spectroscopy, can be observed over a wide range, from lower excited states to ionized continua (several examples are shown in Figure 1-1). As the simplest example of a multiphoton transition, the two-photon transition has several features that are important for spectroscopy[19].

**Figure 1-1.** Various multiphoton absorption processes: a) two-photon transition with resonant intermediate; b) two-photon transition with nonresonant (virtual) intermediate; c) stepwise three-photon transition; and d) three-photon ionization process with resonant intermediate states.

First, the selection rules for two-photon transitions differ from those for one-photon transitions. For centrosymmetric molecules the one-photon transition only has significant oscillator strength when the parity of the electronic wave function changes upon absorption (g-u or u-g). The two-photon absorption process can be thought of as two simultaneous one-photon absorptions, with the first photon achieving an intermediate state and the second photon taking the molecule to the final state. Therefore, in centrosymmetric cases, two-photon excited states will have opposite parity to the one-photon excited states. When the ground state has gerade character, the transition moment is nonzero if the intermediate state has ungerade character and the final state is gerade. Since the intermediate state differs from the initial state by one orbital, the final state may differ by two orbitals. Therefore the final state can result from two promotions of one electron or one promotion of two electrons. The latter is strictly forbidden in one-photon spectroscopy.

Second, during two-photon excitation molecular states may be excited that in the one photon process require a shorter-wave photon to be absorbed; "vacuum UV" energies (200 – 100 nm) are available using photons in the more accessible range 400 to 200 nm. Moreover, additional information, especially about intermediate states, can be obtained from two-photon spectra because the absorption coefficient is measured as a function of two frequencies.

## B. Characteristic Properties of Two-photon Transitions

Two-photon transitions have characteristic features such as radiation field intensity dependence, polarization dependence, and resonance enhancement[20].

### 1. Intensity Dependence

The multiphoton transition probability is formulated according to time-dependent perturbation theory[21]. When two-photons are from the same laser ( $\omega_1 = \omega_2 = \omega_r$ ), for a two-photon absorption from state  $a$  to state  $n$  the transition probability  $W_2$  is given as

$$W_2 \propto I^2 \left( \sum_m \frac{\langle n | \mu | m \rangle \langle m | \mu | a \rangle}{\Delta\omega - \hbar\omega_r} \right)^2 \quad (1-11)$$

where  $I$  is the intensity of the radiation field,  $m$  the virtual intermediate state,  $\Delta\omega$  the energy difference between the intermediate and initial states,  $\mu$  the dipole moment, and  $\omega_r$  is the radiation frequency. This equation shows that the two-photon probability is proportional to the square of the radiation field intensity. More generally, the  $n$ -photon transition probability is proportional to  $I^n$ . If saturation is absent, one determines the order of a multiphoton transition from the slope of the log-log plot of the transition probability as a function of radiation field intensity,

$$\ln W(n) = n \ln I + c. \quad (1-12)$$

## 2. Polarization Dependence

One of the most interesting features of two-photon spectroscopy is the potentiality to identify the nature of the excited state from the polarization studies. The polarization dependence of two-photon transitions in crystals was considered by Bader and Gold[22], and also by Inoue and Toyozawa[23]. For randomly-oriented, nonrotating molecules the exposition was given by Monson and McClain[24,25], who derived an expression for the averaged transition rate and showed how to distinguish states of different symmetries using an appropriate combination of photons with different polarizations. The effects of molecular rotation were considered by Bray and Hochstrasser[26].

Polarization studies in random molecules are uninformative in one-photon absorption because of an averaging out of polarization effects. The one-photon transition probability  $\sigma$  from ground state  $|g\rangle$  to final state  $\langle f|$  is proportional to  $|\lambda \cdot \mu_{fg}|^2$  where  $\lambda$  is the polarization vector of the absorbed photon and  $\mu_{fg}$  is the transition vector between states  $g$  and  $f$ . In randomly oriented systems,  $\sigma$  must be averaged over all orientations of the molecules to obtain  $\langle \sigma \rangle$ . The result is  $\langle \sigma \rangle = 1/3(\lambda \cdot \lambda^*)(\mu_{fg} \cdot \mu_{fg}^*)$ . Since  $\lambda \cdot \lambda^* = 1$  for all polarizations, the absorption is completely independent of the polarization of the incident beam.

In two-photon absorption, the transition probability,  $\delta$ , is given by

$$\delta = |\lambda \cdot S_{ab}^{\alpha} \cdot u|^2, \quad (1-13)$$

where  $\lambda$  and  $\mathbf{u}$  are the polarization vectors of the two absorbed photons and  $\mathbf{S}^{\text{of}}$  is the two-photon transition tensor between states  $\langle 0|$  and  $|f\rangle$ . When the two photon transition of a fluid is considered,  $\delta$  is averaged over all orientations of the molecule to yield  $\langle \delta \rangle$ ,

$$\langle \delta \rangle = \delta_F F + \delta_G G + \delta_H H \quad (1-14)$$

The terms  $F$ ,  $G$  and  $H$  depend only on the polarization of the incident photons, and the terms  $\delta_F$ ,  $\delta_G$  and  $\delta_H$  are molecular parameters independent of the polarization of the photons where

$$\delta_F = \sum_{a=b=1}^3 \mathbf{S}_{ab}^2 \quad (1-15a)$$

$$\delta_G = \sum_{(a,b=1)}^3 |\mathbf{S}_{ab}|^2 \quad (1-15b)$$

$$\delta_H = \sum_{(a,b=1)}^3 \mathbf{S}_{ab} \mathbf{S}_{ba}^* \quad (1-15c)$$

$$\mathbf{S}_{ab}^{\text{of}} = \langle 0 | \mathbf{S}_{ab} | f \rangle \quad (1-15d)$$

and

$$\mathbf{S}_{ab} = \sum_i \left[ \frac{[\mathbf{p}_a | i \rangle \langle i | \mathbf{p}_b]}{(E_i - E_1)} + \frac{[\mathbf{p}_b | i \rangle \langle i | \mathbf{p}_a]}{(E_i - E_2)} \right]. \quad (1-15e)$$

In these equations  $a, b$  are coordinate axes in the molecular frame,  $\mathbf{p}_a$  is the operator for total momentum in the  $a$  direction,  $|i\rangle$  is the intermediate state,  $E_i$  is the transition energy from  $|0\rangle$  to  $|i\rangle$ , and  $E_1$  and  $E_2$  are the energies of the two absorbed photons.

The functions  $F$ ,  $G$  and  $H$  are given by

$$F = 4 |\lambda \cdot \mathbf{u}|^2 - 1 - |\lambda \cdot \mathbf{u}^*|^2 \quad (1-16a)$$

$$G = - |\lambda \cdot \mathbf{u}|^2 + 4 - |\lambda \cdot \mathbf{u}^*|^2 \quad (1-16b)$$

$$H = - |\lambda \cdot \mathbf{u}|^2 - 1 + 4 |\lambda \cdot \mathbf{u}^*|^2 \quad (1-16c)$$

and it follows that  $\langle \delta \rangle$  is a linear function of the  $|\lambda \cdot \mathbf{u}|^2$  and  $|\lambda \cdot \mathbf{u}^*|^2$ . Therefore  $\delta_F$ ,  $\delta_G$  and  $\delta_H$  can be independently determined with carefully designed experiments which require the use of linear and circular polarized light. The values for F, G, and H under different beam polarizations are shown in Table 1-2.

For the "single beam experiment", which we applied to the TPE measurement of perylene, the two-photons come from the same laser beam, ( $E_1 = E_2$ ,  $\lambda = \mathbf{u}$ ). In this case only two independent parameters,  $\delta_F$  and  $\delta_G$  (since  $\delta_G = \delta_H$ ), remain which are determined from the two measurements of  $\delta$  with linearly and circularly polarized light. From Table 1-2,

$$\delta_{\text{lin}} = 2 \delta_F(\omega) + 4 \delta_G(\omega), \quad (1-17a)$$

$$\delta_{\text{cir}} = -2 \delta_F(\omega) + 6 \delta_G(\omega). \quad (1-17b)$$

The two-photon polarization ratio  $\Omega(\omega)$  is defined as

$$\Omega(\omega) = \frac{\delta_{\text{cir}}}{\delta_{\text{lin}}} = \frac{-\delta_F + 3 \delta_G}{\delta_F + 2 \delta_G}. \quad (1-18)$$

The value is bound to the interval

$$0 \leq \Omega \leq \frac{3}{2} \quad (1-19)$$

Table 1-2. Values of the Polarization Variables F, G, and H for Two-Photon Transitions.

Case									
Polarization Value	1	2	3	4	5	6	7	8	
	$\times \times$	$\times \times$	$\times \times$	$\times \times$	$\times \times$	$\times \times$	$\times \times$	$\times \times$	
F	2	-1	-1	$\frac{1}{4}$	$\frac{1}{2}$	$\frac{1}{2}$	-2	3	
G	2	4	4	$\frac{2}{7}$	3	3	3	3	
H	2	-1	-1	$-\frac{1}{4}$	$\frac{1}{2}$	$\frac{1}{2}$	3	-2	

From reference [24].



and is, in symmetric molecules, closely related to the symmetry of the excited state; it corresponds to the "degree of polarization" in Raman spectroscopy. Therefore  $\Omega$  can serve as a symmetry-indicator (Table 1-3). Even if the theoretical limit is not seen in a real spectrum, due to the influence of vibronic coupling or overlapping of peaks arising from different symmetry states, the relative trends in  $\Omega(\omega)$  provide valuable information on the symmetries of the excited states.

### *3. Resonance Effect*

The intermediate state in two-photon absorption can be off-resonance from all ungerade states, so called a virtual state (Figure 1-2), although the total energy of the two photons must satisfy the resonance condition. When the excitation laser is tuned and its frequency approaches a real intermediate electronic state, the two-photon absorption signal will dramatically increase (resonance enhancement),

$$W_2 \sim \left[ \frac{1}{\Delta\omega - \Gamma} \right]^2 \quad (1-20)$$

where  $W_2$  is the probability of the two-photon transition,  $\Gamma$  is the homogeneous half-width of the transition and  $\Delta\omega$  is the energy difference between the laser and real intermediate level. For nonresonant two-photon transitions, the vibronic structure is mainly determined by the Franck-Condon vibrational overlap between the initial and final states, because the energy mismatch to the intermediate level is so large that the vibronic structure of the intermediate state can be neglected. On the other hand, the

Table 1-3. Examples of the Two-Photon Tensor Patterns for Groups.

Tensor Pattern	Point Group Irreducible Representations			Polarizaion Ratio
	$D_2$	$C_{2v}$	$D_{2h}$	
$\begin{pmatrix} \sigma_{xx} & 0 & 0 \\ 0 & \sigma_{yy} & 0 \\ 0 & 0 & \sigma_{zz} \end{pmatrix}$	A - A B <sub>1</sub> - B <sub>1</sub> B <sub>2</sub> - B <sub>2</sub> B <sub>3</sub> - B <sub>3</sub>	A <sub>1</sub> - A <sub>1</sub> A <sub>2</sub> - A <sub>2</sub> B <sub>1</sub> - B <sub>1</sub> B <sub>2</sub> - B <sub>2</sub>	A <sub>g</sub> - A <sub>g</sub> B <sub>1g</sub> - B <sub>1g</sub> B <sub>2g</sub> - B <sub>2g</sub> B <sub>3g</sub> - B <sub>3g</sub> A <sub>u</sub> - A <sub>u</sub> B <sub>1u</sub> - B <sub>1u</sub> B <sub>2u</sub> - B <sub>2u</sub> B <sub>3u</sub> - B <sub>3u</sub>	$\frac{2}{3}$
$\begin{pmatrix} 0 & \sigma_{xy} & 0 \\ \sigma_{yx} & 0 & 0 \\ 0 & 0 & 0 \end{pmatrix}$	A - B <sub>1</sub> B <sub>2</sub> - B <sub>3</sub>	A <sub>1</sub> - A <sub>2</sub> B <sub>1</sub> - B <sub>2</sub>	A <sub>g</sub> - B <sub>1g</sub> B <sub>2g</sub> - B <sub>3g</sub> A <sub>u</sub> - B <sub>1u</sub> B <sub>2u</sub> - B <sub>3u</sub>	$\frac{3}{2}$
$\begin{pmatrix} 0 & 0 & \sigma_{xz} \\ 0 & 0 & 0 \\ \sigma_{zx} & 0 & 0 \end{pmatrix}$	A <sub>2</sub> - B <sub>2</sub>	A <sub>1</sub> - B <sub>1</sub>	A <sub>g</sub> - B <sub>2g</sub> B <sub>1g</sub> - B <sub>3g</sub> A <sub>u</sub> - B <sub>2u</sub> B <sub>1u</sub> - B <sub>3u</sub>	$\frac{3}{2}$
$\begin{pmatrix} 0 & 0 & 0 \\ 0 & 0 & \sigma_{yz} \\ 0 & \sigma_{zy} & 0 \end{pmatrix}$	A - B <sub>3</sub> B <sub>1</sub> - B <sub>2</sub>	A <sub>1</sub> - B <sub>2</sub> A <sub>2</sub> - B <sub>1</sub>	A <sub>g</sub> - B <sub>3g</sub> B <sub>1g</sub> - B <sub>2g</sub> A <sub>u</sub> - B <sub>3u</sub> B <sub>1u</sub> - B <sub>2u</sub>	$\frac{3}{2}$

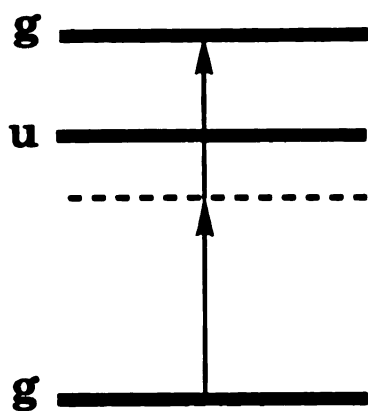
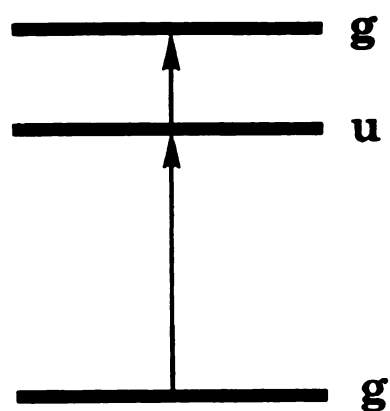
Table 1-3. (continued)

Tensor Pattern	Point Group Irreducible Represents		Polarizaion Ratio
	$C_{4v}, D_4, D_{2d}$	$D_{4h}$	
$\begin{pmatrix} \sigma_{xx} & 0 & 0 \\ 0 & \sigma_{yy} & 0 \\ 0 & 0 & \sigma_{zz} \end{pmatrix}$	$A_1 - A_1$ $A_2 - A_2$ $B_1 - B_1$ $B_2 - B_2$	$A_{1g} - A_{1g}$ $A_{2g} - A_{2g}$ $B_{1g} - B_{1g}$ $B_{2g} - B_{2g}$ $B_{3g} - B_{3g}$ $A_{1u} - A_{1u}$ $A_{2u} - A_{2u}$ $B_{1u} - B_{1u}$ $B_{2u} - B_{2u}$	$< 1$
$\begin{pmatrix} \sigma_{xx} & 0 & 0 \\ 0 & -\sigma_{xx} & 0 \\ 0 & 0 & 0 \end{pmatrix}$	$A_1 - B_1$ $A_2 - B_2$	$A_{1g} - B_{1g}$ $A_{2g} - B_{2g}$ $A_{1u} - B_{1u}$ $A_{2u} - B_{2u}$	$\frac{3}{2}$
$\begin{pmatrix} 0 & \sigma_{xy} & 0 \\ \sigma_{yx} & 0 & 0 \\ 0 & 0 & 0 \end{pmatrix}$	$A_1 - B_2$ $A_2 - B_1$	$A_{1g} - B_{2g}$ $A_{2g} - B_{1g}$ $A_{1u} - B_{2u}$ $A_{2u} - B_{1u}$	$\frac{3}{2}$

Table 1-3. (continued)

Tensor Pattern	Point Group Irreducible Representations	Polarizaion Ratio
$\begin{pmatrix} 0 & 0 & \sigma_{xz} \\ 0 & 0 & 0 \\ \sigma_{zx} & 0 & 0 \end{pmatrix} + \begin{pmatrix} 0 & 0 & 0 \\ 0 & 0 & \sigma_{yz} \\ 0 & \sigma_{zy} & 0 \end{pmatrix}$	<div style="display: flex; justify-content: space-around;"> <div style="text-align: center;"> <math>C_{4v}, D_4, D_{2d}</math>   <math>A_1 - E</math>  <math>A_2 - E</math>  <math>B_1 - E</math>  <math>B_2 - E</math> </div> <div style="text-align: center;"> <math>D_{4h}</math>   <math>A_{1g} - E_g</math>  <math>A_{2g} - E_g</math>  <math>B_{1g} - E_g</math>  <math>B_{2g} - E_g</math>  <math>A_{1u} - E_u</math>  <math>B_{1u} - E_u</math>  <math>B_{2u} - E_u</math> </div> </div>	$\frac{3}{2}$
$\begin{pmatrix} \sigma_{xx} & 0 & 0 \\ 0 & \sigma_{yy} & 0 \\ 0 & 0 & \sigma_{zz} \end{pmatrix} + \begin{pmatrix} \sigma_{xx} & 0 & 0 \\ 0 & -\sigma_{xx} & 0 \\ 0 & 0 & 0 \end{pmatrix} + \begin{pmatrix} 0 & \sigma_{xy} & 0 \\ \sigma_{yx} & 0 & 0 \\ 0 & 0 & 0 \end{pmatrix}$	<div style="display: flex; justify-content: space-around;"> <div style="text-align: center;"> <math>E - E</math>  <math>E_u - E_u</math> </div> <div style="text-align: center;"> <math>E_g - E_g</math> </div> </div>	$<1$

**Figure 1-2. The two-photon absorption processes of a molecule.**

**Nonresonant Intermediate****Resonant Intermediate****Figure 1-2.**

vibronic structure of resonant two-photon transitions cannot be explained by simple Franck-Condon overlap of the vibrational wave functions of the initial and final states, but depends also on the intermediate state.

### C. Experimental Techniques

In the first article on two-photon absorption, Maria Goeppert-Mayer briefly discussed the feasibility of experimentally detecting two-photon processes[27]. She wrote that because of the quadratic intensity dependence, it would be difficult to observe two-photon absorption. Hence, no progress was made in two-photon absorption experiments over a period of some thirty years after Goeppert-Mayer's prediction. Compared with a one-photon cross section for a typical molecule ( $\sim 10^{-17} \text{ cm}^2$ ), the cross section of multiphoton transitions are  $\sim 10^{-50} \text{ cm}^4\text{s}$  and  $\sim 10^{-82} \text{ cm}^6\text{s}^2$  for two-photon and three-photon transitions, respectively. The first successful visible-region experiment was performed by Kaiser and Garrett[28] using a high power ruby laser beam at  $\lambda = 6943 \text{ \AA}$  focused into a  $\text{Eu}^{2+}$ -doped  $\text{CaF}_2$  crystal. The emission of blue light from the two-photon excited state was observed.

Since two-photon absorption is a second-order process, it is weak at moderate light intensities. This demands a sensitive technique for detecting two-photon absorption in a sample. In principle, higher light intensities could be used, but then higher-order processes become more probable and the measured spectrum may be a superposition of two-, three-, or more than three-photon spectra. Indeed, even ionization and fragmentation of a molecule is possible at high radiation intensities. For

these reasons highly sensitive detection techniques and moderate light intensities are more favorable than high light intensities and nonsensitive detection techniques.

Several experimental techniques have been developed to measure two-photon spectra. These include, direct two-photon measurement[29,30], indirect fluorescence excitation measurement[31,32], thermal blooming[33], and multiphoton ionization[34,35]. Only direct two-photon absorption yields absolute cross section  $\delta$ -values, although with very low accuracy and sensitivity[36,30(b)].

The absorption law obeyed by two-photon transitions is similar to that for one-photon absorption, except that the absorbance is intensity dependent. The fraction of light absorbed can be determined by

$$\frac{\Delta P}{P} = \left[ \frac{\delta P}{A} \right] l C, \quad (1-21)$$

where  $P$  is the incident power,  $\Delta P$  is the change due to absorption,  $\delta$  is the two-photon cross section,  $C$  is the concentration,  $l$  is the path length, and  $A$  is the transverse area of the incident beam. For the case where fluorescence from same excited state follows two-photon absorption, it can be seen from eq. 1-21 that the fluorescence intensity is proportional to  $\Delta P$ ;  $P_f = q \Delta P$ , and is therefore proportional to  $P^2$ , where  $q$  depends on the fluorescence quantum yield and on geometrical factors of the experimental set-up[37,38]. Monitoring the intensity of the fluorescence initiated by two-photon absorption as a function of the laser frequency can allow the  $\delta$ -value measurements to be made over a wide spectral range, although only the relative values of  $\delta$  at different laser wavelengths are obtained. Because of



its sensitivity and convenience, the indirect fluorescence measurement is the most widely utilized method to obtain (relative)  $\delta$ -values.

The details of the experimental aspects of the above methods are well reviewed in the literature. Because they are the most common methods, fluorescence excitation and multiphoton ionization are the measurement techniques reviewed here.

### *1. Fluorescence Measurement*

The most convenient and sensitive method for measurement of two-photon spectra is the detection of the fluorescence from the excited molecules. Two-photon excitation (TPE) of fluorescence spectroscopy is based on the detection of the fluorescence as a function of the incident laser energy, and is the technique used to determine the low-lying one-photon forbidden gerade state of the perylene described in this dissertation. In this method the sample to be studied is irradiated with one or two laser pulses, of which at least one must be tunable. The two-photon induced fluorescence is collected by an optical system after appropriate filtering (chemical or optical filters, and/or monochromator), and detected by a photomultiplier. For a "single-beam" experiment the signal from the detector is normalized at each wavelength to the square of the incident laser power. The TPE method requires that emission from same excited state follows the two-photon absorption by the excited states of interest.

## *2. Detection of Two-photon Absorption by Multiphoton Ionization of Molecules*

The multiphoton ionization technique for obtaining information from excited molecules was demonstrated for the first time by Lineberger and Patterson in 1972[34] and developed by Johnson[35]. This method involves collecting electrons released from molecules after irradiation by one or more laser pulse(s). After a molecule has been excited by two-photon absorption, it absorbs subsequent photons, which finally results in ionization. The ion signal is recorded as a function of the laser frequency. The sensitivity of ion detection is quite high compared with that of absorption. However, this method is more complicated in interpretation because different absorption steps may overlap, giving rise to congested spectra from different transitions. An interesting feature of multiphoton ionization is the signal enhancement by resonant intermediate states. Since the ionization efficiency is strongly enhanced when the photon energy is in resonance with a real intermediate state, scanning the wavelength of the laser leads to a modulation of the ion current, which reflects the spectrum of the intermediate states. This method is sometimes abbreviated as REMPI or RE2PI. A new branch of multiphoton ionization called multiphoton ionization mass spectroscopy (MPIMS), in which a mass spectrometer is used to identify the ionization products, has been developed[39,40]. MPIMS yields important information on the dynamic behavior involving both energy relaxation and fragmentation reactions that take place in the excited states of neutral and ionic molecules.

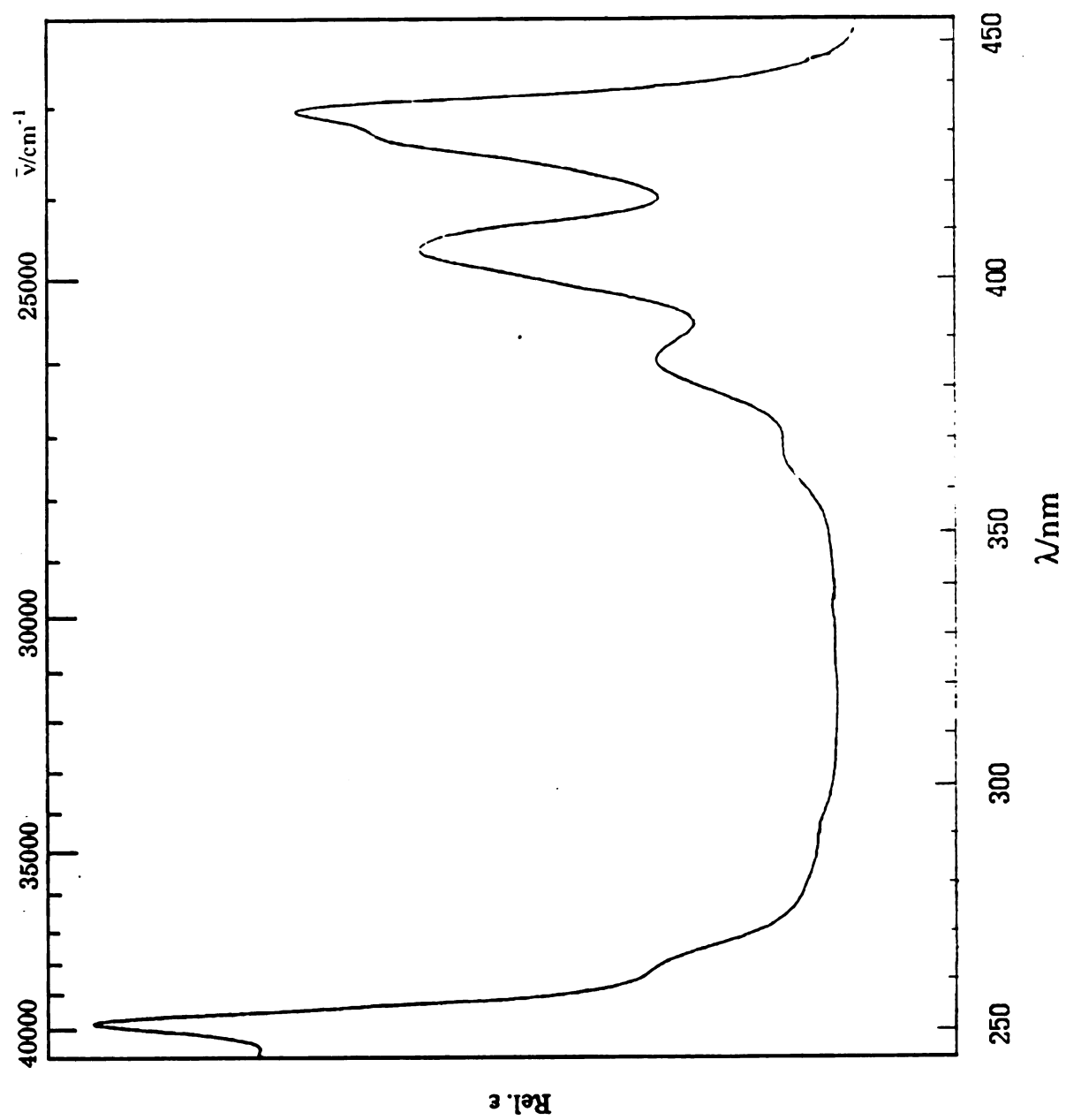
For comparison, the differences between the spectra from above two methods are summarized as follows: 1) the ionization technique is more sensitive to states with high excitation energies near the ionization continuum that barely fluoresce; 2) the ionization technique is especially sensitive for detection of Rydberg states, whose relaxation rates are supposed to be not as fast as relaxation from valence states; 3) with fluorescence detection one preferentially obtains pure two-photon spectra, since fluorescence from higher, three-photon states that might be simultaneously excited by the absorption of a third photon, is not very probable; and 4) in many cases the ionization technique may produce overlapping spectra from two-, or three-photon intermediate states, and therefore assignment is not always unambiguous.

### III. MOTIVATION

Considerable attention has been paid to the electronic spectroscopy of condensed aromatic compounds because of their importance as chromophores in photochemical and biological systems, such as carcinogens and laser dyes, etc., as well as their intrinsic interest[41-44].

As a model of centrosymmetric polycyclic aromatic compounds, perylene is an interesting molecule from the spectroscopic point of view. Unlike other condensed aromatic compounds the lowest singlet one-photon transition (weak in most other molecules of this type) of perylene is the strongest band. Also, the two lowest electronic transitions observed in the one-photon spectrum are separated by an unusually large energy spacing ( $>10,000\text{ cm}^{-1}$ , see Figure 1-3). In the gas phase and in solution perylene

**Figure 1-3.** UV-visible electronic absorption spectrum of perylene ( $10^{-4}$  M) in *n*-hexane solution.



has a high molecular point symmetry,  $D_{2h}$ , and the transitions in the visible and near UV region can be correlated only to  $\pi$ -electron excitations of the aromatic rings. Negligible conjugation is indicated by the consideration of Kekule structures for the two central bonds joining the two naphthalene group rings (Figure 1-4), and both theoretical calculations and experimental results indicate that the  $\pi$ -electron bond order changes with electronic excitation (Figure 1-5)[45].

In addition to investigations in the condensed phase, perylene has been well studied even in supersonic jets with regard to energy transfer[46], intramolecular vibrational relaxation[47], and excimer formation[48], as well as the absorption and emission spectra[49]. Most of the studies, however, are limited only to the first excited state, and only one two-photon measurement (at the  $14,400\text{ cm}^{-1}$  fundamental of the ruby laser for gas phase perylene) has been reported. However, theoretical calculations[50], dichroism analysis of perylene embedded in a stretched polymer[50(a), 51], fluorescence analysis in the gas phase[52], and low temperature absorption spectra[53] all indicate that one-photon forbidden gerade states, as well as a  $B_{2g}^-$  state forbidden in conventional spectra by the  $+$   $-$  pseudo-parity selection rule[54], exist between the first two absorption bands.

Transitions to gerade excited states are normally forbidden by one-photon selection rules because the electronic ground state is  $A_g^-$ , and only u-g transitions are permitted for centrosymmetric chromophores in conventional (one-photon) spectroscopy. The unique even-parity selection rule and the dependence of the fluorescence intensity on the polarization of the excitation beam in two-photon spectroscopy reveal important information regarding such "hidden" states.

**Figure 1-4.** The nine Kekule structures of perylene classified according to symmetry.

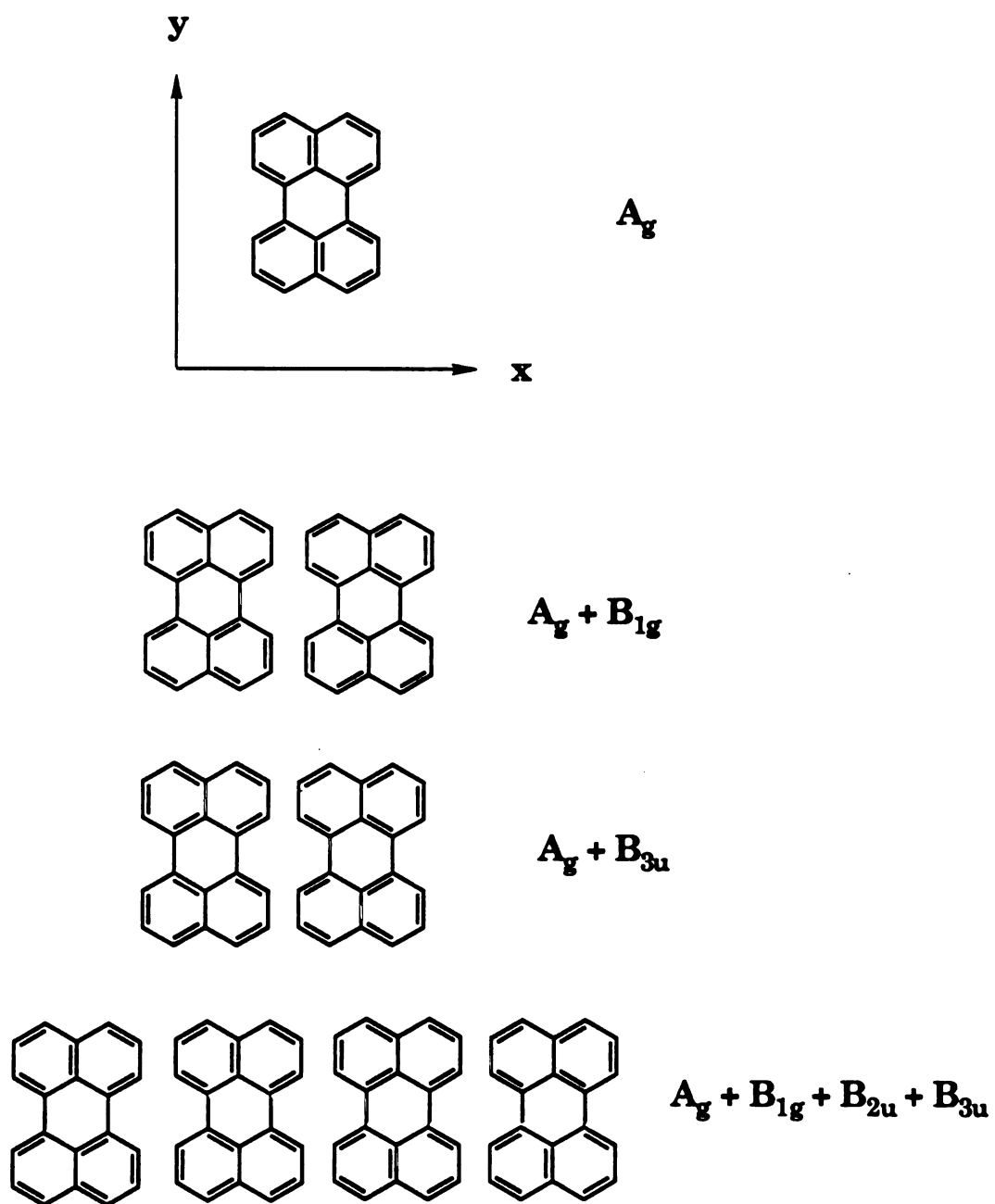
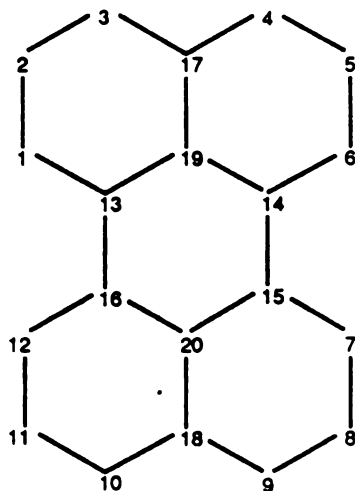


Figure 1-4.



**Figure 1-5.** The bond length ( $\text{\AA}$ ) in the ground and excited state of perylene.

From ref. [45a].



Bond	1-2	2-3	13-6	17-9	14-6	16-20	4-17
Ground State	1.45	1.38	1.50	1.44	1.38	1.45	1.42
1 <sup>st</sup> Excited State	1.39	1.40	1.43	1.42	1.42	1.42	1.418

Figure 1-5.

In this dissertation, the observation and assignment of hidden electronic states of perylene by two-photon excitation spectroscopy will be described. This work contains two parts. Firstly, the TPE spectra of perylene in *n*-hexane solution at room temperature over the dye laser wavelength spectral region 560 – 840 nm, and in isopentane solution at 77 K over the region 650 – 840 nm have been measured. These spectra were obtained using two photons from the same laser. For polarization analysis, the ratio of the fluorescence intensity generated by circularly and linearly polarized laser beams was also measured. Symmetry assignments are given to the observed features based on the polarization ratio,  $\Omega = I_{\text{cir}} / I_{\text{lin}}$ . Secondly, to obtain highly resolved spectra, TPE of perylene in a jet was attempted. As an initial step, the one-photon spectra of perylene in the  $A_g \rightarrow B_{2u}$  transition region (~410 – 420 nm), of iodine over the spectral region 578 – 596 nm ( $X(^1\Sigma) \rightarrow B(^3\Pi)$ ), and of [2,2]paracyclophane ( $A_g \rightarrow B_{1g}$   $\lambda$  (280 – 320 nm)) were obtained.

## **CHAPTER II**

### **TWO-PHOTON EXCITATION SPECTROSCOPY OF PERYLENE IN SOLUTION**

## **I. EXPERIMENTAL**

### **A. Materials**

Perylene (99.<sup>+</sup> % purity) and spectroscopic grade *n*-hexane were purchased from Aldrich Chemical Co. and EM Science, respectively, and used without further purification. The high purity isopentane used for low-temperature experiments was prepared by degassing isopentane, obtained from Burdick and Jackson, by repeated freeze-pump-thaw cycles and then vacuum distilling onto NaK alloy contained in a high vacuum flask.

### **B. Absorption and Emission Spectra**

UV-visible absorption spectra of perylene were recorded on a Perkin-Elmer Lambda Array 3840 spectrometer before and after two-photon excitation spectra were obtained to ensure that no photochemistry had occurred due to laser irradiation. The sample was dissolved in the spectroscopic grade *n*-hexane ( $\sim 10^{-4}$  M) and placed in a square quartz cell with 1 cm pathlength. The dispersed emission spectrum was obtained by using a home-built emission spectrometer which is described in detail in reference 55, housed in Nocera's laboratory at Michigan State University.

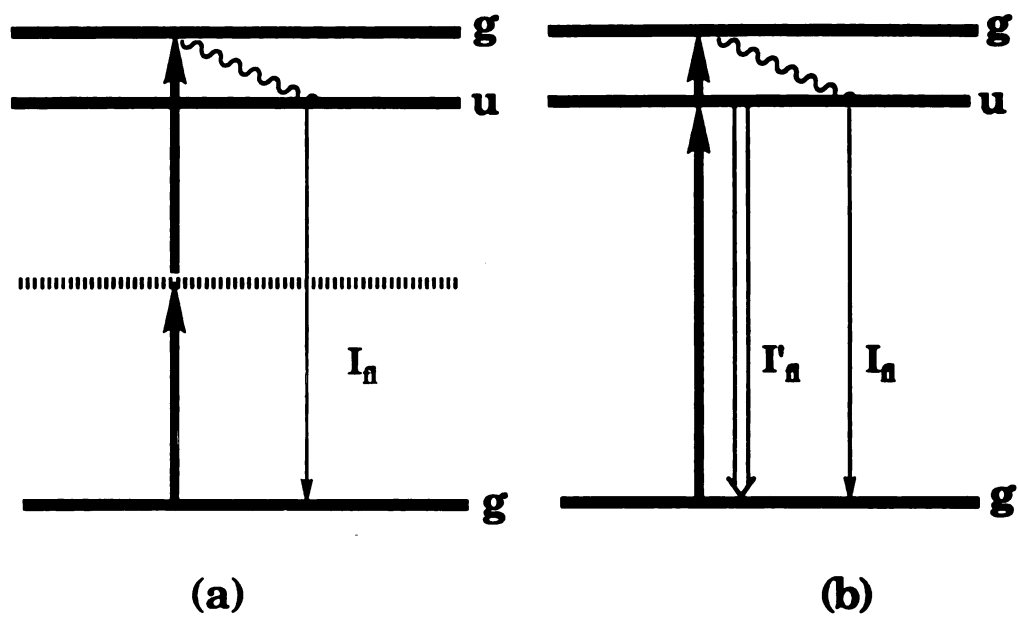
## C. Two-photon Excitation Spectra

### 1. General Considerations

Two-photon excitation (TPE) spectrum can be obtained by (1) two-beam two-photon excitation ( $\omega_1 \neq \omega_2$ ), or (2) one-beam two-photon excitation ( $\omega_1 = \omega_2$ ). In method (1), the first photon, of energy  $\omega_1$ , can be in resonance with a real electronic excited state of the molecule; the two-photon cross section is thus much higher, and this method strongly enhances the emission intensity in comparison to method (2). The latter involves a process in which the intermediate state is a virtual state (see eq 1-20). Also, with the use of two different beams more information can be obtained, since more combinations of the polarization of each beam can be applied. However, the two-beam method could not be applied in experiments with perylene because a series of red and near infrared tunable lasers (not available in our laboratory) would be required for the tunable beam,  $\omega_2$ , in order to cover the two-photon region of interest, and the fluorescence signal monitored is the emission from the first excited state of perylene (Figure 2-1). If two beams are used to achieve the two-photon transition, the pump beam would be in resonance with the first excited state, which emits strongly. Thus it would be extremely difficult to distinguish the signal which results only from the two-photon transition.

In general, a two-photon excitation spectrum is displayed as a TPE profile, which consists of a plot of the two-photon induced fluorescence intensity divided by the product of the powers of the two exciting photons (method 1) or the square of the exciting laser power (method 2) versus excitation energy. In order to perform polarization analysis, the TPE

**Figure 2-1.** Two-photon transition processes, where  $I_{\text{fl}}$  is an intensity of fluorescence from the two-photon induced state, and  $I'_{\text{fl}}$  is an intensity from the one-photon induced excited state.



One-beam two-photon excitation    Two-beam two-photon excitation

Figure 2-1.



profile must be measured under several different conditions of incident laser polarization.

The experimental apparatus is schematically depicted in Figure 2-2. A Nd:YAG (Quanta-Ray DCR-2) pumped tunable dye laser (PDL-2) was used as the excitation source. The Nd:YAG laser was operated at 15 Hz with average pulse energy of approximately 1 mJ/pulse. The output from the dye laser was completely linearly polarized with a Glan-Thompson prism  $P_1$ , and a set of three Fresnel rhombs ( $P_2$  and  $P_3$ ) were used to produce linearly or circularly polarized light without changing the beam intensity and position. The use of these rhombs to control the polarization of the laser beam in the TPE experiment is described in detail in the section on polarization measurement procedure. The outcoming beam from the third rhomb was focussed onto the sample (1 cm pathlength quartz cell) using a glass focussing lens L ( $f = 10$  cm).

The fluorescence measurement sample chamber, shown in the Figure 2-3, contained two quartz spherical lenses which collected the emitted light at  $90^\circ$  from the incident dye laser beam ( $f = 10$  cm each). These lenses focused the two-photon induced fluorescence onto the entrance slit of a Spex 1680A monochromator, M, after it passed through a combination of UV-transmitting filters  $F_2$  (Corning 5-57 or 4-96). The wavelength of the monochromator was set at  $470 \pm 5$  nm. The energy region selected contains the strong 0 - 1 emission band ( $0 - 1298$   $\text{cm}^{-1}$  and  $0 - 1369$   $\text{cm}^{-1}$  fluorescence). The signal was detected using a Hamamatsu R928 photomultiplier tube,  $D_1$ , which is characterized by low dark current, fast rise time ( $\sim 2$  ns), and high spectral response in the region of interest. The PMT was mounted in a Pacific Instruments 3150RF housing at room temperature and normally operated at 960 V. The intensity of each pulse of

**Figure 2-2.** A schematic diagram of the two-photon excitation of fluorescence measurement. Here SH is a second harmonic generator, M is a mirror, BS a beamsplitter, OP is opal glass, and Osc. is an oscilloscope.

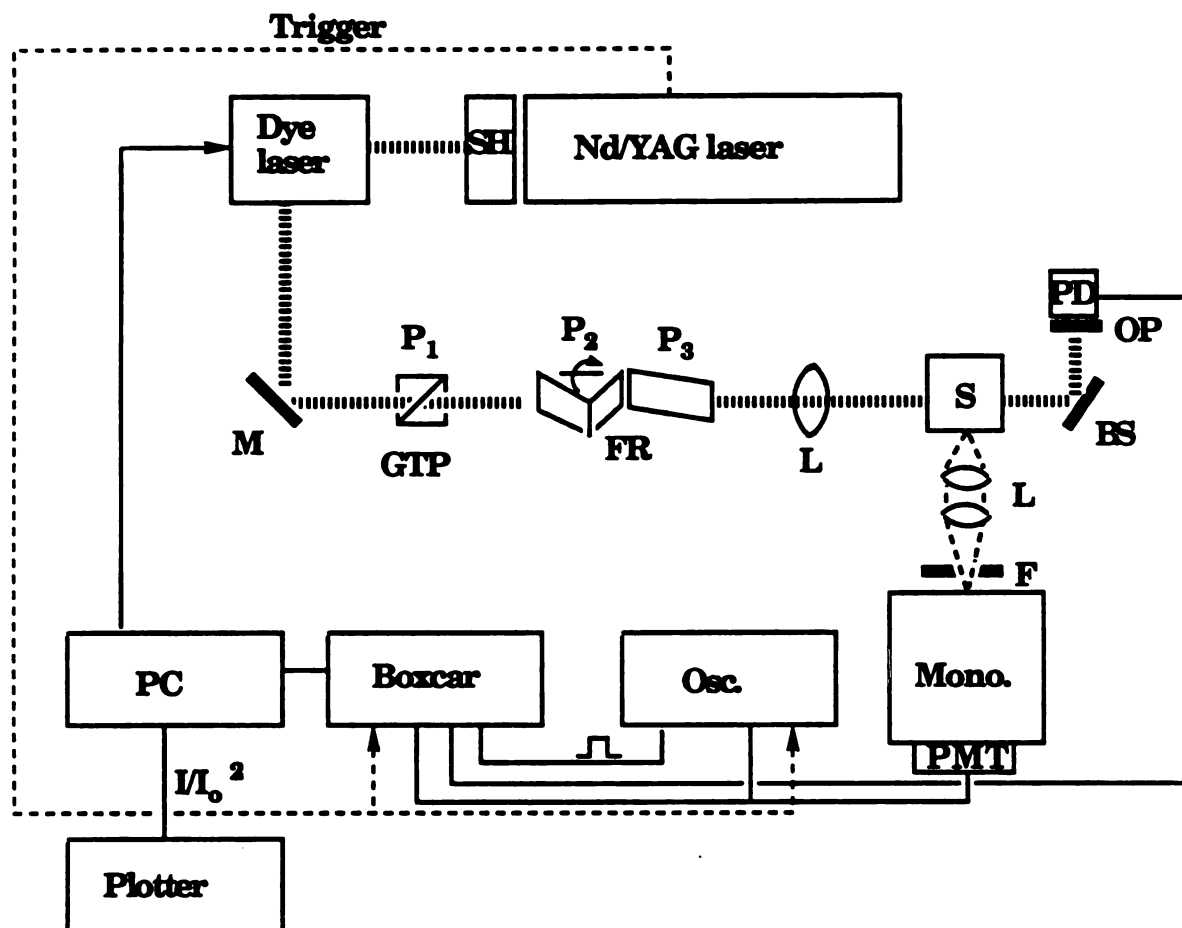
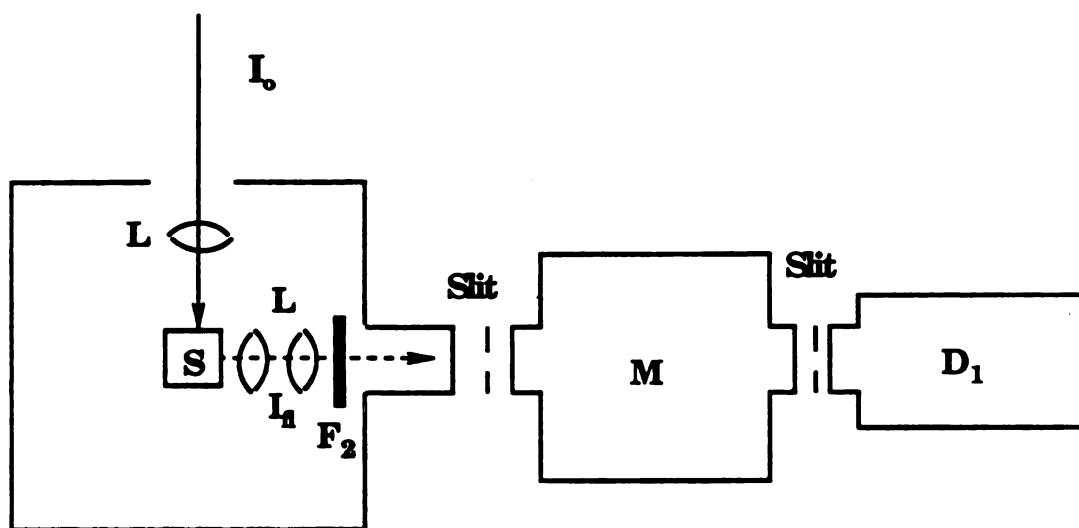


Figure 2-2.

**Figure 2-3.** The fluorescence measurement sample chamber for TPE.



**Figure 2-3.**

the exciting laser was measured by deflecting a small portion of the beam with a beamsplitter through opal glass to a fast photodiode (Hewlett Packard 5082-4200) after it had passed through the sample. The photodiode is indicated as PD in Figure 2-2. This arrangement provided for accurate relative measurement of the reference power, since less than  $1 \times 10^{-5}$  of the total number of photons in an excitation pulse are absorbed by the sample in a virtual two-photon process. Before the collection of TPE data, the pure solvent background was measured. Also, the dispersed emission spectrum induced by the two-photon transition (Figure 2-4) and the necessary quadratic intensity dependence of the TPE fluorescence on the exciting laser power (Figure 2-5) were confirmed.

Under control of the trigger from the variable output of the Nd:YAG laser, peak signals from the sample and the reference photodiode (i.e., the peak height was assumed to be proportional to the peak intensity of the TPE) were integrated (gatewidth set at 10 ns) and 30 of these integrated signals were averaged for each data point by the boxcar integrator/averager (Stanford SR 232). To prevent signal ringing through the cable connections, 50- $\Omega$  terminators were first attached to the PMT output and the averaged outputs from the boxcar integrator/averager. The averaged outputs from the boxcar integrator were collected, and the signal from the sample was normalized to the square of the exciting laser intensity by a personal computer (PC). This procedure was followed because the signal from the two-photon excited state ( $I_{\eta}$ ) is proportional to the square of the exciting laser power,  $\langle \delta \rangle \sim \langle I_{\eta} \rangle / \langle I_0^2 \rangle$ . Under computer control, the wavelength setting of the dye laser was changed and the process repeated for each excitation point of the spectrum within the tuning range of the dye. Nine dye solutions were used to cover the spectral range from 560 to 840 nm.

**Figure 2-4.** Dispersed fluorescence spectra: (a) one-photon excitation,  $\lambda_{\text{ex}} = 365$  nm: (b) two-photon excitation,  $\lambda_{\text{ex}} = 584$  nm.

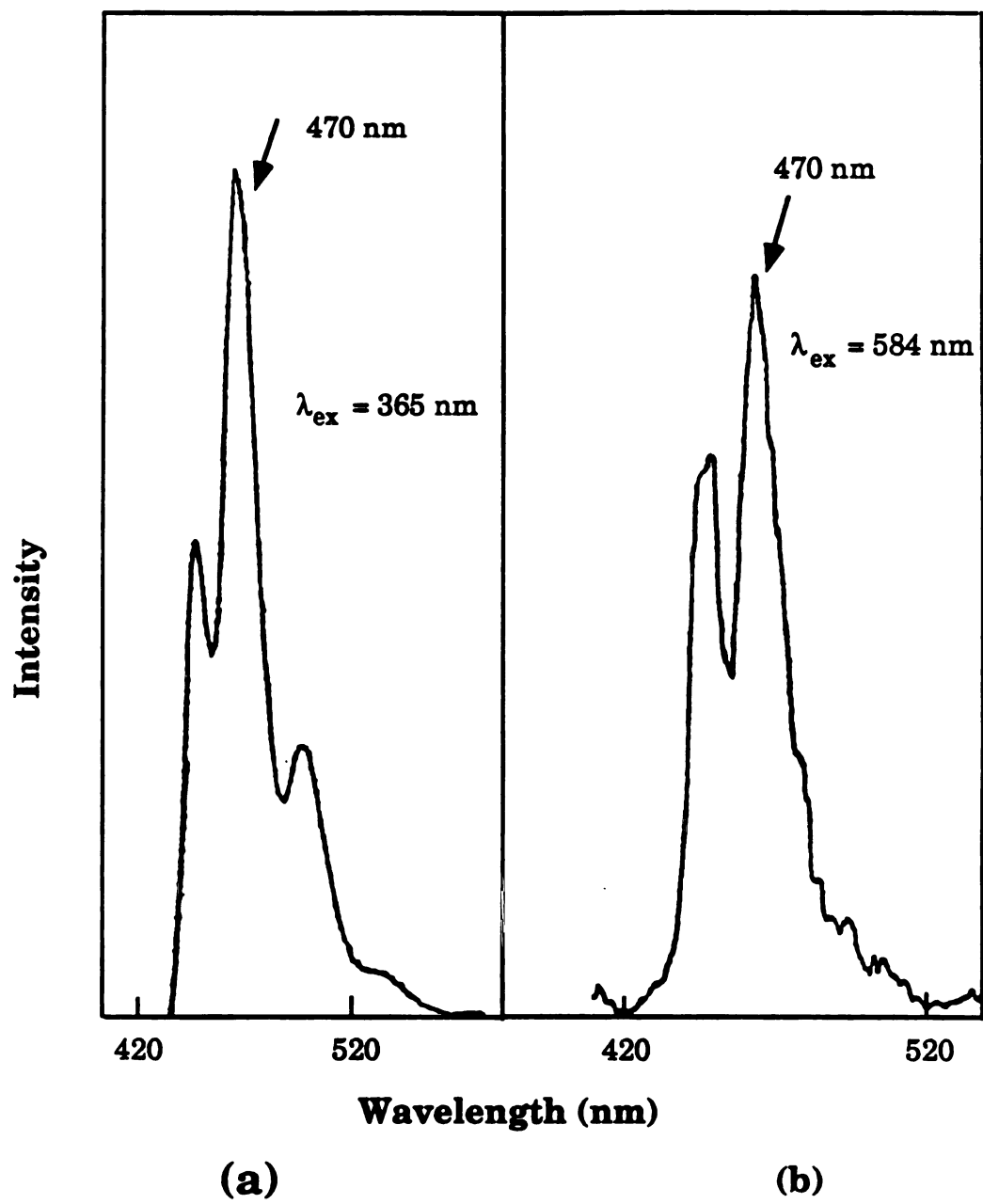


Figure 2-4.



**Figure 2-5.** Power dependence of the two-photon induced fluorescence of perylene ( $\sim 10^{-4}$  M in *n*-hexane) at two-different initial laser wavelengths.

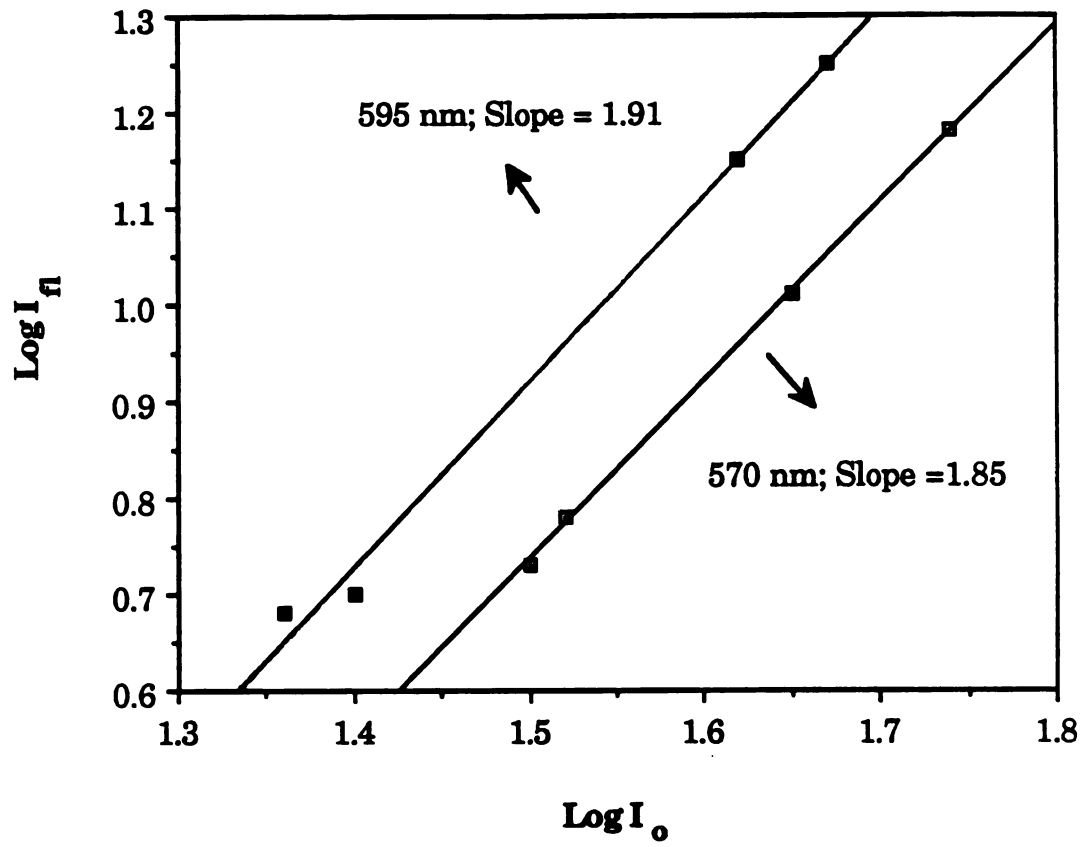


Figure 2-5.

They were selected in such a way that the tuning ranges overlapped by at least 5 nm. Since it is not possible to measure the absolute  $\delta$  values from the fluorescence measurements, the partial spectra that were measured with different dyes needed to be matched in the overlapping range. The ranges covered by the dyes used in our experiment are shown in Figure 2-6. The TPE spectrum measured was not corrected for variations in the fluorescence quantum yield or the spectral response of the photodiode as a function of excitation energy (Figure 2-7). Data from the literature[56, 57] indicate that the quantum yield varies only little with excitation energy for perylene in the energy range 435 – 250 nm.

The two-photon excitation spectrum of perylene at 77 K over the 780 – 650 nm dye laser wavelength region was also obtained as described below. The sample solution was prepared by using a high-vacuum cell consisting of a 1 cm square quartz cuvette attached to a sidearm terminating with a 10 ml round bottom flask (Figure 2-8). These two parts were separated from one another with a high vacuum valve. Perylene was placed in the cuvette and isolated from the side arm with the valve. High purity isopentane was degassed by freeze-pump-thaw cycles and transferred to the side-arm round bottom flask by bulb-to-bulb vacuum distillation, and then mixed with the perylene. To make a homogeneous glass solution, the sample cell was slowly immersed in the liquid nitrogen contained in a silver-coated Dewar, also shown in Figure 2-8, having three quartz windows located along orthogonal axes (i.e., "entrance" and "exit" windows along an excitation axis and one window along a "fluorescence monitoring" axis). Nitrogen gas was blown across the surface of the windows to prevent moisture condensation. The procedure for obtaining the 77 K spectrum was the same as the room temperature measurement, except that the reference beam

**Figure 2-6.** The tuning range and relative output power of dyes used in the two-photon excitation of perylene.

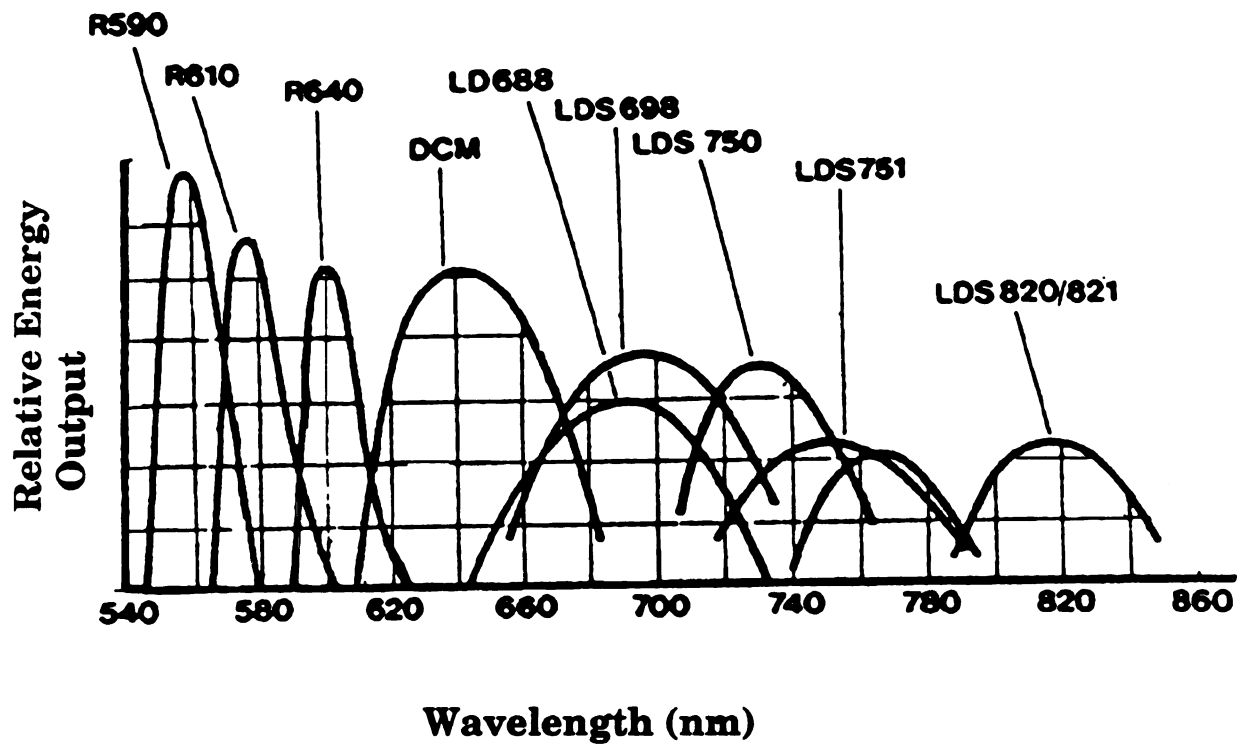
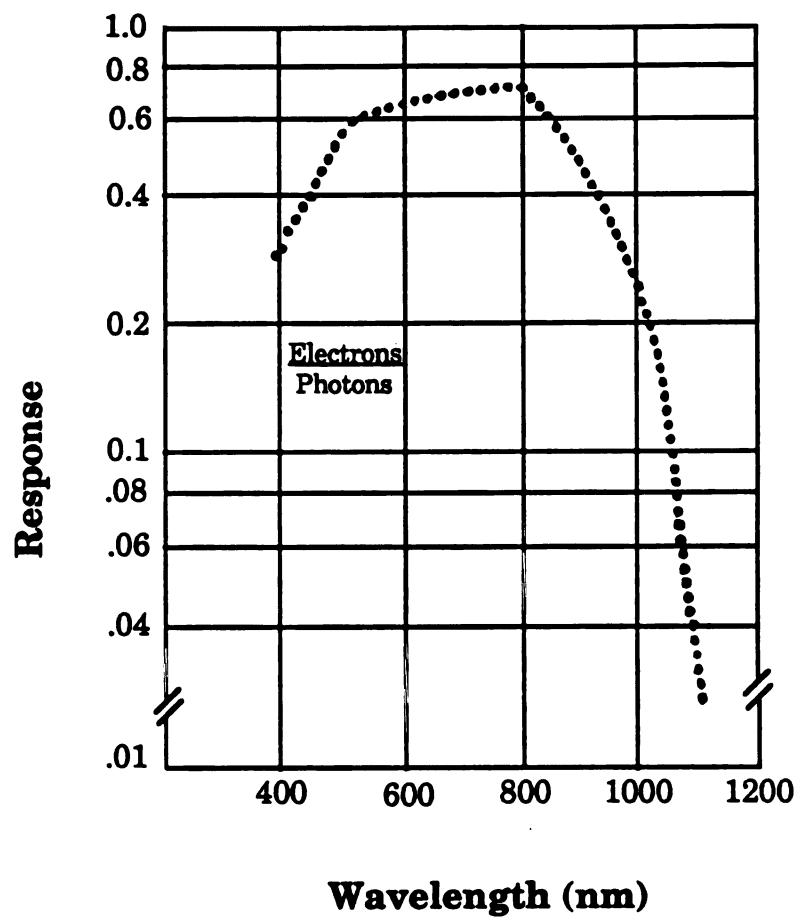


Figure 2-6.

**Figure 2-7. The spectral response of the photodiode.**

**Figure 2-7.**





**Figure 2-8. Liquid nitrogen Dewar and High-vacuum cell for 77 K TPE measurement.**

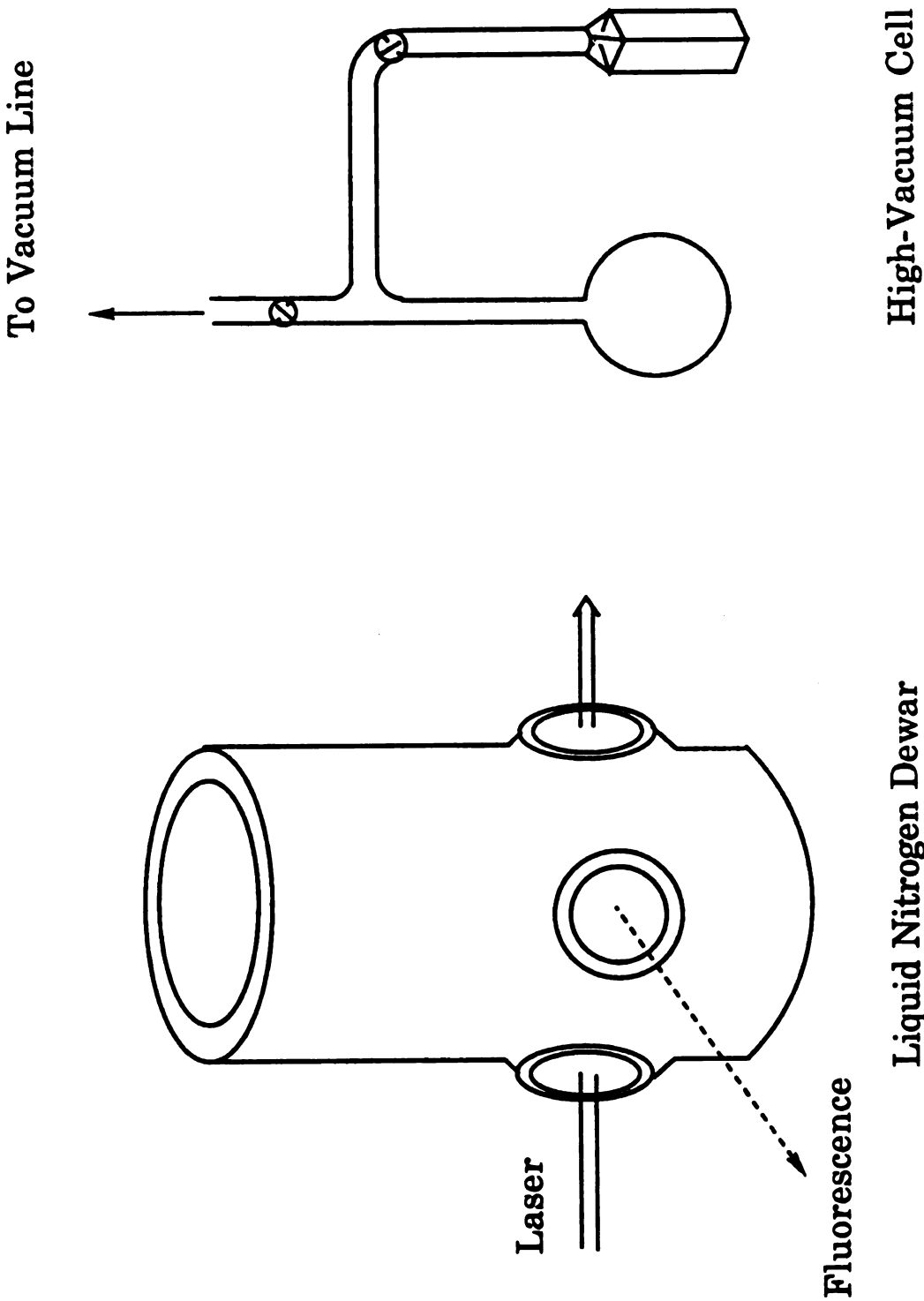


Figure 2-8.

intensity was monitored before the beam had passed through the Glan-Thompson prism,  $P_1$ .

## *2. Polarization Measurement Procedure*

The polarization ratio of interest is the ratio of the two-photon cross-sections for circularly and linearly polarized incident beams:  $\Omega = \delta_{\text{cir}} / \delta_{\text{lin}}$ . To obtain the polarization ratio,  $\Omega$ , one has to measure the normalized fluorescence intensity under both polarizations of the incident light,  $I_{\text{cir}}$  and  $I_{\text{lin}}$ . Two different experimental methods can be used. One is the simultaneous measurement in two different samples, and the second utilizes two consecutive runs with the same sample, with the polarization of the laser light changed between the two measurements[59-61]. In the first case, all optical and opto-electronic parts of the experimental setup must have the same excitation energy ( $\omega$ ) dependence, and in the second case the light source and detector system must have a very good long term stability. For the two-photon excitation  $\Omega$  measurement of perylene the second method was used.

The polarization changing device (Figure 2-9) consists of a fixed Glan-Thompson prism (linear polarizer)  $P_1$ , a double-Fresnel rhomb configured such that it can be rotated around the optical axis of the laser beam (achromatic  $\lambda/2$  retarder)  $P_2$ , and a fixed Fresnel rhomb (achromatic  $\lambda/4$  retarder)  $P_3$ . The laser output from the dye laser is completely linearly polarized with the Glan-Thompson prism  $P_1$ . If the double-Fresnel rhomb,  $P_2$ , is rotated around the axis of the light propagation, the vector of the outcoming light is rotated with respect to the linearly polarized incident beam. Therefore rotation of  $P_2$  changes the angle between the orientation of

**Figure 2-9.** The alignment of the polarization changing optics: here  $P_1$  is a Glan-Thompson prism,  $P_2$  is a double-Fresnel polarization rotator,  $P_3$  is a Fresnel rhomb, and M is a mirror.

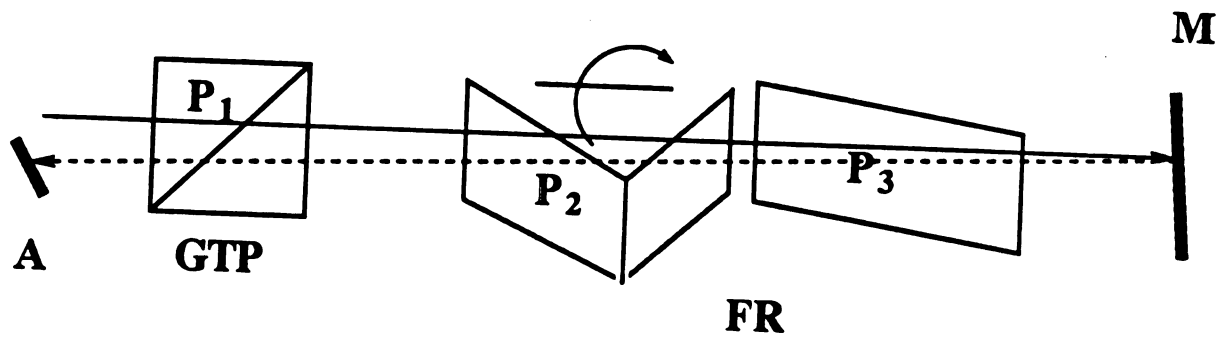


**Figure 2-9.**

the linearly polarized light and the optical axis of the third Fresnel rhomb,  $P_3$ . The light leaving  $P_3$  is linearly polarized every  $45^\circ$  increment of rotation about the optic, and circularly polarized light is obtained halfway between two positions which yield linearly polarized beams (Figure 2-10). To confirm whether the light leaving the third Fresnel rhomb is completely circularly polarized, the outcoming beam was reflected back through the incoming path using mirror M (Figure 2-9), and the intensity of the reflected image was monitored in front of the linear polarizer  $P_1$ . When the outcoming beam was completely circularly polarized, no reflected beam was observed at position A. The polarization ratio,  $\Omega$ , was measured every 1 nm, and each point represents the average over 1000 laser shots at each polarization.

### *3. Dye Laser Wavelength Scan*

To scan the two-photon excitation spectrum the grating position of the dye laser was computer controlled. The dye laser scanning procedure is as follows. The variable output from the Nd:YAG laser triggers the boxcar integrator to start collecting data. The busy output signal from the SR232 triggers the boxcar interface. After the user-specified number of busy output pulses are received, the interface sends a signal to the stepping motor transformer. Then the stepping motor attached at the dye laser scans the wavelength a preset amount, and data collection is initiated again. To scan the stepping motor two signals are required. One is the TTL pulse for the stepping and the other is a logic level high (5 V) or low (0

**Figure 2-10.** Representation of the electric field vector in space, (a) and (b), and the projection, (c), of the electric field vector of the initial incoming beam and the electric field after the rotator. Here  $Z$  is the optical axis of the rotator,  $E_0$  is the incoming beam strength;  $E_x$  and  $E_z$  are the  $x$  and  $z$  components of the electric field, respectively;  $E_{2\lambda}$  and  $E_{4\lambda}$  are the electric field vectors of the outgoing beam from the rotator and the third Fresnel rhomb, respectively,  $Z_0$  is the optical axis of the third Fresnel rhomb; and  $\alpha$  is the rotation angle of the rotator with respect to the incoming beam and the optical axis of the third Fresnel rhomb.

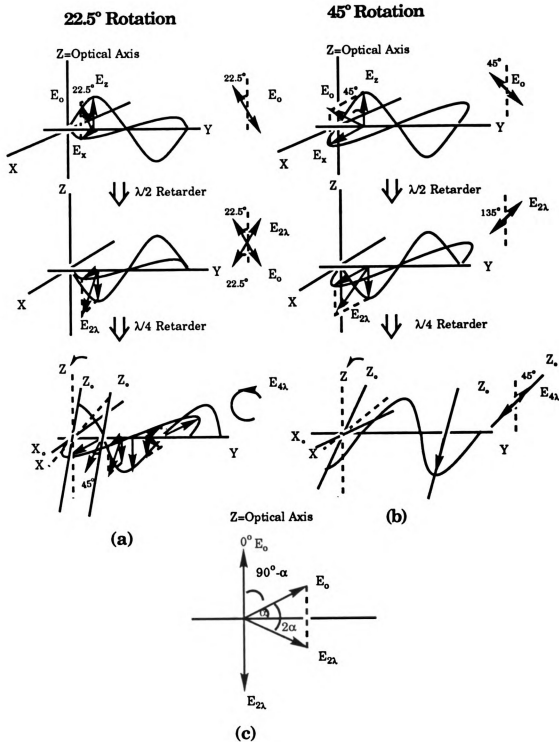


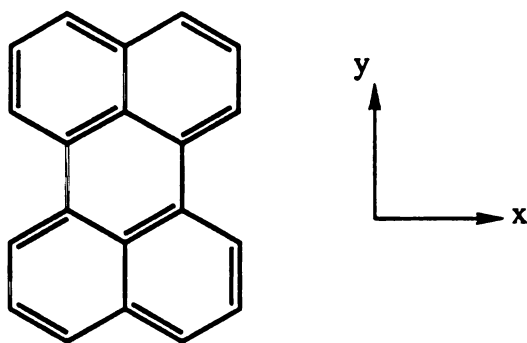
Figure 2-10.



V) for the stepping direction. The electronic circuit diagram of the stepping motor transformer designed by Ralph Thiim[58] is shown in Figure 2-11.

## II. RESULTS AND DISCUSSION

Assuming that perylene, 1, in solution has  $D_{2h}$  molecular symmetry (the long and short in-plane axes being  $y$  ( $B_{2u}$ ) and  $x$  ( $B_{3u}$ ), respectively),



**Perylene**

1

the two-photon active electronic states that can couple with the totally symmetric ground state,  $A_g^-$ , belong to the  $A_g$ ,  $B_{1g}$ ,  $B_{2g}$ , and  $B_{3g}$  symmetries. Additionally, making the reasonable assumption that the lower excited states which lie in the visible and the near UV region are  $\pi\pi^*$ ,

**Figure 2-11.** The electronic circuit diagram of the stepping motor interface.

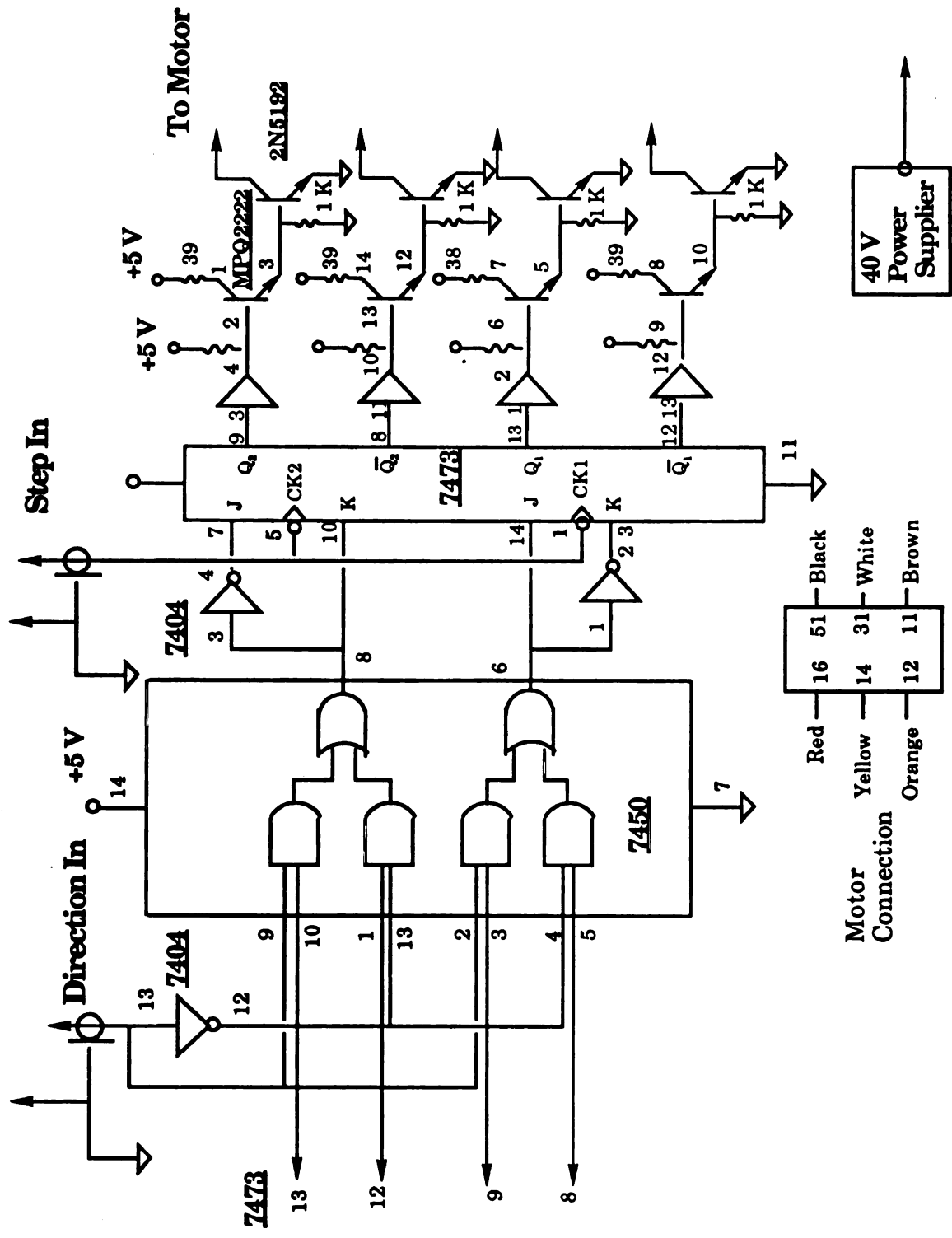


Figure 2-11.

i.e. having in-plane transition moments, the two-photon activity is further restricted to  $A_g$  and  $B_{1g}$  (xy) states (Figure 2-12).

The normal one-photon absorption spectrum of perylene in *n*-hexane at room temperature is shown in Figure 2-13. The two-photon fluorescence excitation spectrum, obtained under linear polarization of the incident laser radiation is superimposed.

The UV-visible absorption spectrum of perylene has a strong first absorption band ( $\log \epsilon \sim 5$ ) in the visible region ( $\sim 435$  nm), which has been assigned to the  $A_g^-(S_0) \rightarrow B_{2u}^+(S_1)$  transition, polarized along the long molecular axis[50(a)]. The second strong absorption band ( $\log \epsilon \sim 4$ ) is in the UV region ( $\sim 250$  nm) and has been assigned to the  $A_g^-(S_0) \rightarrow B_{3u}^+(S_n)$  transition, which is polarized along the molecular short axis. At the same time, perylene has a fluorescence quantum yield of about  $\sim 1$  over the entire spectral range 435 – 250 nm in solution at room temperature. It is noteworthy that the energy region below  $\sim 13,000$   $\text{cm}^{-1}$  (laser wavelength above 750 nm) does not produce notable two-photon absorption within our experimental error limit, although the one-photon spectrum has strong absorption in the region of twice this energy.

To reveal more detail, the TPE intensity and a point-by-point plot of the polarization ratio  $\Omega$  vs. incident laser wavelength are reproduced in Figure 2-14. In addition, the TPE spectrum of perylene in isopentane at 77K over the two-photon energy region of 23,600 - 35,700  $\text{cm}^{-1}$  (dye wavelength 780 - 650 nm) is shown in Figure 2-15.

Seven major absorption maxima are observed in the two-photon spectrum at room temperature, being located at 26,530 (754 nm), 27,860 (718 nm), 28,950 (690 nm), 30,300 (660 nm), 32,000 (625 nm), 33,900 (590 nm), and

**Figure 2-12.** The symmetries of the  $\pi$ -electron cloud of the ground state and the low-lying excited electronic states of perylene.

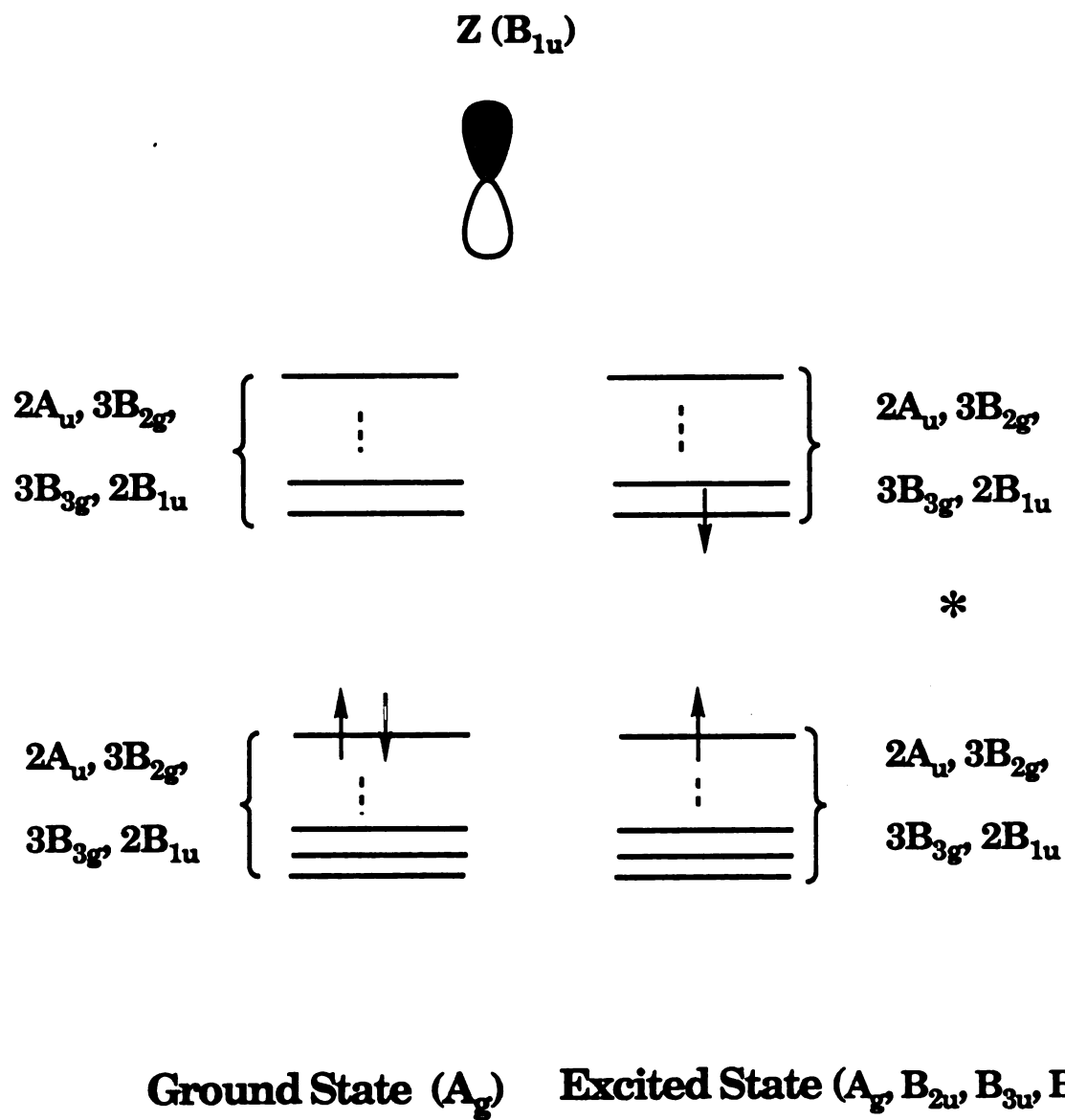
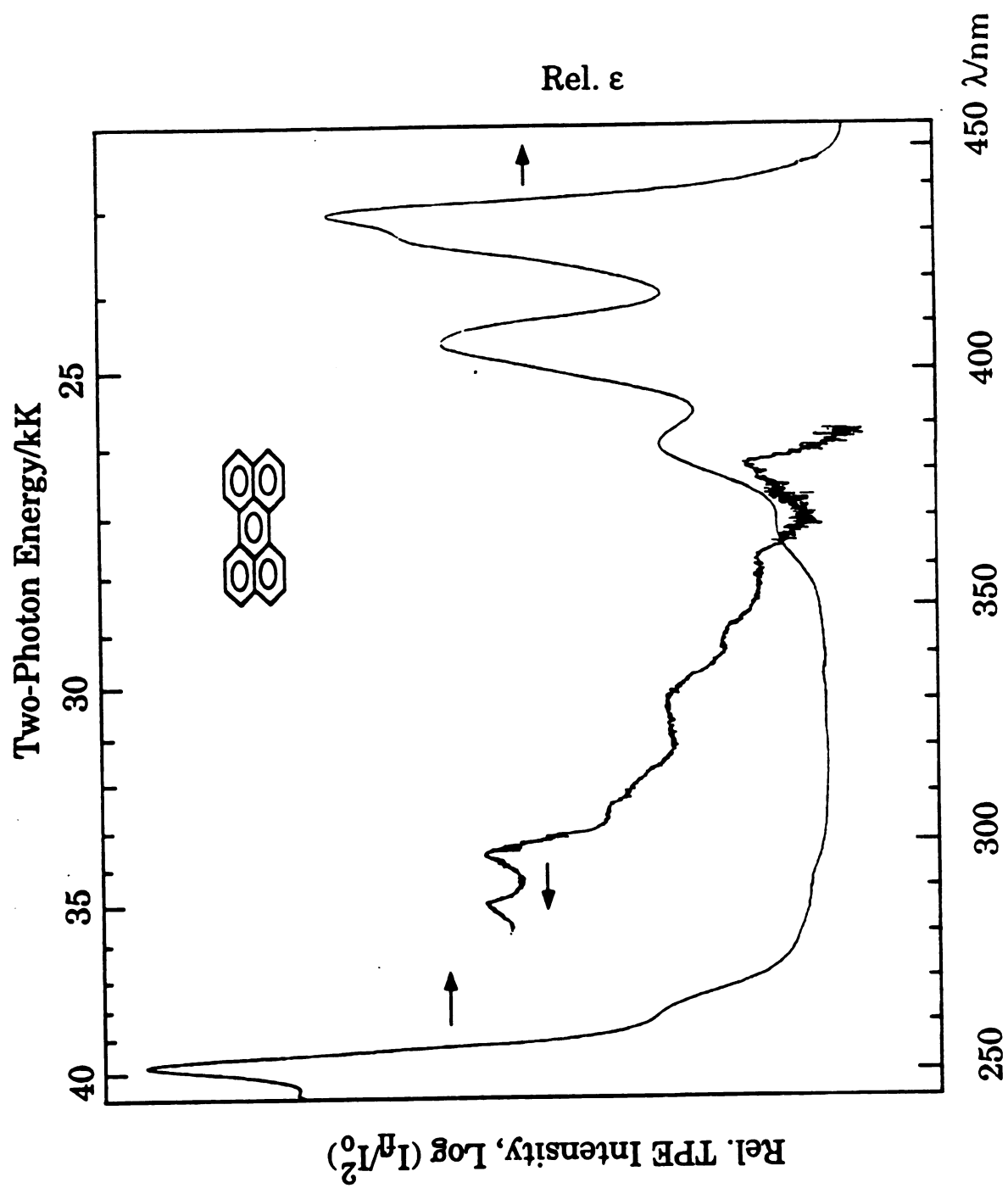


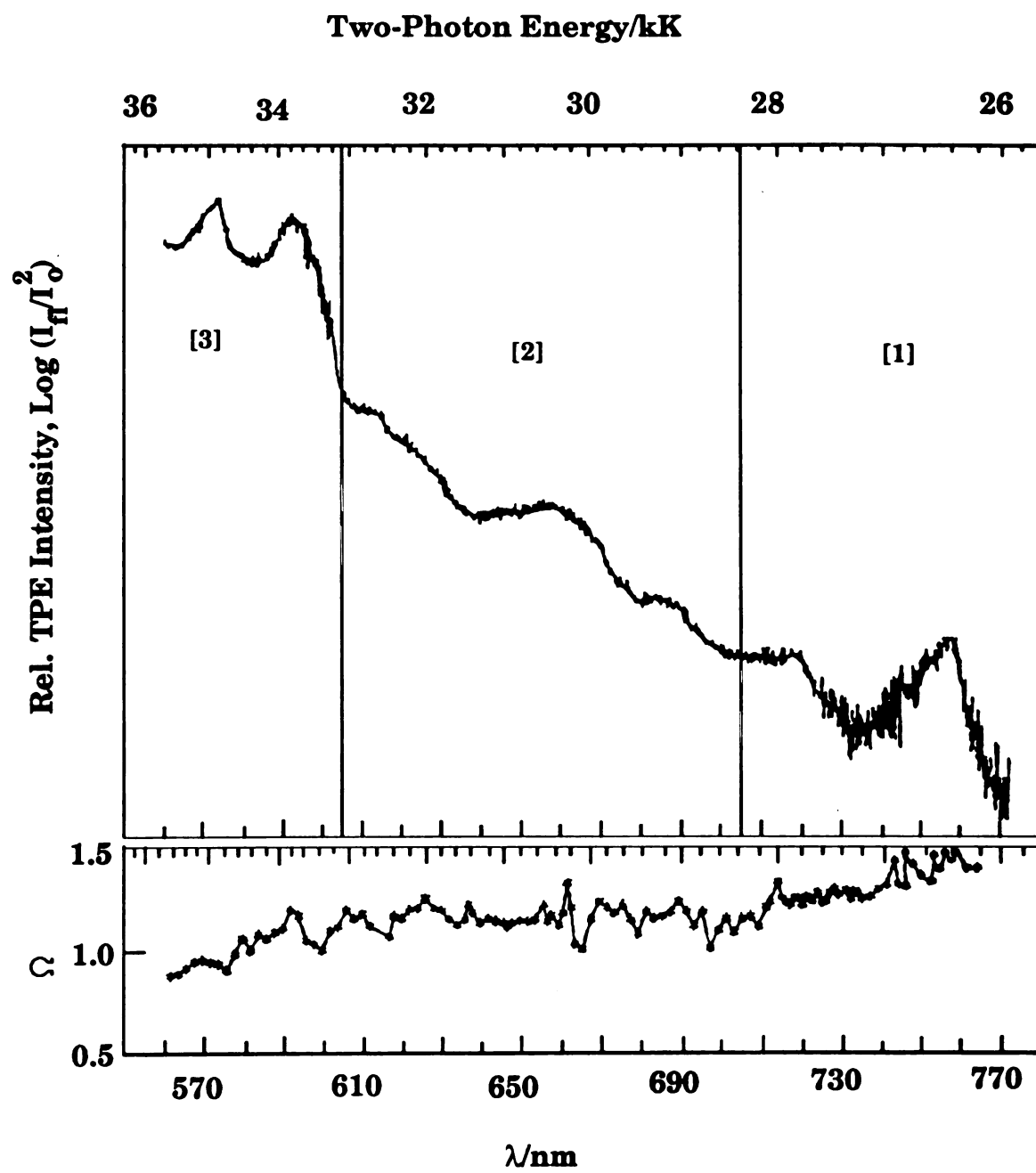
Figure 2-12

**Figure 2-13.** One-photon UV-visible absorption and two-photon excitation spectra of perylene in *n*-hexane solution.

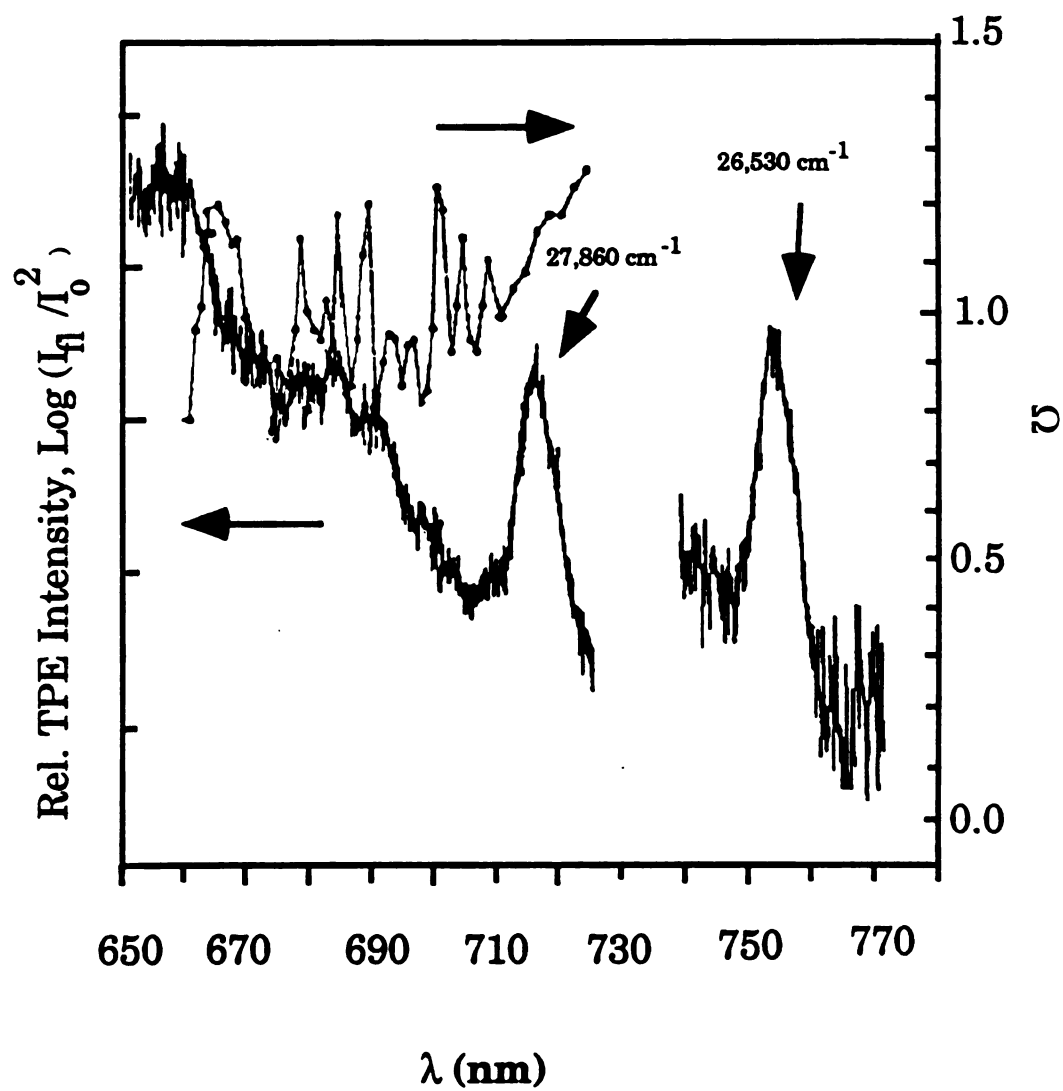




**Figure 2-14.** TPE of perylene in *n*-hexane ( $10^{-4}$  M) and polarization ratio,  $\Omega$ , plotted as a function of the incident dye laser wavelength.

**Figure 2-14.**

**Figure 2-15.** TPE spectrum of perylene in isopentane at 77 K. The polarization ratio over a somewhat narrower incident laser wavelength range is also included.

**Figure 2-15.**

34,900  $\text{cm}^{-1}$  (573 nm); the two-photon induced fluorescence intensity is strongly enhanced as one moves from lower to higher energies. The two-photon polarization parameter,  $\Omega$ , starts with a value close to the theoretical upper limit of 1.5[25] in the region of 26,530  $\text{cm}^{-1}$  (754 nm) and reaches a value of 1.35 in the vicinity of the maximum of the peak at 27,860  $\text{cm}^{-1}$  (718 nm). The polarization ratio remains between 1.25 – 1.00 in the region 28,170 – 32,790  $\text{cm}^{-1}$  (710 – 610 nm). The  $\Omega$  curve drops from  $\sim 1.2$  to  $\sim 0.85$  near 34,500  $\text{cm}^{-1}$  (580 nm) and shows a distinct decrease below 570 nm, indicating either a superposition of two different symmetry transitions or vibronic coupling. In the energy region above 28,570  $\text{cm}^{-1}$  (700 nm), the vibronic structure of the spectrum and the values of the polarization ratio become complex.

On the basis of the intensity of the TPE and the value of the polarization ratio,  $\Omega$ , it is convenient to consider the TPE spectrum in three parts (Figure 2-14).

The first band system [1] in the two-photon excitation (TPE) spectrum of perylene, in the region 780 - 705 nm (25,600  $\text{cm}^{-1}$  – 28,400  $\text{cm}^{-1}$  two-photon energy) shows distinct sub-structures: a sharp maximum at 758 nm (26,380  $\text{cm}^{-1}$ ); and a shallow maximum at 716 nm (27,900  $\text{cm}^{-1}$ ). The structure is better resolved at 77 K, where two relatively strong and comparatively broad ( $\sim 280 \text{ cm}^{-1}$  FWHM) peaks are revealed at about 26,530  $\text{cm}^{-1}$  and 27,860  $\text{cm}^{-1}$ . The polarization ratio at 758 nm is close to the theoretical limiting value of 1.5, which indicates that this peak is the result of a transition from the  $A_g^-$  ground state to an excited state of  $B_{1g}^-$  vibronic symmetry. From the bandwidth and enhanced intensity of the peaks at liquid nitrogen temperature, it is likely that the bands at 716 nm and 758 nm belong to the same electronic state.

The experimentally and/or theoretically obtained energy levels of the excited states of perylene in the energy region near  $26,500\text{ cm}^{-1}$  are depicted in Figure 2-16 [50(a)-(c)]. Here  $B_{2u}^+$  is the one-photon allowed lowest singlet excited electronic state ( $S_1$ ),  $B_{3u}^-$  is the experimentally and theoretically predicted second excited electronic state of perylene[50(a), 50(c), 52, 53, 61],  $B_{1g}^-$  is the predicted and observed lowest "g" state, and the dotted line represents our observed peak at  $\sim 26,500\text{ cm}^{-1}$ . The one-photon allowed lowest singlet excited state,  $B_{2u}^+$ , is observed at  $23,000\text{ cm}^{-1}$  (435 nm). It seems highly questionable to assign the band at  $26,530\text{ cm}^{-1}$  (754 nm) as a vibronically induced  $B_{2u}^+ b_{3u}$  ( $= B_{1g}^-$ ) false origin. In this case, it would be necessary to assume for the inducing  $b_{3u}$  vibrational mode in the excited state a value of  $\sim 3,500\text{ cm}^{-1}$  above the  $23,000\text{ cm}^{-1}$   $B_{2u}^+$  origin, which is unreasonable. A  $B_{1g}^-$  allowed transition in this spectral region also seems to be excluded. The experimentally-observed first  $B_{1g}^-$  state occurs at  $\sim 29,000\text{ cm}^{-1}$ [50(a)-(c)] although the two-photon data do not provide sufficient information to confirm the reliability of those experiments. Also, theoretical calculations predict the first  $B_{1g}^-$  state at  $29,000 - 30,600\text{ cm}^{-1}$ . On the other hand, several calculations predict a  $B_{3u}^-$  state at  $\sim 27,400\text{ cm}^{-1}$  [50(a), 50(c)]. From these facts it seems likely that the bands are vibronically-induced transitions to the  $B_{3u}^-$  state. The somewhat high intensity for a vibronically allowed transition is probably due to the near-resonance with allowed transitions.

Having an almost vanishing oscillating strength and being hidden under the strong  $A_g^- \rightarrow B_{2u}^+$  transition, the  $B_{3u}^-$  state was not observed in the conventional one-photon spectroscopy of perylene. However, the existence of the  $A_g^- \rightarrow B_{3u}^-$  transition in the absorption and photoelectron spectra of the perylene was already inferred by Clar[53, 62]. A linear dichroism

**Figure 2-16.** Observed and calculated energy level diagram of the excited electronic states of perylene near the peak at  $26,500\text{ cm}^{-1}$ .

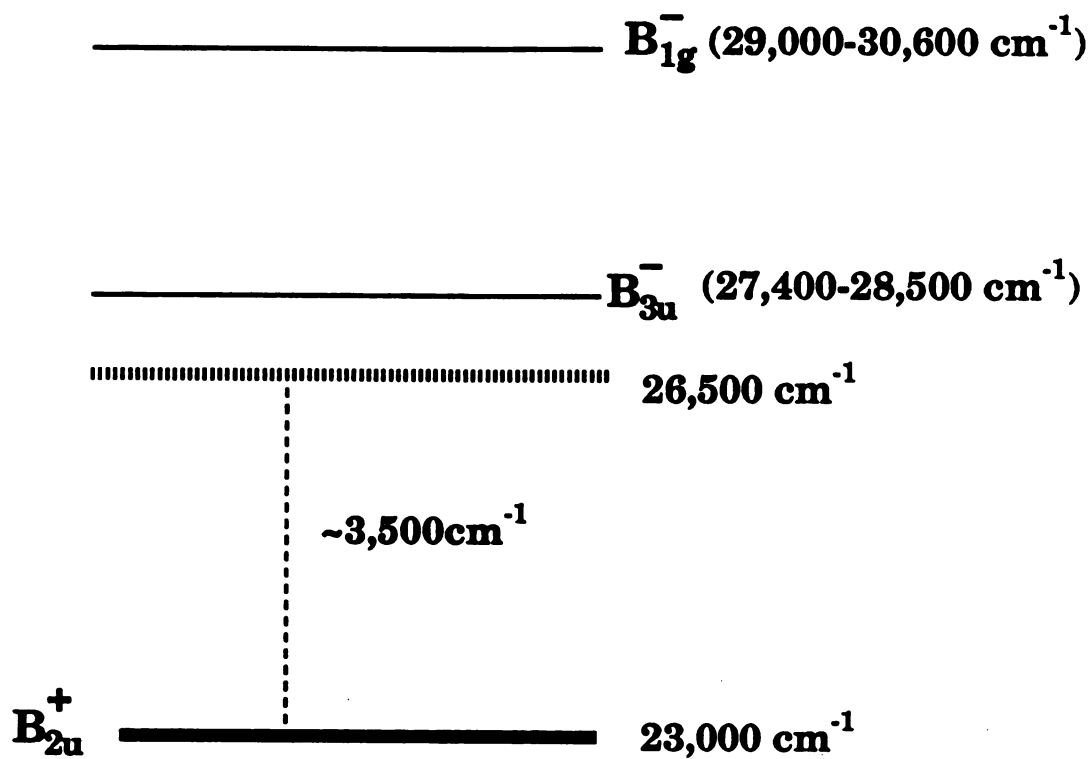


Figure 2-16.



measurement on perylene embedded in stretched polymer sheets has revealed a weak short-axis polarized contribution in the high energy region of the first absorption band[50(a)]. An indication of the  $B_{3u}^-$  state at ~365 nm is also found in polarization spectrum of perylene in the gas phase[52]. According to the pseudoparity selection rules of alternant hydrocarbon theory ( $- \rightarrow -$  is forbidden for one-photon transitions)[54], a  $B_{3u}^-$  state is expected in two-photon absorption( $A_g^- \rightarrow B_{3u}^-$ ) to be vibronically allowed.

Perylene ( $C_{20}H_{12}$ ) has ninety normal vibrations which are classified as follows:

$$\Gamma_{\text{vib}} = 16 a_g + 15 b_{1g} + 15 b_{2u} + 15 b_{3u} + 7 a_u + 8 b_{1u} + 6 b_{2g} + 8 b_{3g}$$

where  $a_g$ ,  $b_{1g}$ ,  $b_{2u}$ , and  $b_{3u}$  are the symmetries of the planar vibrations. Because of the  $g \rightarrow g$  selection rule for two-photon absorption, the active vibrations in the  $B_{3u}^-$  electronic state will be of "u" symmetry. All such vibrations:  $b_{1u}$ ,  $b_{2u}$ ,  $b_{3u}$ , and  $a_u$  may be active since

$$B_{3u}^-(b_{3u}, b_{1u}, b_{2u}, a_u) = (A_g, B_{2g}, B_{1g}, B_{3g}),$$

respectively. Vibrations of symmetries  $a_u$  and  $b_{1u}$  are out-of-plane motions, and can be ignored for the vibronic mixing of  $\pi\pi^*$  states. On the basis of the polarization ratio value in the region of the lowest-energy peak (~1.5), it is likely that a higher excited  $B_{1g}^-$  state lends intensity to the transition through vibronic coupling. And the somewhat high intensity for a vibrationally-induced transition is probably due to the small energy gap between the  $B_{3u}^-$  and  $B_{1g}^-$  states (Figure 2-16). Therefore, the active vibrations

for the vibronic coupling are likely to be of  $b_{2u}$  symmetry. From these considerations, the lowest-energy peak in our two-photon spectrum, at  $26,530\text{ cm}^{-1}$ , is assigned to a "false origin" of the symmetry forbidden transition  $A_g^- \rightarrow B_{3u}^-$ , whose true electronic origin is located at a lower energy. The observed transition terminates in a state of  $B_{1g}$  vibronic symmetry, lying above the origin by the energy of a  $b_{2u}$  vibrational mode. Bands of  $b_{2u}$  symmetry ranging from  $300\text{--}3,000\text{ cm}^{-1}$  have been observed in the ground state vibrational spectrum of perylene (see Table 2-1) obtained from ir and Raman measurements[52, 63-65], and the  $B_{3u}^-$  origin would thus be placed in the  $23,500\text{--}26,200\text{ cm}^{-1}$  range.

The vibrational mode which contributes to the vibronically induced transition at  $27,860\text{ cm}^{-1}$  (718 nm) can be a  $b_{2u}$  vibrational mode which has an energy difference of  $\sim 1,330\text{ cm}^{-1}$  from the  $b_{2u}$  vibration which induces the first  $B_{3u}^- * b_{2u}$  band at 754 nm, an odd overtone band of  $b_{2u}$  symmetry ( $B_{3u}^- * b_{2u}^n$ ), or a combination band involving an  $a_g$  ( $B_{3u}^- * b_{2u} * a_g$ ) vibrational mode. From Table 2-1, the first possibility can be excluded. If one of the overtone bands of a  $b_{2u}$  mode is responsible for the transition at  $27,860\text{ cm}^{-1}$ , then it cannot be a second overtone of  $b_{2u}$ , which would have  $B_{3u}^-$  vibronic symmetry [ $B_{3u}^- * b_{2u} * b_{2u} = B_{3u}^-$ ] and thus be forbidden in two-photon spectroscopy (Figure 2-17). If  $b_{2u}^n$  is responsible for the observed peak, it must be a third overtone [ $B_{3u}^- * b_{2u} * b_{2u} * b_{2u} = B_{1g}^-$ ], and the frequency of the responsible  $b_{2u}$  mode should be half of the vibrational interval from the band at  $26,530\text{ cm}^{-1}$  (754 nm) to the band at  $27,860\text{ cm}^{-1}$  (718 nm),  $\sim 665\text{ cm}^{-1}$ . No  $b_{2u}$  mode near  $665\text{ cm}^{-1}$  is listed among the fundamental frequencies in Table 2-1. Because distortion of the ring can be ignored for the lower  $\pi\pi^*$  excited state of perylene, the vibrational frequencies in the excited electronic state will be little shifted. Thus, the possibility of a third overtone is also excluded. The

Table 2-1. Observed and Calculated In-Plane Vibrational Frequencies ( $\text{cm}^{-1}$ ) of Perylene.

Fluorescence[52]	ir[64, 65]	Raman[63, 64]	Form of the Vibration[52]	Symmetry Type	Theory[52, 64]
298		297	CCC	$a_g$	298, 271
			CCC, CCH	$b_{1g}$	316, 309
	417		CCC	$b_{2u}$	336, 403
358		364, 358	CCC, CCH	$a_g$	358, 399
550		548, 551	CCC	$a_g$	550, 445
			CCC, CCH	$b_{1g}$	568, 557
	585, 583		CCC, CCH	$b_{2u}$	584, 527
			CCC, CCH	$b_{1g}$	634, 672
793		784, 797	CCC	$a_g$	792, 807
	850, 847	850	CCC, CCH	$b_{2u}$	849, 689
			CCC, CCH, CC	$b_{1g}$	962, 883
	963, 977		CCC, CCH, CC	$b_{2u}$	960, 815
973		979	CCC, CCH	$a_g$	973, 908
	980, 988	982	CC	$b_{2u}$	983, 957
		1103(?)	CCC, CCH, CC	$a_g$	1024, 926
			CCC, CCH, CC	$b_{1g}$	1071, 958
1104		1140(?), 1105	CCH	$a_g$	1104, 1096
	1151, 1148	1145	CCH	$b_{2u}$	1154, 1097
	1217, 1215	1225	CCH	$b_{2u}$	1223, 1199
1252		1222	CCH	$b_{1g}$	1239, 1096

Table 2-1. (Continued)

Fluorescence[52]	ir[64, 65]	Raman[63, 64]	Form of the Vibration[52]	Symmetry Type	Theory[52, 64]
1298	1288, 1287	1299, 1296	CCH CCH CCH CC CC, CCH CC, CCH CC, CCH CC, CCH CC, CCH, CCC CC, CCH CC, CCH, CCC CC, CCH, CCC CC, CCH CC, CCH CC, CCH CC, CCH, CCC CH	b <sub>1g</sub> b <sub>2u</sub> a <sub>g</sub> b <sub>1g</sub> b <sub>2u</sub> a <sub>g</sub> a <sub>g</sub> b <sub>2u</sub> a <sub>g</sub> b <sub>1g</sub> b <sub>2u</sub> b <sub>1g</sub> a <sub>g</sub> a <sub>g</sub> b <sub>1g</sub> b <sub>2u</sub> a <sub>g</sub> b <sub>2u</sub>	1271, 1206 1282, 1392 1289, 1236 1316, 1419 1364, 1430 1370, 1339 1380, 1448 1377, 1471 1452, 1480 1501, 1534 1508, 1520 1538, 1578 1574, 1523 1580, 1665 1583, 1649 1592, 1611 3031, 3029 3053, 3029 3056, 3035
1369	1367, 1365	1367, 1370			
1380	1382, 1381	1373, 1378			
1574	1513, 1508				
1581		1568, 1574 1582			
3031	1592, 1591	1592			
		3052, 3012 3054, 3045			

**Figure 2-17.** Two-photon transitions to various vibrational levels of a  $B_{3u}^-$  electronic symmetry state. The right sides of (a) and (b) represent the symmetry of the vibrational levels, and left sides levels show the corresponding total vibronic symmetries.  $A_g^-$  is the symmetry of the ground state of perylene.

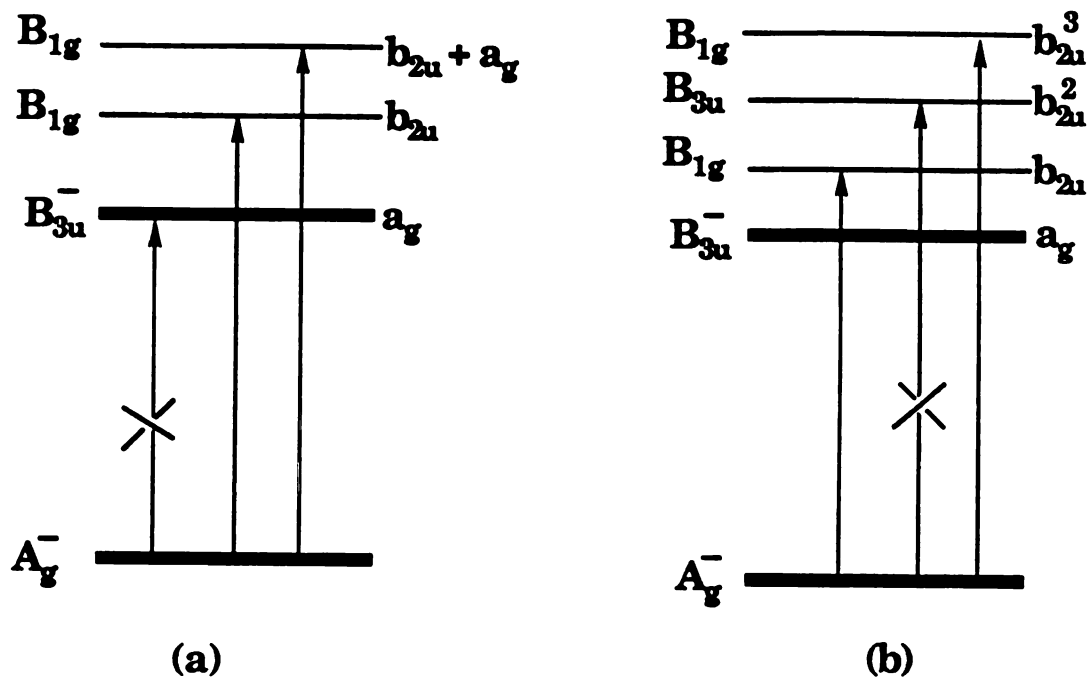


Figure 2-17.

band at 718 nm should probably be assigned to combination of the ( $B_{3u}^- * b_{2u}$ ) level with an  $a_g$  vibration, which likely corresponds to the  $1,370\text{ cm}^{-1}$  ground-state frequency (C=C, C=C-H ring stretching motion) measured from Raman spectroscopy.

The TPE in region [2],  $28,400\text{ cm}^{-1}$  (705 nm) –  $33,000\text{ cm}^{-1}$  (605 nm), is more intense than that in region [1] and continues to rise slowly. It consists of a broad band with maxima at  $28,990\text{ cm}^{-1}$  (690 nm) and  $30,300\text{ cm}^{-1}$  (660 nm), and a weaker shoulder at  $32,000\text{ cm}^{-1}$  (625 nm) having three substructures, at  $32,790\text{ cm}^{-1}$  (610 nm),  $32,260\text{ cm}^{-1}$  (620 nm), and  $31,750\text{ cm}^{-1}$  (630 nm). Above  $28,400\text{ cm}^{-1}$  (below 705 nm) at 77 K, the vibrational structure and the polarization ratio value in the spectrum become complex (Figure 2-15). It is reasonable to assume that the discontinuity corresponds to the onset of a different electronic transition. However, the mean value of the polarization ratio stays approximately constant at  $\sim 1.2$  throughout this region, indicating that all the bands likely belong, whatever their origin, to the same electronic system. These bands are not seen in the one-photon solution spectrum in the same energy region. From this fact and the relatively large intensity it is suggested that the observed bands are due to symmetry-allowed  $g \rightarrow g$  electronic transitions.

Several theoretical calculations place the lowest  $B_{1g}^-$  state at  $29,000 - 30,600\text{ cm}^{-1}$  (690 – 654 nm) [50(a)-(c)]; other  $B_{1g}^-$  states may be nearby [50(a), 50(c)]. We also suggest that  $B_{1g}^-$  electronic states are responsible for the fluorescence obtained following TPE in this region. At the origin, and for other  $B_{1g}$  vibronic levels,  $\Omega$  should be 1.5. In-plane  $b_{1g}$  vibrations will have  $A_g$  vibronic symmetry, for which  $\Omega = 0.67$  is expected [25]. In low resolution spectra the measured polarization ratio will reflect the vibronic symmetry of the specific state being accessed ( $3/2$  or  $2/3$  in the case of perylene), plus

contributions from overlapping bands, as well as underlying levels built on lower-energy origins, which have other symmetry. Thus deviation from the mean  $\Omega \sim 1.15$  may be more diagnostic of the symmetry of a state reached by two-photon excitation than the numerical value is. On this basis, we tentatively assign the origin of the first  $B_{1g}^-$  electronic state to the lowest-energy component of the 77 K triplet obtained with laser radiation near 685 nm, at  $28,950 \text{ cm}^{-1}$ , where  $\Omega$  exhibits a local maximum.

The TPE spectrum at 77 K in the wavelength region below 705 nm reveals several peaks [ $28,410$  (704 nm),  $28,650$  (698 nm),  $28,940$  (691 nm),  $29,150$  (686 nm), and  $29,410 \text{ cm}^{-1}$  (680 nm)]. Since two different electronic states ( $B_{3u}^-$  and  $B_{1g}^-$ ) contribute here, definitive assignments cannot be made from our low-resolution spectrum.

From the remaining structure in the  $31,750 \text{ cm}^{-1}$  (630 nm) region, it is not clear how to make an assignment from the observed polarization ratio at room temperature; however, the presence of another  $B_{1g}^-$  state near  $32000 \text{ cm}^{-1}$ , where a polarization maximum is obtained, cannot be ruled out.

In region [3], we observe a very strong band with maxima at  $33,900 \text{ cm}^{-1}$  (590 nm) and  $35,100 \text{ cm}^{-1}$  (570 nm). On the long wavelength side of the  $33,900 \text{ cm}^{-1}$  peak a shoulder is discerned. In the region of this shoulder,  $\Omega$  drops down to  $\sim 1$  and then rises up to 1.2 at the maximum near  $33,900 \text{ cm}^{-1}$  (590 nm). Regardless of the differing levels of sophistication, all calculations predict a  $A_g^-$  electronic state in the neighborhood of  $34,000 \text{ cm}^{-1}$  [50(a)-(d)]; there may be other g-states nearby[50(a)]. CARS[50(d)] and picosecond[66] dynamics measurements on perylene in the  $S_1$  ( $B_{2u}^+$ ) state both show a strongly-allowed one-photon transition to a (presumably  $A_g^-$ ) state which lies  $35,300 - 38,400 \text{ cm}^{-1}$  above the ground state. On the basis of



the observed polarization ratio, however, the absorption maximum at ~590 nm should be assigned to a  $B_{1g}$  vibronic symmetry state rather than to an origin of  $A_g$  symmetry. Thus we place the origin of the lowest  $A_g^-$  excited state at  $33,450\text{ cm}^{-1}$  where a polarization minimum is obtained in *n*-hexane solution at room temperature. The peak at 590 nm ( $\sim 330\text{ cm}^{-1}$  higher than the assigned  $A_g^-$  state origin) may be due to presence of a  $b_{1g}$  vibration in the  $A_g^-$  excited electronic state, corresponding to the  $b_{1g}$  mode at  $316\text{ cm}^{-1}$  in ground state. On the other hand, one calculation[50(a)] predicts a  $B_{1g}^-$  state close to the  $A_g^-$  state ( $\sim 200\text{ cm}^{-1}$ ), so the polarization maximum near  $33,900\text{ cm}^{-1}$  could signify the origin of a  $B_{1g}^-$  excited state. In the region of  $35,090\text{ cm}^{-1}$  (570 nm),  $\Omega$  drops from 1.2 to 0.8, indicating that most of the TPE intensity above 570 nm is related to final states of symmetry  $A_g$ . However, it is not clear whether the peak at 570 nm is due to an electronic origin of symmetry  $A_g$  or to vibronic perturbation; there are several strong  $1300 - 1600\text{ cm}^{-1}$   $a_g$  vibrations in the ground state. Approximately  $330\text{ cm}^{-1}$  higher than this value there is local maximum in the  $\Omega$ -curve. Again, this may be due to the presence of a  $b_{1g}$  vibration with frequency similar to the ground state mode at  $316\text{ cm}^{-1}$ .

The results of this work are shown in Figure 2-18, and collected in Table 2-2, where they are compared with values of perylene excited state origins predicted by various calculations, or observed by one-photon experiments in low temperature glasses, stretched films, etc. The theoretical predictions are generally slightly higher than the experimental values in *n*-hexane solution, but the correlation is surprisingly good. In order to obtain better resolved spectra, which would provide more definitive assignments and compare more directly to theory, we tried to obtain the

**Figure 2-18.** Energy diagram of the lower excited electronic states of perylene.

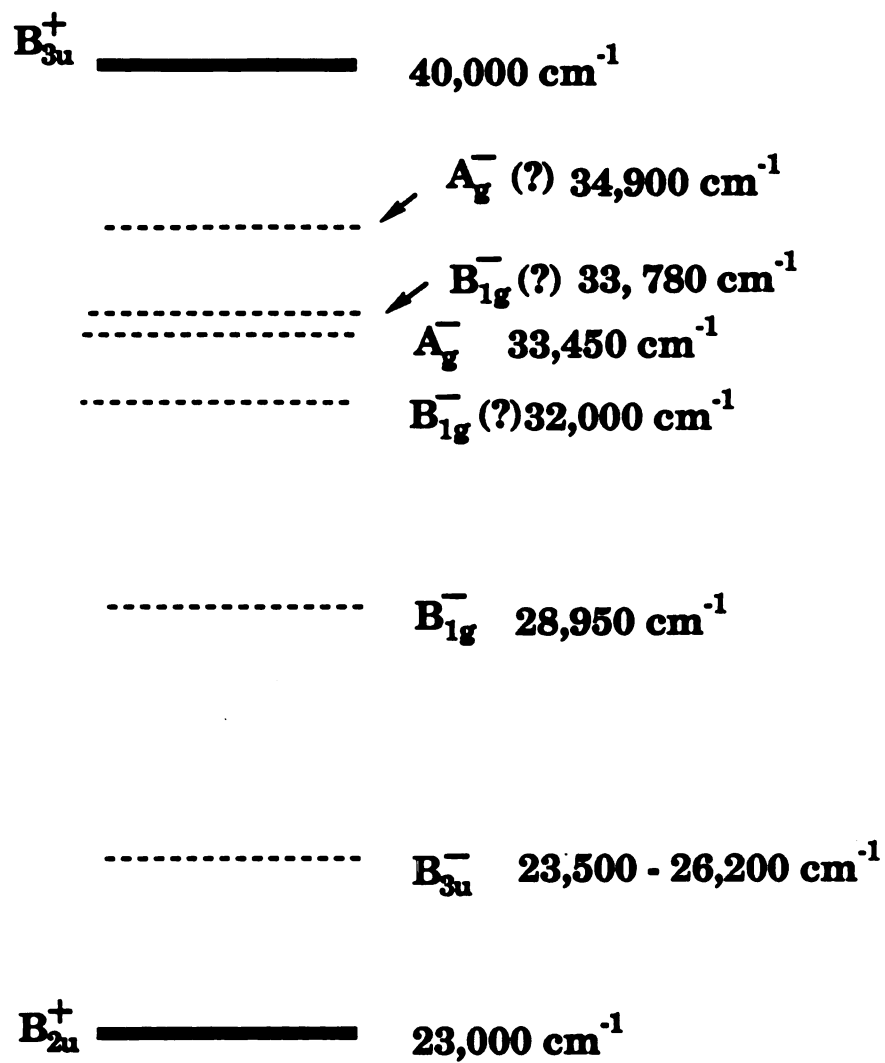


Figure 2-18.

**Table 2-2. Comparison of Experimental and Calculated Values ( $\text{cm}^{-1}$ ) of Transition Energies to Low-Lying Symmetry-Forbidden Excited States from the Ground ( $A_g^-$ ) State of Perylene.**

Table 2-2.

Two-Photon		One-Photon	
Assignment	Experiment <sup>a</sup>	Assignment	Theory
$B_{3u}^-$	(23,500 - 26,200)	$B_{3u}^-$	27,300 [50(a)] 27,960 [50(c)]
$B_{3u}^- + b_{2u}$	26,530		28,600 [50(a)]
$B_{3u}^- + b_{2u} + a_g$	~27,000		
$B_{3u}^- + b_{2u} + a_g$	27,860		
$B_g^-$	28,950	$B_g^-$	29,090 [50(a)] 29,400 [50(a), 67, 68] 29,330 [50(c)]
$B_g^- + (b_{1g} a_g)$	(29,200 - 32,800)		29,500 [51] 30,570 [50(d)]
$B_g^-$	32,000(?)		29,600 [53] 31,780 [50(a)] 34,460 [50(a)]
$A_g^-$	33,450	$A_g^-$	~33,000 [50(a)] 34,140 [50(c)]
$A_g^- + b_{1g}$ (or $B_g^-$ )	33,780		34,300 [53, 51] 34,560 [50(a)]
$A_g^- + a_g$ (or new $A_g^-$ )	34,900		34,500 [50(c), 67, 68] 35,670 [50(d)]
$A_g^- + b_{1g}$	35,210		36,280 [50(a)]

<sup>a</sup> This work.<sup>b</sup> From solid state of film measurements; no source is given for the experimental numbers listed in ref. 50(c).

**TPE spectrum of perylene vapor *via* supersonic jet spectroscopy; this is described in Chapter III.**

## **CHAPTER III**

### **TWO-PHOTON SPECTROSCOPY IN A SUPERSONIC JET**

## **I. INTRODUCTION**

One of the most powerful methods for investigating the microscopic properties of a compound is molecular spectroscopy. In principle, the more complex the molecular spectrum is, the more information about the molecule it contains. However the spectrum of a molecule can be so complex that analysis is impossible.

The laws of quantum mechanics require that the frequency of an absorbed photon is proportional to the difference in energy between the initial state and the final state of a molecule. If the molecules are found in many different initial energy states, the possible energy transitions can be extremely large. On the other hand, if the number of initial energy states is limited, the number of possible transitions is reduced. The most practical way to limit the number of initial states is to lower the temperature of the molecules. At low temperature, however, molecules tend to condense into the liquid or the solid state, and the interactions of the molecules with one another bring about significant changes in the spectrum. It is also important to study the properties of the individual molecules, free from interaction with their surroundings. Such a study is best carried out in the gas phase. Therefore the problem is to make a gas cold enough to limit the number of initial energy states without allowing the gas to condense and form a liquid or a solid.

In order to study molecules in the gas phase at low temperature, Levy, Wharton and co-workers used a refrigerant technique which cools the molecules very quickly and then thins them out before they can





condense[69, 70]. The refrigerant is an uncollimated, free jet of gas ejected into an evacuated chamber under conditions where the flow is many times faster than a sound wave in that medium; the technique is called *supersonic free jet spectroscopy*; the speed of mass flow is larger than the speed of sound not because the speed of the mass flow is large, but because the local speed of sound (proportional to  $T^{1/2}$ ) is so low. If the flow is collimated with devices downstream from the nozzle, a *supersonic molecular beam* is produced. Therefore the use of a supersonic jet or beam allows the preparation of internally cold, isolated, gas phase molecules and thereby retains the advantages of solid state or matrix isolation spectroscopy without the disadvantage of molecular perturbations.

As a molecular beam source, the supersonic jet was proposed by Kantrowitz and Grey to increase the intensity of the molecular beam in 1951[71]. However, its implementation was prevented by insufficient pump capacity. Then the realization that supersonic expansion may also be useful in spectroscopic applications, due to the partial cooling of rotational and vibrational degrees of freedom, was reported by several workers[72-73]. In 1974, Levy, Wharton and co-workers applied the supersonic jet technique to molecular spectroscopy; they took advantage of the rotational cooling effect of seeded continuous nozzle expansion to dramatically simplify the fluorescence excitation spectra of  $\text{NO}_2$  (seeded in helium)[70].

## II. SUPERSONIC EXPANSION

An effusive beam is one in which the hole diameter ( $D$ ) is smaller than the mean free path ( $\lambda_0$ ) of the molecules in the reservoir; no collisions

between gas molecules downstream of the orifice are present, and the distribution of internal molecular states is identical with that in the reservoir. The velocity distribution is given by the Maxwell-Boltzmann distribution characteristic of the reservoir temperature (Figure 3-1). On the other hand, in a gas that has expanded through a supersonic nozzle, where the hole diameter is larger than the mean free path of the molecules in the vicinity of the hole, there will be many collisions among molecules in the vicinity of the hole area. The expansion converts the enthalpy associated with random motion into direct mass flow and therefore causes the mass flow velocity to increase. Moreover, the effect of a large number of collisions in the orifice vicinity is to make the velocity uniform and cause the cooling. The velocity distribution in the direction of the mass flow is also shown in Figure 3-1. Because of the increase in the velocity, the peak of the distribution shifts and because the gas has cooled, the distribution narrows. In supersonic nozzle expansion the reservoir pressure or the orifice size is increased to the point where  $D \gg \lambda_0$ .

The feature of a supersonic expansion that distinguishes it from ordinary cooling is the fact that the molecules of interest are only in contact with the cold bath for a limited time, and therefore the final state of the system is determined more by kinetics than by thermodynamics. Since the cooling is due to kinetic phenomena, all particles will cool in such a free expansion regardless of their ideality. In fact, the most ideal gas, helium, was found to attain the lowest temperature yet achieved in a free jet expansion, with a translational temperature of 0.006 K[74].

The importance of establishing a supersonic flow condition is that as the gas propagates supersonically, a shock wave due to collisions, with background gas molecules is established around the flow, Figure 3-2. The

**Figure 3-1.** Velocity distribution in an effusive molecular beam(a), and a supersonic beam(b).

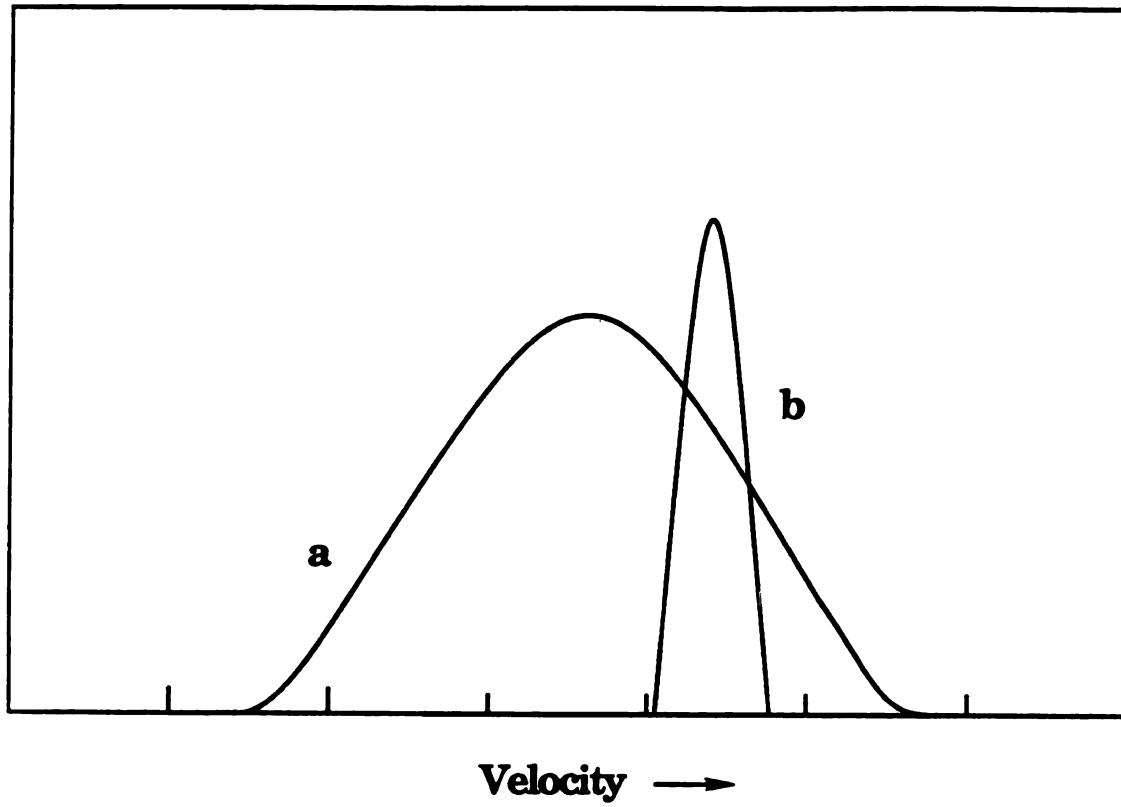
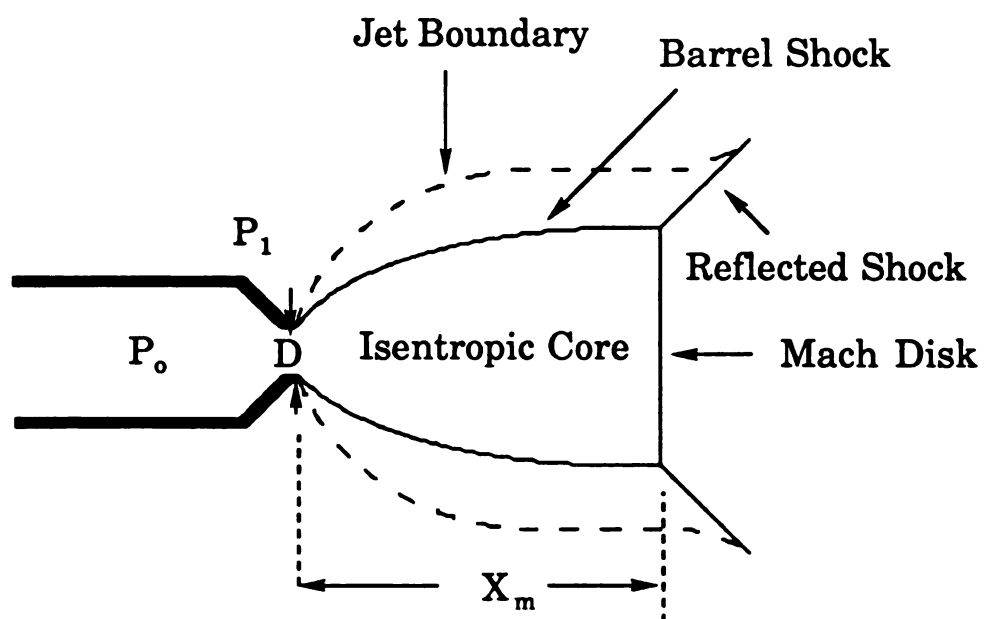


**Figure 3-1.**

**Figure 3-2.** Shock structure surrounding the expanding gas of a free jet. Nozzle pressure is  $P_0$ , the pressure in the expansion chamber is  $P_1$ ,  $D$  is the diameter of the nozzle,  $X_m$  is the distance to the Mach disk from the nozzle. From ref. [131].



$$\frac{X_m}{D} = 0.67 \left( \frac{P_o}{P_1} \right)^{\frac{1}{2}}$$

**Figure 3-2.**

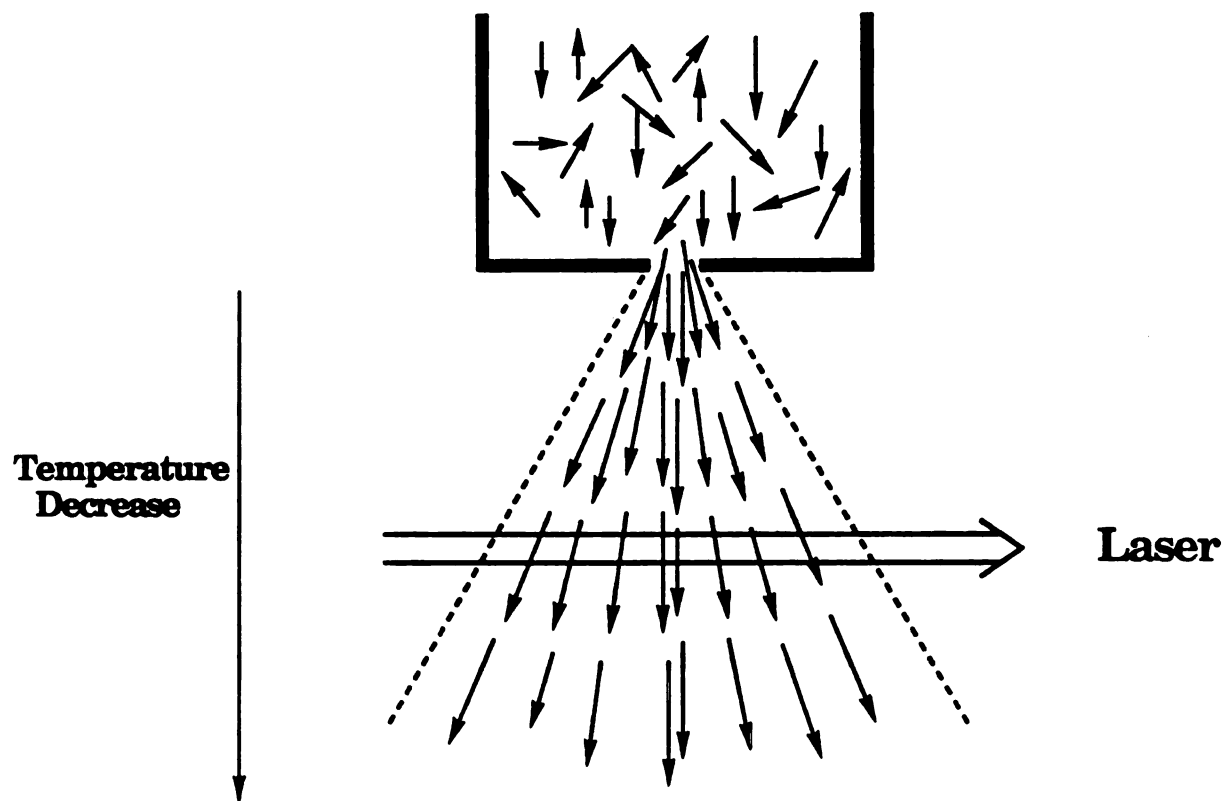
effect of this shock wave is to develop a region around the beam protected from intrusion by warm background gas in the vacuum chamber. Thus one can take full advantage of the cooling effects of the expansion for spectroscopy. The components of the shock wave are referred to as the barrel shock which extends outward from the orifice to the Mach disk, which is a circular shaped area perpendicular to the flow direction.

### A. Translational Cooling

In a supersonic expansion the molecules of interest, either pure or seeded in a carrier gas, are expanded through a small nozzle. As the expansion proceeds, molecules with small perpendicular velocities tend to congregate close to the center line of the jet, while molecules with large perpendicular velocities tend to move far away from the center line (Figure 3-3)[75]. Since the translational temperature is determined by the width of the velocity distribution not by the position of the peak, the narrowing of the velocity distribution which takes place in a supersonic expansion is called translational cooling. Therefore, a cooling of the translational degrees of freedom can be achieved without collisions, and the cold translational bath acts as a refrigerant for the other degrees of freedom; however, the cooling of internal degrees of freedom cannot be obtained without collisions. Through binary collisions, various degrees of freedom (translational, vibrational and rotational) are equilibrated with the cold bath by means of cooling of the perpendicular velocity, which is transferred to the parallel component *via* the collisions.



**Figure 3-3.** The geometric cooling of the translational degrees of freedom in relation to the expansion axis.

**Figure 3-3.**

A supersonic expansion requires a reservoir with gas at a relatively high pressure  $P_0$ , a small orifice of diameter  $D$ , an expansion volume at lower background pressure  $P_1$ , and pumps to maintain the downstream pressure in the presence of the gas discharge through the nozzle. By using the assumptions that the expansion is isentropic (without viscous forces, heat conductivity, shock waves, and heat sources or sinks such as chemical reactions) and that the gas mixture is an ideal gas, the relations are[76]

$$\frac{T}{T_0} = \left(\frac{P}{P_0}\right)^{(\gamma-1)/\gamma} = \left(\frac{\rho}{\rho_0}\right)^{\gamma-1} = \frac{1}{1 + \frac{1}{2}(\gamma-1) M^2} \quad (3-1)$$

where  $T_0$ ,  $P_0$ , and  $\rho_0$  are the temperature, pressure, and density in the reservoir,  $T$ ,  $P$ , and  $\rho$  are the same quantities in the beam and  $\gamma$  is the heat capacity ratio  $C_p/C_v$ . The Mach number,  $M$ , is the ratio of the flow velocity,  $\mu$ , to the local speed of sound,  $a$ , where for an ideal gas the speed of sound is given by  $a = [\gamma(C_p - C_v)T]^{1/2}$ . For a continuous flow, the Mach number is given by[77]

$$M = A \left(\frac{x}{D}\right)^{\gamma-1} \quad (3-2)$$

where  $x$  is the downstream distance,  $D$  is the nozzle diameter, and  $A$  is a constant that depends on  $\gamma$  and is 3.26 for a monatomic gas ( $\gamma = 5/3$ ).

Eqs 3-1 and 3-2 suggest that if one took a spectrum sufficiently far downstream, an arbitrarily low translational temperature could be achieved. However, there are fundamental limitations to the amount of translational cooling attainable. As the expansion proceeds, the density of the gas drops and eventually becomes too low to provide sufficient collisions, and the Mach number and temperature are frozen from this

point on downstream. Anderson and Fenn[78] have predicted that the terminal Mach number,  $M_t$ , is

$$M_t = \epsilon \left( \frac{\lambda}{D} \right)^{(1-\gamma)/\gamma} \quad (3-3)$$

where  $\lambda$  is the mean free path in the nozzle and  $\epsilon$  is a constant which is characteristic of the gas in question. For a monatomic gas the terminal Mach number,  $M_t$ , is a function only of the product ( $P_0 D$ ) and is, using an experimentally determined value of  $\epsilon$  for argon, given by[78]

$$M_t = 133(P_0 D)^{0.4} \quad (3-4)$$

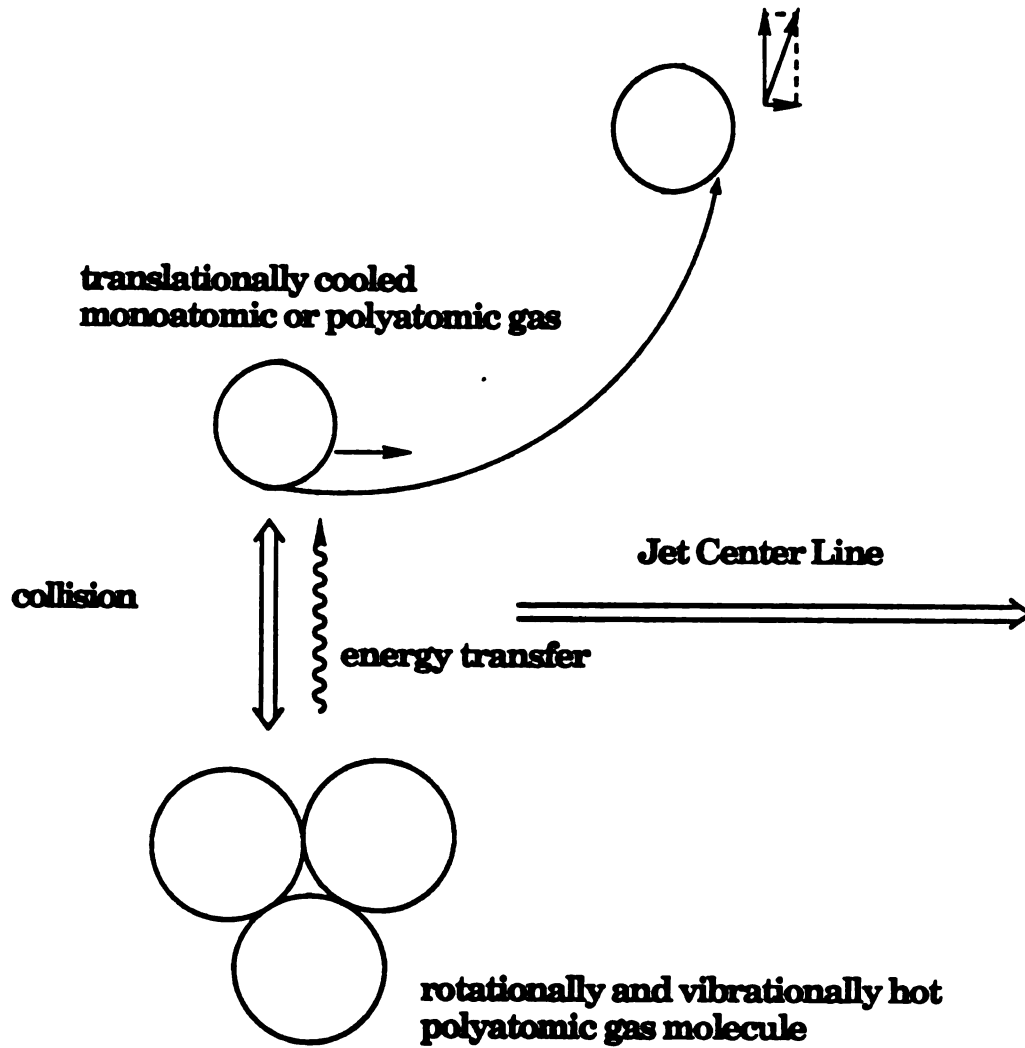
In the case of helium, quantum effects cause the collisional cross-section to increase with decreasing relative energy, and this leads to very much larger terminal Mach numbers than those predicted by eq 3-4[79].

## B. Vibrational and Rotational Cooling

As described above, the primary process in a supersonic jet expansion is the cooling of the translational degrees of freedom. Near the orifice, where the pressure of the gas in the jet is relatively high, the atoms in the jet collide with one another continually. These collisions allow full or partial equilibrium between the transverse velocity components and the other degrees of freedom in the motion of the molecules (Figure 3-4).

As long as the molecules collide at low velocity with the cold atoms, the energy of rotational and vibrational motion of the molecules is

**Figure 3-4.** Vibrational and rotational cooling *via* collisions in a jet.

**Figure 3-4.**

transferred to the translational cold bath. As the gas flows downstream from the nozzle, the density of the gas drops and eventually becomes too low to provide the collisions necessary to connect the internal degrees of freedom (vibrational and rotational) with the translational cold bath. Thus, cooling of the molecules caused by the exchange of energy in collisions is a self-limiting process, and the degrees of freedom which equilibrate with the translational bath are the coldest at the point where the expansion runs out of collisions.

The actual state of the beam depends on the rate at which the internal degrees of freedom come into equilibrium with the cold translational bath. The cooling attained in the expansion for any particular degree of freedom depends on the collisional cross-section for relaxation for that degree of freedom. For the rotational degrees of freedom this cross-section is roughly equal to gas kinetic cross-section. In general, the rate of equilibrium between translations and rotations is relatively fast, and therefore extensive rotational cooling takes place before the molecules enter the collision-free region. The vibrational degrees of freedom have collisional relaxation cross-sections considerably smaller than those of gas kinetics. Thus vibrational excitation is more difficult to cool in a free jet expansion, and usually cooling occurs to a temperature below the original temperature but above the final translational temperature. However, the vibrations having the smallest cross-sections have a high vibrational frequency and therefore have a small Boltzmann population in the excited states.

In order to further cool a molecular gas of interest, a small amount of this gas is mixed with a large quantity of a monatomic carrier gas, which cannot store energy in internal degrees of freedom. Although the

lowest translational temperature from a pure expansion has been attained with helium, it does not always produce the most efficient cooling of seed molecules. For seeded beams with large differences in size and weight between the seed (sample) and carrier molecules (e.g.  $m_{\text{heavy}}/m_{\text{light}} > \sim 50$ ), there is a velocity slip effect[80-83]. For large, heavy, rigid molecules Amirav *et al.*[82] found that cooling varied in the order Xe > Kr > Ar > Ne > He. However, the frequency of three-body collisions, which lead to condensation, depends on the mass and interatomic potentials of the atoms, and lighter species have been found to create lower terminal temperature because of the reduced rate of condensation[84].

### C. Condensation and Complex Formation

The main advantage of the supersonic jet as a refrigerant is that the molecular motions can be cooled for spectroscopic purposes before the molecules condense. An important factor controlling the cooling in a supersonic expansion is the possibility of condensation. Compared to translational cooling, condensation is slow because its initiation requires simultaneous collisions among three or more particles. Unlike cooling, which requires only that energy be exchanged between two colliding particles, condensation requires that at least two particles are bound together. To form a bond, a third particle must collide with the first two particles during the time of the two-body collision so that the third particle can carry off the binding energy of the pair as translational energy. Three-body collisions (roughly proportional to  $P_0^2 D$  [85]) require much higher density in the gas than two-body collisions, and normally the cooling is



complete before a significant number of three-body collisions can take place. Nevertheless, three-body collisions do occur; the heat of formation of these complexes is liberated into the translational degrees of freedom of the expanding gas, and this limits the cooling that is ultimately attained. One explanation for the fact that helium attains lower energy in a free expansion than any other gas might be that the ground state potential of the  $\text{He}_2$  molecule is thought to be too weakly attractive to support a bound state[86]. Therefore, condensation must initiate with the far more unlikely occurrence of four-body collisions in the expansion to form  $\text{He}_3$ [87].

The practical limit of the cooling in a supersonic expansion is the requirement of adequate pumping capacity to handle the gas discharge through the nozzle. Since the amount of complex formed in the expansion is proportional to  $P_0^2 D$ , the cooling attained in the expansion is proportional to  $P_0 D$ , and the total mass throughput from the nozzle is proportional to  $P_0 D^2$ , in order to increase the cooling attained in the expansion by a factor of  $\Delta$  while ratio  $P_0/D$  is adjusted to keep a constant value of  $P_0^2 D$  (the amount of complexes formed constant) the throughput would have to be increased by a factor of  $(\Delta)^3$ [120].

To overcome the pumping limitation, *pulsed nozzles* and *moderate background pressure augmentation* ( $P_1 \sim 10^{-2}$  to 1 Torr; Campargue-type) have been used. In the first method, the gas flows only a small fraction of time, so the use of a pulsed nozzle increases the effective pumping speed in a small apparatus. The effective pumping speed of the system will be the true speed of the pumping system multiplied by the inverse of the pulsed nozzle duty cycle. The second method was developed by Campargue[88-90]. The main idea is that the chamber pressure is increased at a constant  $P_0/P_1$  ratio, instead of decreasing the chamber pressure; pumps of a fixed

volumetric pumping speed have a mass throughput that increases linearly with pressure. At higher background pressures, the developing free jet is encased in a shock-wave structure. The shock wave extends from the nozzle tip to the Mach disk, and it is thick and dense enough to prevent penetration of the core of the jet by warm background gas. By increasing the pressure in the nozzle  $P_0$ , it is possible to reach a mode of operation where the expanding gas in the region upstream of the shock structure is unaffected by the background gas and is equivalent to the same region of a free jet expanding into an infinite vacuum. This is true even though the increase in the nozzle pressure has brought about a corresponding increase in the pressure in the expansion chamber. In contrast to the Campargue-type expansion, the Fenn-type[91, 92] expansion utilizes a low background pressure ( $10^{-3}$  to  $10^{-6}$  Torr). Due to the decrease of the collision frequency in a jet of relatively low density, the expansion becomes frozen at a distance from the nozzle much smaller than the distance  $X_m$ , at which the Mach disk of a free jet shock wave structure would be formed. Nevertheless, downstream distances where significant molecular cooling has occurred are accessible to interrogation by focussed, transverse laser beams. All the measurements described in this dissertation were taken under low background pressure ( $P_1 < 10^{-3}$  Torr) conditions.

### III. SPECTROSCOPY IN SUPERSONIC JETS

Supersonic jet spectroscopy has been applied to the study of a various molecules, from diatomics to large organic molecules such as porphyrins[93]. Although detection methods and the molecule sizes vary

somewhat, laser spectroscopic studies in supersonic jets fall into four categories: 1) Studies of molecular spectra to provide information about the molecule itself[94-98]; 2) Studies of the physical phenomena of supersonic expansion[99-104]; 3) Dynamic studies of intramolecular dynamics and radiationless processes[105-112]; and 4) Investigations of formation and structure of molecular complexes, such as van der Waals and hydrogen-bonded complexes[114-119].

The first two categories, 1 and 2, are generally applied to small-size or medium-size molecules, for which we can obtain resolved rotational structure in the electronic spectrum; two-photon spectroscopy of perylene is in this first category. Taking advantage of the collision-free conditions and low temperatures, categories 3 and 4 represent more recent, and very promising applications of supersonic jet spectroscopy. Subjects of such experiments include energy flow from one particular state to another, preparation of an intense beam of highly reactive and unusual free radicals, and formation of highly selective photofragments. Also, if the molecules of interest are cooled sufficiently, then van der Waals complexes may form which are too weak to form stable bonds under ordinary laboratory conditions. In this dissertation studies in the latter two categories will not be reviewed.

### **A. The Number of Excited Molecules**

When a molecule is mixed with monatomic gas at a number density ratio  $c$ , and expanded from a supersonic nozzle of diameter  $D$  at a pressure

$P_0$  and a temperature  $T_0$  the number density of the molecule in the nozzle is

$$\rho_0 = \frac{P_0}{k T_0} \quad (3-5)$$

where  $k$  is Boltzmann's constant. As the gas expands into the vacuum chamber, the density falls as[77]

$$\rho \propto \rho_0 \left(\frac{D}{x}\right)^2, \quad (3-6)$$

where  $x$  is the distance downstream from the nozzle. If a laser beam crosses the molecular beam at a distance  $x$  downstream of the nozzle, a column of excited molecules will be produced in the molecular beam. The column length  $L$  is given by[120]

$$L \propto x \quad (3-7)$$

If the laser pulse duration is much shorter than the time required for a molecule in the supersonic beam to pass across the laser beam then, neglecting saturation effects, each laser will produce a total of  $N_e$  excited molecules[120],

$$N_e = L \rho E \sigma \quad (3-8)$$

where  $\rho$  is the number density of the absorbing molecule,  $E$  is the number of laser photons per pulse,  $\sigma$  is the absorption cross section of the molecules for these photons, and all possible decay routes out of the excited state have been neglected. Thus,

$$N_e \propto \frac{1}{x}; \quad (3-9)$$

$N_e$  depends only on the inverse power of the distance from the nozzle even though the jet density falls as  $x^{-2}$ . Usually  $N_e$  is sufficiently large, even for moderate laser powers, for spectroscopic measurements to be made. Therefore there are no advantages obtained by decreasing the laser beam size, and in fact this can only increase the possibility of saturation. For long pulses or continuous lasers, however, if the laser beam is focussed at the interaction region with the molecular beam then the time dependence and coherence of the excitation can be reduced.

## B. Detection

Although a jet-cooled molecule is collision-free and in a well defined state, the concentration of molecules is so low that normal spectroscopic methods such as direct absorption spectroscopy are difficult to apply. As an indirect method, *molecular fluorescence* (total undispersed and dispersed fluorescence) has been the principal method for detecting the formation of excited states and for characterizing the structure and time evolution of those states in supersonic jets. In laser fluorescence excitation spectroscopy, which was applied for all measurements described in this chapter, the wavelength of the exciting light is tuned and the total undispersed fluorescence is collected. In dispersed fluorescence spectroscopy, the intensity of the emission is recorded as a function of the wavelength of the emitted light. In contrast to the fluorescence spectrum of

molecules in a matrix, that of an isolated molecule can be strongly dependent on the particular excited state that is originally populated when the laser light is absorbed.

However, even with carefully designed detection systems only ~5 % of the fluorescence can be collected, and to obtain this value a detector with excellent quantum efficiency is required. For molecules which do not fluoresce with good quantum yields within a sufficiently short time to be detected (with a space-fixed detector), such that the excited molecule passes out of the field of view, other detection methods must be used. Basic requirements for laser induced fluorescence (LIF) analysis of large molecules are considered to be an emission quantum yield exceeding  $10^{-3}$ , and a volatility such that a vapor pressure  $> 10^{-5}$  Torr ( $10^{-7}$  Torr for a slit nozzle) can be attained[121].

One approach to avoiding these limitations is *multiphoton ionization(MPI)*. In the simplest case MPI is an n-photon absorption process leading to ionization and obeys the condition

$$nE_{ph} > IP \quad (3-10)$$

where  $E_{ph}$  is the photon energy and IP is the molecular ionization potential. The signal is provided by ions generated by multiphoton ionization of a molecule, and ions are detected as the final product in a mass spectrometer. Thus the ionization cross section reflects the absorption-excitation spectrum of the intermediate states. However, such a process is entirely nonselective; any sample which can satisfy eq 3-10 will be ionized. When one of the absorption processes terminates in a real excited state of the molecule, the ion signal intensity of that molecule can be greatly

enhanced (see eq 1-20), and through the use of a time-of-flight mass spectrometer (TOFMS, in which ions starting at different points will reach the detector at different times) in conjunction with the jet this problem can be solved[121].

*Direct absorption* can be utilized as a detection method for molecules in supersonically cooled samples, although the sensitivity is low[122-124]. Under normal expansion conditions, the concentration of molecules in a jet is extremely low ( $< 10^{15}$  molecules within the laser/jet intersection) and the optical pathlength of the jet available for the absorption measurement is generally too short to make the method viable. To improve the number density of molecules, Jortner and co-workers[122] developed the planar supersonic expansion technique, in which a pulsed slit nozzle (90 mm length, 0.27 mm width) is employed. The jet emanating from the slit, produced by the supersonic expansion, provided sufficient optical pathlength for absorption measurements in jets, and increased the sensitivity by up to two orders of magnitude.

Recently, highly excited electronic states of molecules have been extensively studied by the use of *double resonance excitation*. A jet-cooled molecule is excited to an allowed excited state by the absorption of one photon of laser frequency  $\nu_1$ , then the excited state is further promoted to a higher state by the absorption of another photon of frequency  $\nu_2$ . Various methods for the detection of highly excited states by double resonance excitation are shown in Figure 3-5. The principles, advantages, and disadvantages of these double resonance spectroscopies are described well in reference [125].

**Figure 3-5.** Various two-beam double resonance spectroscopies: (a) two-color multiphoton ionization spectroscopy, (b) two-color MPI assisted by autoionization, (c) two-color MPI assisted by collision, (d) two-color fluorescence dip spectroscopy, (e) two-color ionization dip spectroscopy, (f) stimulated emission pumping, (g) stimulated emission spectroscopy utilizing the ion dip technique, and (h) population labeling spectroscopy. Here X is the ground electronic state, A and R are resonant excited electronic states, and I marks the onset of the ionization continuum. From ref. [125].



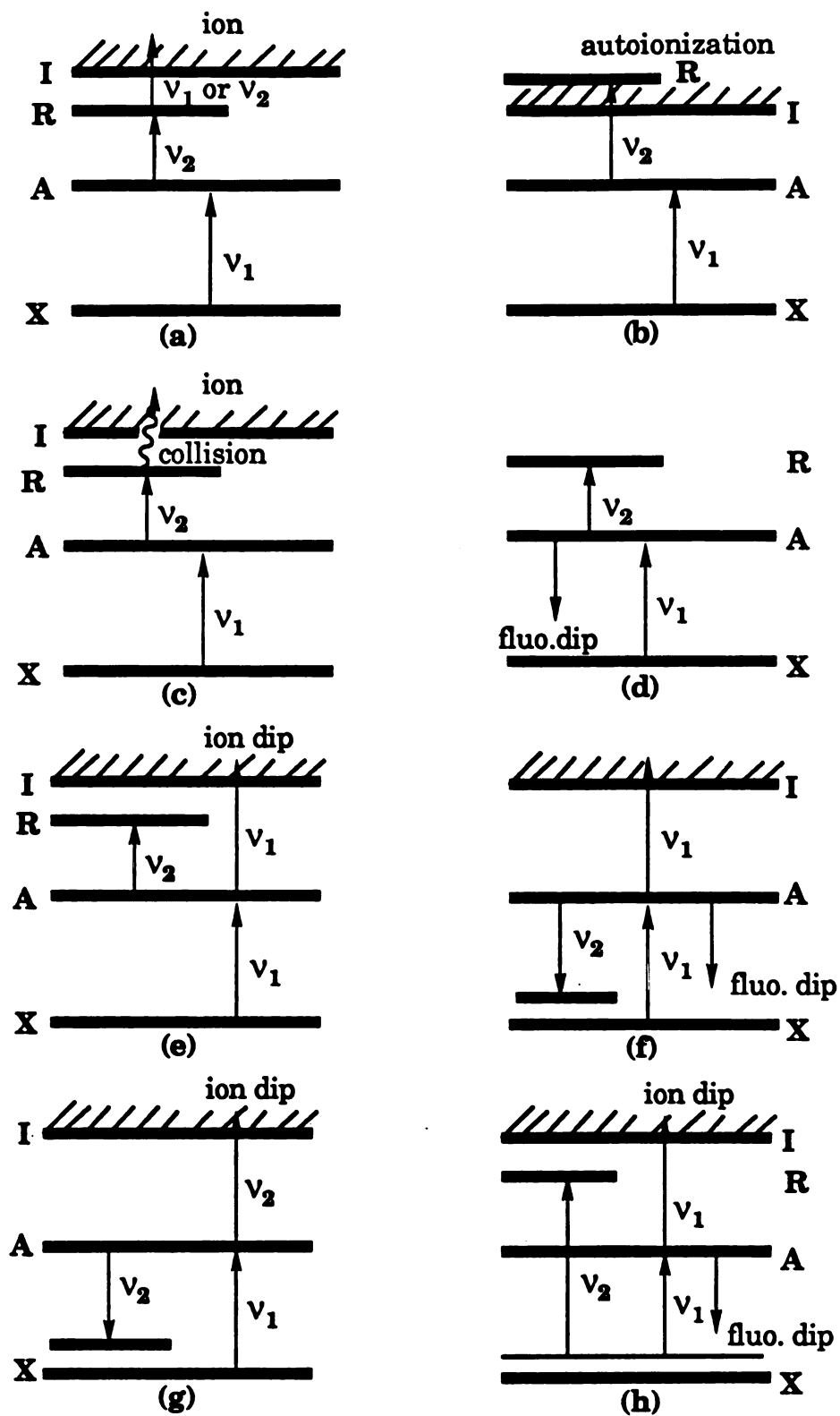


Figure 3-5.

#### IV. LIMITATIONS OF SUPERSONIC JET SPECTROSCOPY

##### A. Vaporization

The jet technique requires the vaporization of the molecule, yet many molecules of interest have very low volatility. Such molecules are often thermally labile and cannot be vaporized by the simple expedient of increased heating. Several techniques have been developed to achieve the vaporization of large molecules, such as laser desorption[121] and supercritical fluids[126, 127].

*Laser desorption* involves the use of a pulsed laser to induce rapid heating effects such that the molecules desorb from a surface before they have time to decompose. In the laser desorption process, both ions and neutrals are formed, in a ratio that depends on the surface temperature induced by the laser. Thus the power density of the laser at the surface is the most critical parameter in desorption efficiency, and the desorption process is not strongly wavelength dependent. The limitation of laser desorption is the formation of ions. However, often desorption conditions can be arranged so that primarily neutral molecules are desorbed and then entrained in a supersonic flow. A native chlorophyll with relative molecular mass of 892 was obtained by Grotemeyer et al.[128], and adenine and cytosine were studied by Tembreull and Lubman by laser desorption-jet expansion-MPI[121]. Figure 3-6 shows a schematic representation of the experimental set-up for the laser desorption-jet expansion-TOFMPI apparatus.

Another method of introducing low volatility, thermally labile species into jets involves *supercritical fluids*, where organic solvents are used as

**Figure 3-6.** The experimental set-up of a time of flight mass spectrometer coupled with apparatus for laser desorption into a supersonic jet followed by laser MPI. Here GV is a gate valve, and  $\text{LN}_2$  is a liquid nitrogen trap. From ref. [121].

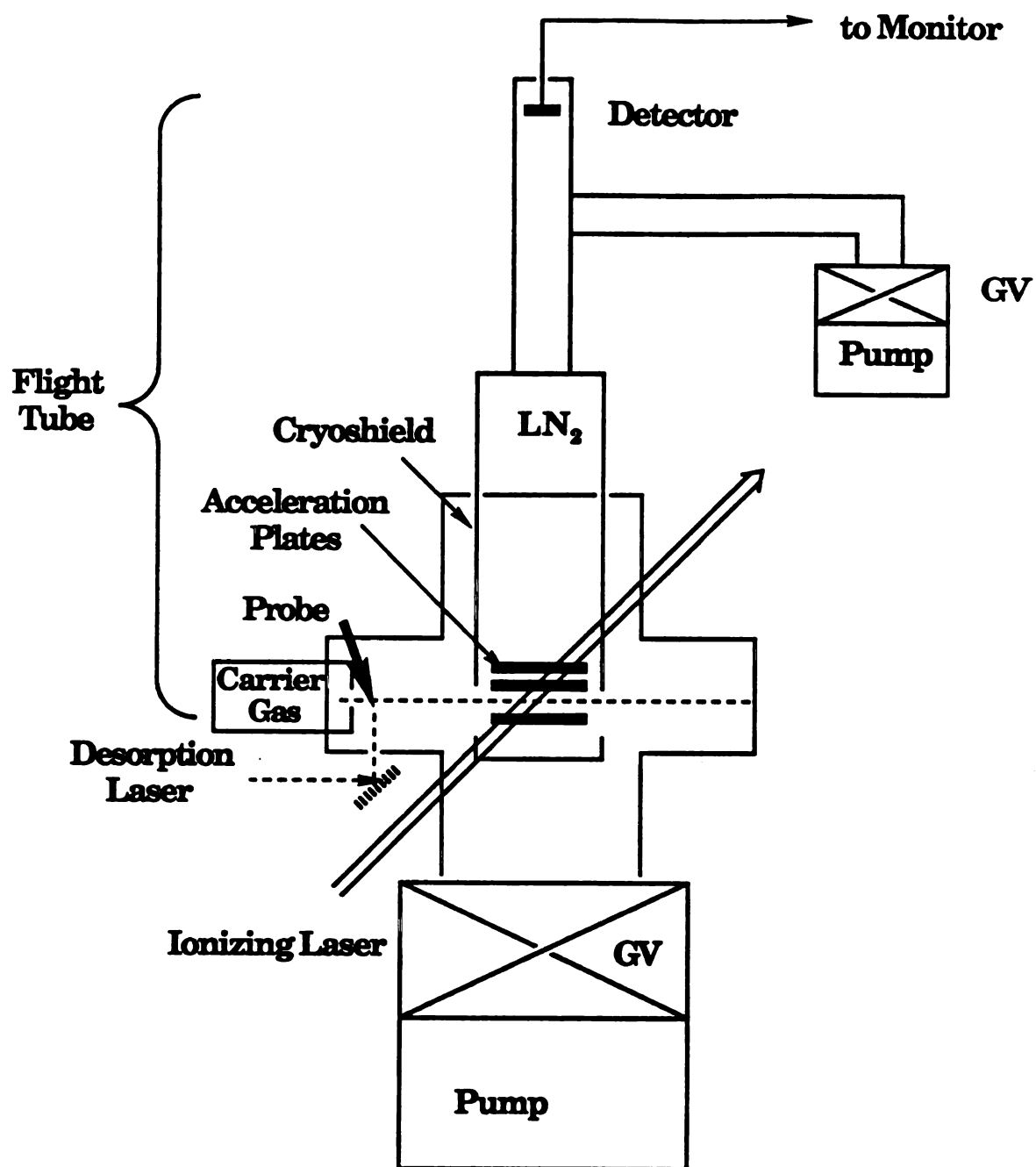


Figure 3-6.

carriers. The solubility of large molecular weight organic species is considerably higher in such a fluid than in a rare gas. Additionally, in the expansion process the supercritical fluid carrier will itself rapidly vaporize as the pressure drops from high pressure ( $\sim 100$  atm) to low pressure ( $< 1$  atm). However the cooling in a supercritical fluids is considerably less than that in rare gases, and it is difficult to remove solvent molecules from the sample cluster. Polyatomic molecules have internal degrees of freedom which need to be cooled, and the high pressure differential required for the expansion to obtain the lowest translational temperatures is not within the experimentally convenient range.

## B. Sensitivity

Although the supersonic expansion places the molecule to be studied in a collision-free environment and in well defined rotational and vibrational states (even for large molecules), the number density of the molecules is very low, which limits jet spectroscopy. Detection limits in the 10-100 ng range for naphthalene ( $10^{13} - 10^{14}$  molecules,  $f = \sim 10^{-4}$ ,  $\phi_f \sim 0.2$ ) were demonstrated by Hayes and Small[129], who used a continuous jet. Perylene ( $f = 0.332$ ), with its near-unity quantum yield  $\phi_f$ , lies in the high-sensitivity end of the above range. Pepich *et al.*[130] coupled a pulsed expansion to GC and laser induced fluorescence detection, and molecules with fluorescence quantum yields similar to the molecules studied by Hays and Small could be detected in the picogram range.

## V. EXPERIMENTAL

Figures 3-7 and 3-8 are schematic block diagrams of the instrument used for our experiment. The experimental components used to observe the signal from molecules expanded in a supersonic jet can be separated into three main parts: the apparatus for generating the jet, the laser system for exciting the gas molecules in the jet, and the detector system utilized to obtain the signal from the excited molecules. (In our experiments, fluorescence from the laser-irradiated molecules was detected.)

### A. Jet Generating System

The jet generating system consists of a sample compartment and a vacuum pumping system. The sample compartment is composed of a sample cell, a heating device, and a nozzle (Figure 3-9). The carrier gas (argon) at pressure  $P_0$  (0.5 – 2 atm) is passed through a quartz sample tube, C, packed with solid sample  $S_1$  (iodine, perylene, or [2,2]paracyclophane), and the resultant gas mixture is expanded into the vacuum chamber through a supersonic continuous nozzle,  $N_1$ . To prevent dispersion of the unvaporized solid sample into the vacuum chamber, the sample is packed with glass wool. To produce the jets, perylene (Aldrich, m.p. 277 – 279 °C) and [2,2]paracyclophane (Aldrich, m.p. 285 – 288 °C) were heated to 220 °C (60 V variac setting) and 150 °C (50 V variac setting), respectively. The temperature is monitored by an iron-constantan thermocouple (Omega J type, TC in Figure 3-8, with an upper temperature limit of 600 °C) attached to the surface of the heating tape. The continuous nozzle  $N_1$  is placed

**Figure 3-7.** Schematic block diagram of the supersonic jet experiment.  
Here B are baffles, T is a telescope, and BD the beam dump.

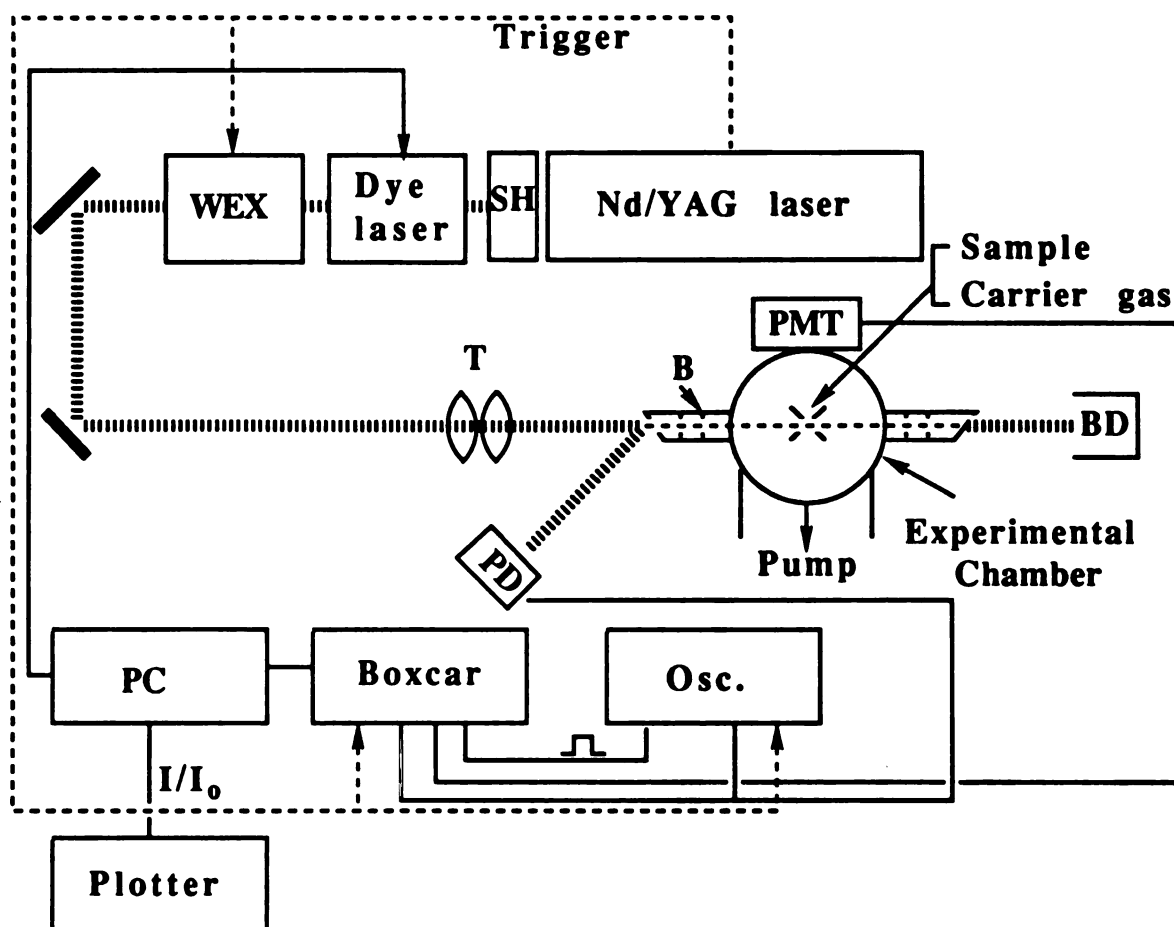


Figure 3-7.



**Figure 3-8. Schematic diagram of the chamber employed for supersonic expansion experiments.**

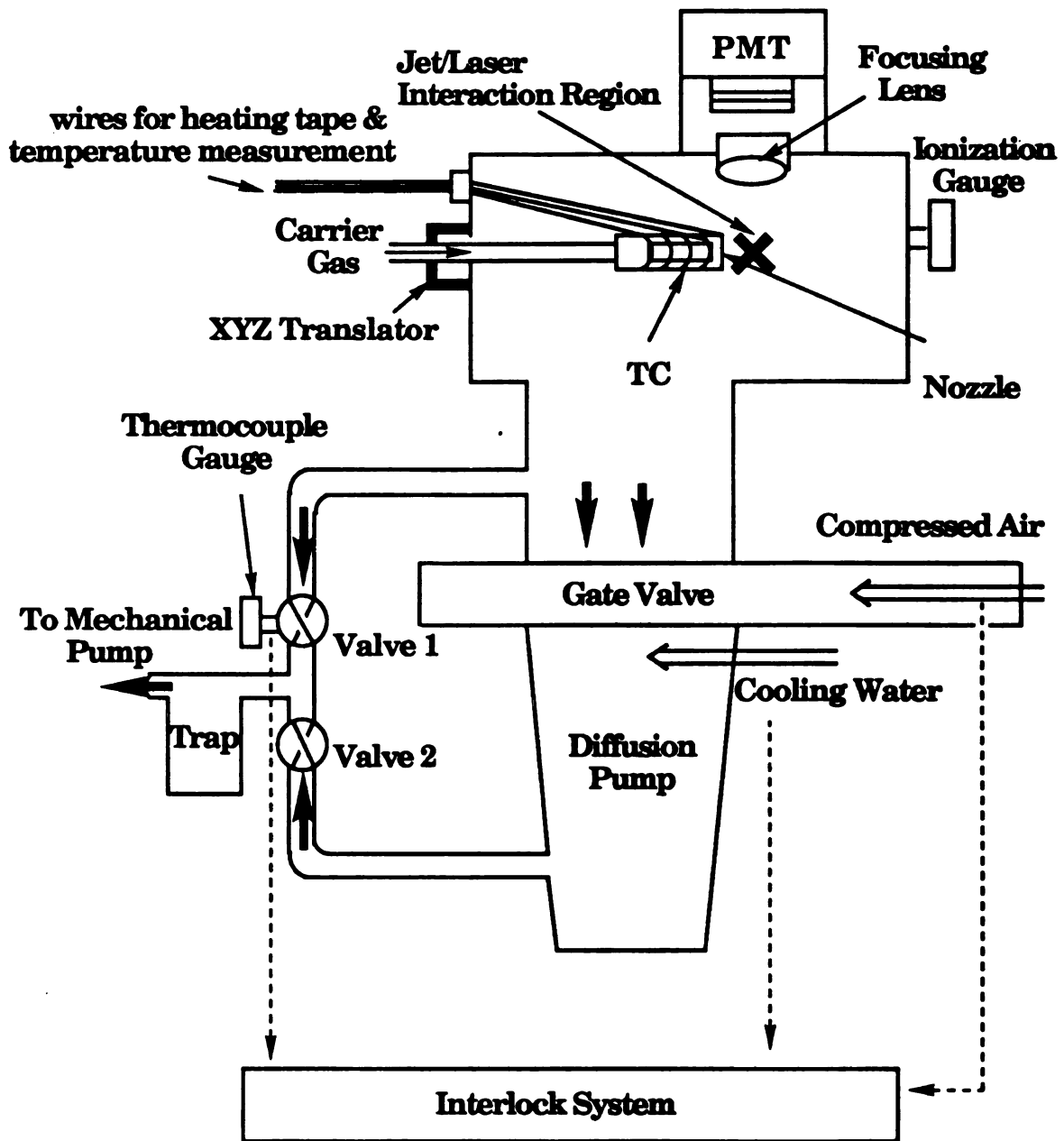
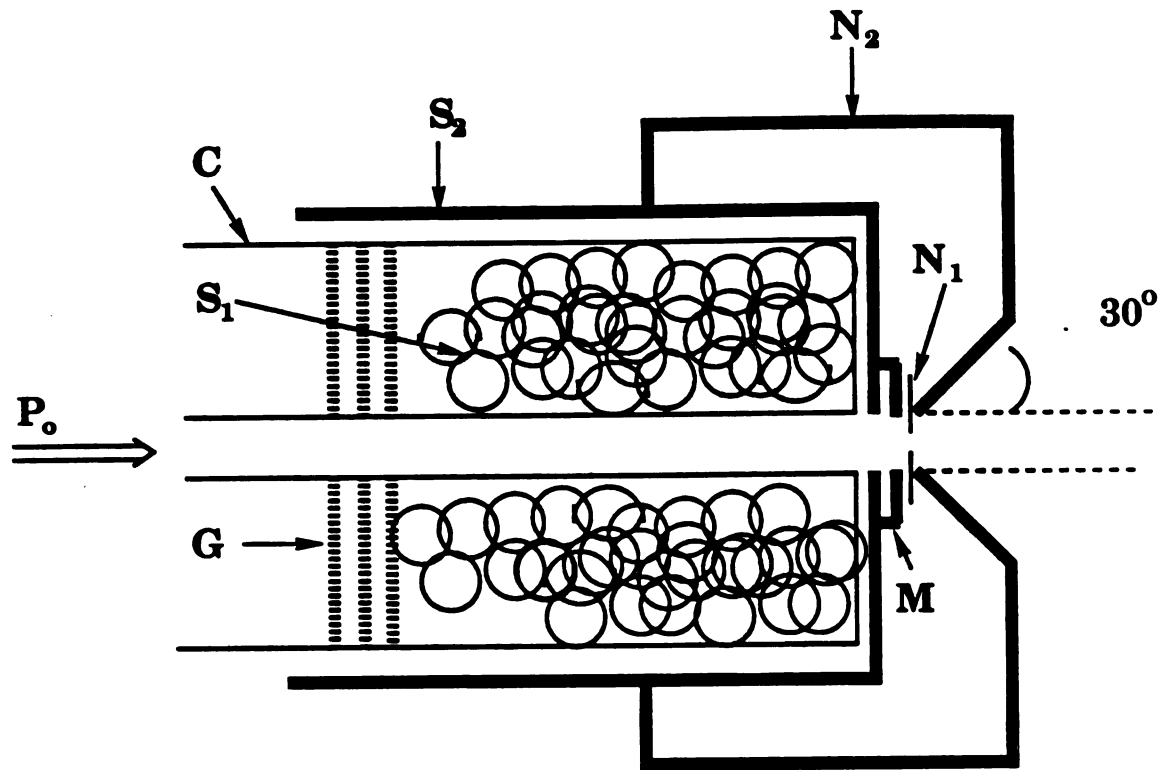


Figure 3-8.

**Figure 3-9.** A side-view cross section of the sample compartment. C is the sample chamber,  $S_1$  the sample,  $S_2$  the sample cell holder,  $N_1$  the continuous nozzle (comprised of an interchangeable pinhole orifice),  $N_2$  the nozzle holder, G is glass wool, and M a magnet.

**Figure 3-9.**

between the nozzle holder and sample cell holder. The nozzle holder,  $N_2$ , shown in Figure 3-9 is made from stainless steel with a round-shaped end plate having an  $\sim 3$  mm diameter hole and a  $30^\circ$  conical tip. The holder threads onto sample cell holder  $S_2$ , which is made from a length of stainless steel tubing, also having an approximately 3 mm diameter hole. A magnet  $M$ , which holds the nozzle  $N_1$  in place, is mounted on the exterior of the sample holder. Various diameter nozzles (15-1000  $\mu\text{m}$ ) purchased from Ealing are used for different experiments. All the measurements described in this Chapter were made with a continuous nozzle. The XYZ translator shown in Figure 3-8 is used for smooth translation of the nozzle in all directions to permit the supersonic jet to be centered, and to control the distance from the nozzle to the laser intersection point while the experiment is in progress.

The expansion chamber is evacuated by Varian VHS 10" oil diffusion pump with pumping speed 5300 l/s for air, backed by a 500 l/min mechanical pump (Varian Hi-vac-45). In our experiments typical background (chamber) pressures of  $< 10^{-4}$  Torr are attained with the jet running (without jet :  $\sim 2 \times 10^{-5}$  Torr). The pumping system is protected by an interlock system which monitors the flow rate of cooling water (set at 1.5 l/min.), the foreline pressure (set at 600 mTorr), and the air pressure on the gate valve (set at 75-120 lb). If the preset conditions are not maintained, an electropneumatic gate valve automatically seals the vacuum chamber and disconnects the power to the diffusion pump. The interlock control circuit was designed and implemented by Marty Rabb, the MSU Chemistry Department's Electronic Designer.

## B. Excitation Source

A Nd:YAG-pumped dye laser was used as the excitation light source for fluorescence excitation spectra of jet-cooled perylene and iodine. For [2,2]paracyclophane, the output from the dye laser was frequency doubled by a doubling crystal (Spectra Physics WEX). The dyes R590, S420, and DCM were used for iodine and two-photon excitation of perylene, for one-photon excitation of perylene, and for [2,2]paracyclophane, respectively; all dyes were purchased from Exciton. The procedure used to scan the dye laser wavelength is described in Chapter II. At the same time that the wavelength of the dye laser is stepped the Q-switch output from the Nd:YAG laser triggers the WEX to rotate the doubling crystal. The scan rate of the PDL must not exceed 0.05 nm/s. However, if the scan rate is slow, e.g. a PDL scan rate less than 0.1 nm/min, then the system loses its feedback lock, which will result in the detuning of the crystal due to ambient temperature change.

To minimize the extent of laser light scattering into the fluorescence detection system, the output from the dye laser or WEX is focussed into the vacuum chamber with a telescope; the laser beam has  $\sim 1$  mm diameter as it intersects the supersonic jet. Also the laser beam is baffled within the entrance and exit arms, each of which carries a quartz window set at Brewster's angle at its extremity. The purpose of the baffles (B in Figure 3-7) is to reduce scattered laser light. The baffle apertures define the laser beam which intersects the sample beam; uncollimated laser light reflects from the baffles rather than hitting the nozzle and being scattered. The Brewster angle windows help reduce reflected laser light from the exit and the entrance windows, and also remove any unpolarized portion of the laser

beam since only parallel polarized laser beams would be transmitted by windows set at this angle.

### C. Detection

The undispersed total fluorescence from the sample was collected for all measurements reported here. Figure 3-10 shows the detection system used to collect and detect the fluorescence from the laser-illuminated free jet. Lens L ( $d = 5$  cm,  $f_l = 5$  cm, glass) collected the fluorescence from the sample and focused it onto the photocathode of an electronically cooled Hamamatsu R562 photomultiplier tube. The PMT is mounted in a magnetically and electronically shielded Pacific Instrument housing, and was normally cooled to  $-20$  °C. The distance between the collecting lens and the crossed beams can be adjusted (from 45 to 75 mm) from inside the vacuum chamber. Since the largest source of noise was from scattered laser light, various filters were placed in front of the PMT. A slit in front of the PMT was used to transmit the fluorescence and to block the light scattered from other parts of the vacuum chamber. (To more effectively reject light scattered from other parts of the apparatus and fluorescence from molecules not in the cold portion of the molecular beam, an imaging optical system can be used[131].) In order to normalize the fluorescence signal to the exciting laser intensity, the laser beam reflected from the Brewster angle entrance window was collected by a photodiode, PD. [See Figure 3-7.] The remainder of the data processing procedure was the same as that utilized in the two-photon excitation fluorescence measurement of

**Figure 3-10. Schematic diagram of the detection system. W represents a glass window.**



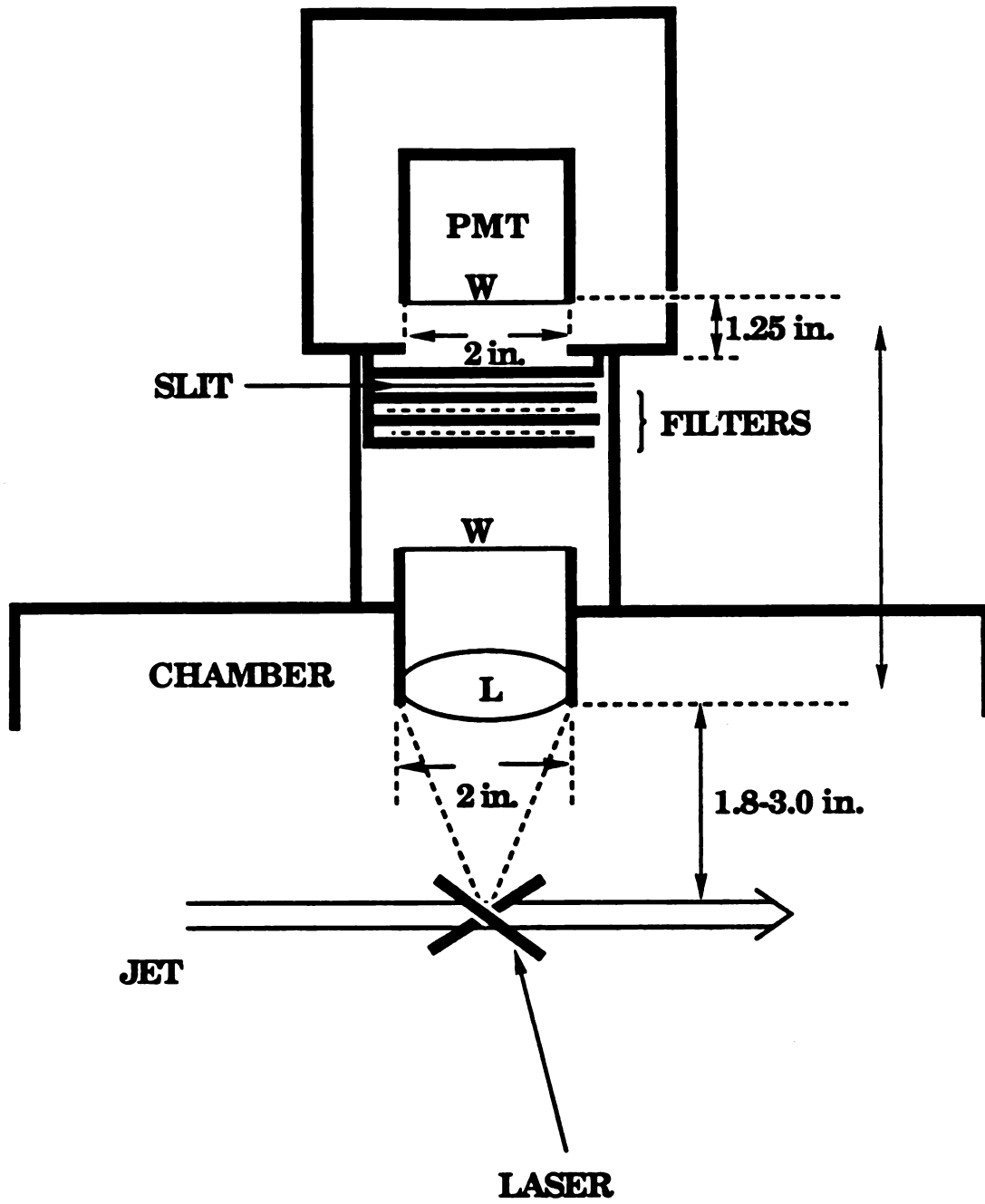


Figure 3-10.

perylene described in Chapter II, except that the signal was normalized to the laser intensity  $I_0$  for one-photon excitation, instead of to  $I_0^2$ .

A typical experimental procedure can be described as follows: 1) The laser beam is aligned at the center line of a nozzle. 2) The vacuum chamber is sealed and the mechanical pump starts to evacuate the chamber. Only valve 1 in Figure 3-8 is opened. 3) When the pressure in the chamber reaches  $< 50$  mTorr, valve 1 is closed and valve 2 is opened to evacuate the diffusion pump. 4) After the pressure inside the diffusion pump falls below 50 mTorr, the cooling water of the diffusion pump is circulated and the air pressure of the gate valve is set between 75 - 120 lb (above 125 lb the piston of the gate valve can be damaged). 5) The diffusion pump is turned on and the gate valve is then opened. If preset conditions of the interlock are not maintained, the diffusion pump power will not be connected. 6) When the pressure in the vacuum chamber is  $< 10^{-5}$  Torr and stabilized, the jet is generated. 7) The laser wavelength is set at a known peak position of the sample and the carrier gas pressure is changed until a signal from the laser-irradiated molecules is detected with the PMT. 8) The conditions of the jet and the detection system are optimized; to prevent hitting the nozzle surface with the exciting laser beam, all the measurements are started at the minimum value of the distance between the nozzle and the laser/jet intersection region, and the distance is increased.

## VI. RESULTS AND DISCUSSION

To utilize the home-built supersonic jet (for which plans were drawn by Tun-Li Shen of Prof. Leroi's group), we tested and characterized the jet

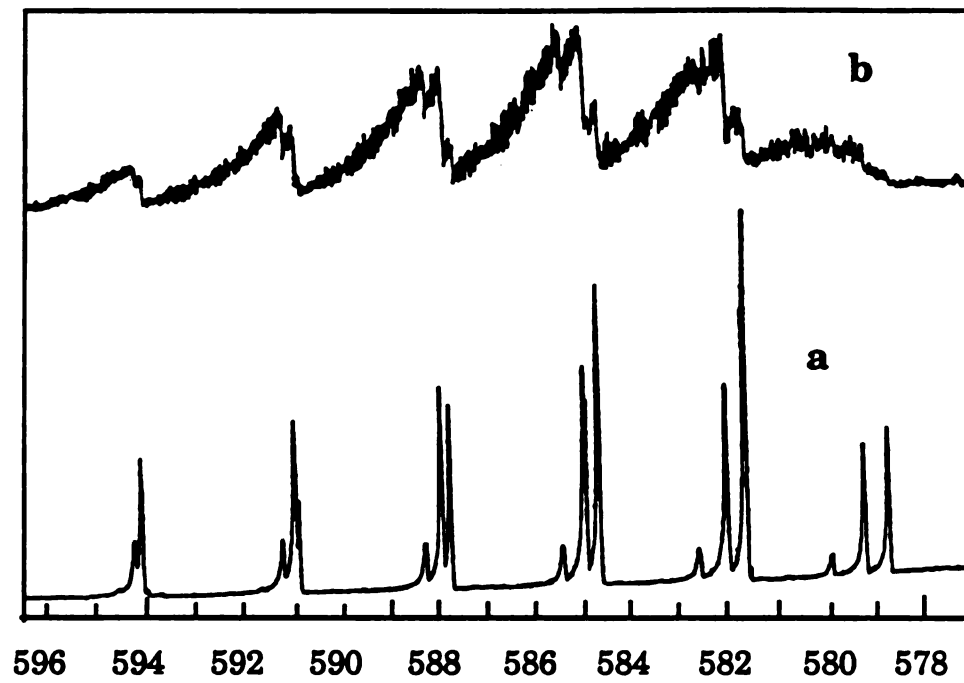
system with one-photon spectra of iodine, perylene and [2,2]paracyclophane. Since the translational, and to a slightly lesser extent the vibrational and rotational, cooling depends mainly on the reservoir pressure and diameter of the nozzle, and on the distance from the nozzle to the laser intersection, these parameters in particular were examined. Also, two-photon excitation of perylene with a single laser was attempted. Measurements reported in Chapter III monitored undispersed fluorescence as the signal; all spectra are plotted as the normalized total fluorescence *vs.* the incident dye laser wavelength.

## A. Pressure Effect

### 1. Chamber Pressure

Figure 3-11 shows a portion of the fluorescence excitation spectrum of a supersonic jet containing molecular iodine (sample tube held at room temperature, vapor pressure  $\sim 0.2$  Torr) over the 578 – 596 nm excitation range ( $X^1\Sigma \rightarrow B^3\Pi$ ). In scan (a) the Ar carrier gas pressure is 0.5 atm, the nozzle diameter is 100  $\mu\text{m}$  ( $X/D = 100$ ) and chamber pressure is  $2 \times 10^{-4}$  Torr. The upper portion of this figure, scan (b), shows the LIF (laser induced fluorescence) spectrum over the same spectral range at a chamber pressure of  $2 \times 10^{-1}$  Torr. The translational temperature obtained from eq 3-1 was 1.4 K. From spectrum (a) we can deduce that the rotational temperature is nearly equilibrated with the translational temperature. From the relative Frank-Condon factors reported in the literature[132] the vibrational temperature is calculated to be about  $\sim 150$  K. When the

**Figure 3-11.** The laser induced fluorescence spectra of jet-cooled iodine molecules at different chamber background pressures. (a)  $P_1 = 2 \times 10^{-4}$  Torr, (b)  $P_1 = 2 \times 10^{-1}$  Torr.



**Wavelength (nm)**

**Figure 3-11.**

chamber pressure is increased to 200 mTorr (mechanical pump only) under otherwise the same conditions, the spectrum becomes congested and the unresolved vibrational and rotational structure reproduced in (b) is measured.

## 2. Carrier Gas Pressure

The effect of the carrier gas pressure was measured with perylene over the dye laser spectral range 417 – 413 nm. The laser induced fluorescence excitation spectra of perylene at different argon carrier pressures ( $P = 150 - 760$  torr) are shown in Figure 3-12. The carrier gas pressure was increased from traces (1) to (5). The nozzle diameter is 100  $\mu\text{m}$  and the laser beam crossed the supersonic jet  $\sim 7$  mm down stream from the nozzle,  $X/D \sim 70$ . By increasing the carrier gas pressure, the cooling of the vibrational and rotational degrees of freedom is increased and the spectrum becomes better resolved. On the other hand, the number density of perylene molecules is decreased, and as a result the intensity of the signal is decreased. The most intense peak, at 415.7 nm, is the 0-0 origin of the  $A_g \rightarrow B_{3u}$  transition of perylene. Above a certain argon carrier pressure, the appearance of new spectral features is observed, exemplified by the marked peak in trace (5). This additional feature, appearing on the low energy side of the 0-0 transition of the bare perylene molecule ( $\sim 50 \text{ cm}^{-1}$  lower than the 0-0 transition) is assigned to a vibration in the perylene-Ar 1:1 van der Waals complex[133]. Generally, the position of the peaks attributed to van der Waals complexes depend on the identity of the carrier gas (the positions of fluorescence from isolated molecules are independent

**Figure 3-12.** The laser induced fluorescence spectra of perylene in a jet as a function of the carrier gas pressure. The argon carrier pressure is increased from (1) to (5). The arrow represents a vibration of a perylene-Ar vdW complex.

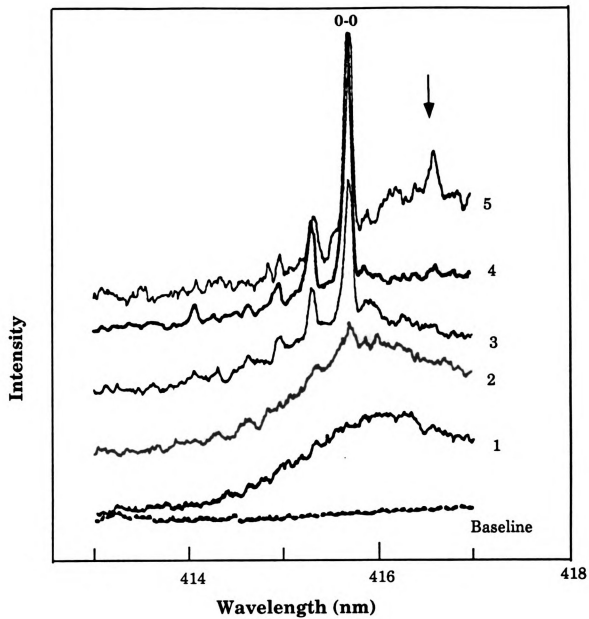


Figure 3-12.

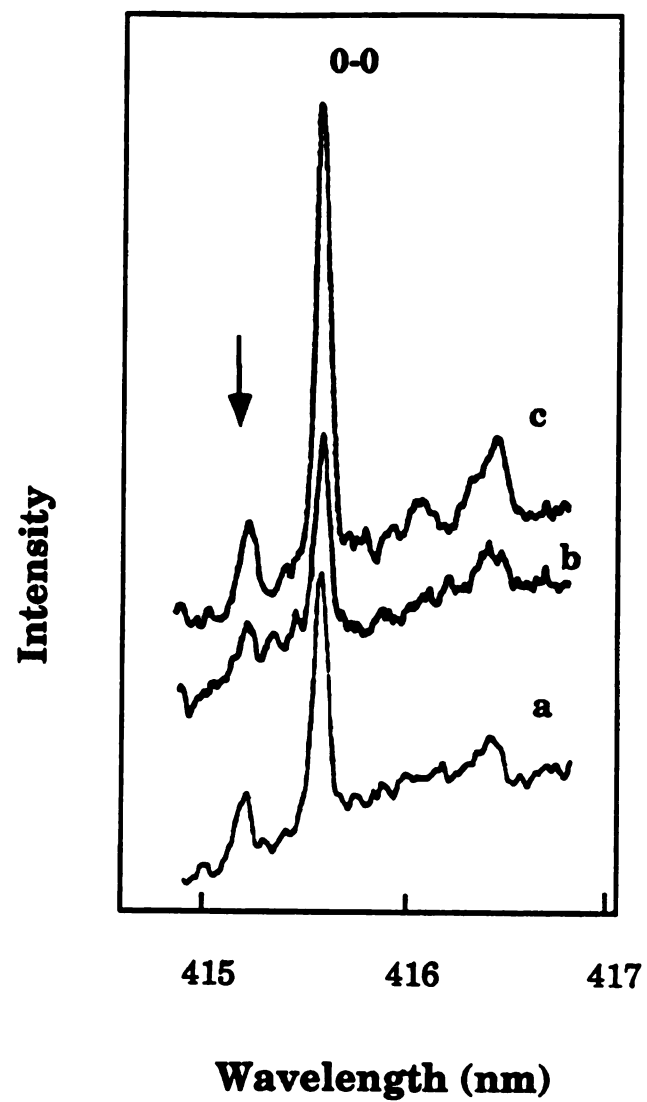


of the carrier gas) and the relative intensity of peaks attributed to (carrier gas)<sub>n</sub>-sample vdW complexes exhibit a dependence of the form  $P^{2n}$  on the carrier gas pressure  $P$ . Above an argon backing pressure of 760 Torr, with a 100  $\mu\text{m}$  diameter nozzle, the pumping speed of the pump could not handle the throughput from the nozzle, and backstreaming of diffusion pump oil occurred.

### B. Distance Effect

The energy of rotational and vibrational motion of a polyatomic sample molecule is transferred to the translational cold bath through collisions. As long as the molecules make a collision, the number of collisions is a function of the distance from the nozzle to the laser cross section,  $X$ ; the cooling of the internal degrees of freedom increases as the distance increases. The LIF spectra of perylene plotted in Figure 3-13 were obtained at different distances  $X$ , between 5 mm and 10 mm ( $D = 100 \mu\text{m}$ ). The intensity of the scattered laser beam is increased by decreasing the distance, but the signal is increased because the number density of the sample also increases.  $X/D = 50$  is the minimum distance under our experimental conditions at which the scattered laser light could be sufficiently discriminated. From the spectra shown in Figure 3-13 the dependence of sample cooling on the distance,  $X$ , is not clear; there is little difference among the three traces. The likely reason for this observation is that cooling is already complete even at the shortest distance ( $X/D = 50$ ) accessible in these measurements.

**Figure 3-13.** Laser induced fluorescence spectra of perylene in a jet at different distances from the nozzle to the laser intersection;  $X/D = 100$ (a), 70(b), and 50(c). The arrow designates a hot band.

**Figure 3-13.**

### C. Nozzle Size Effect

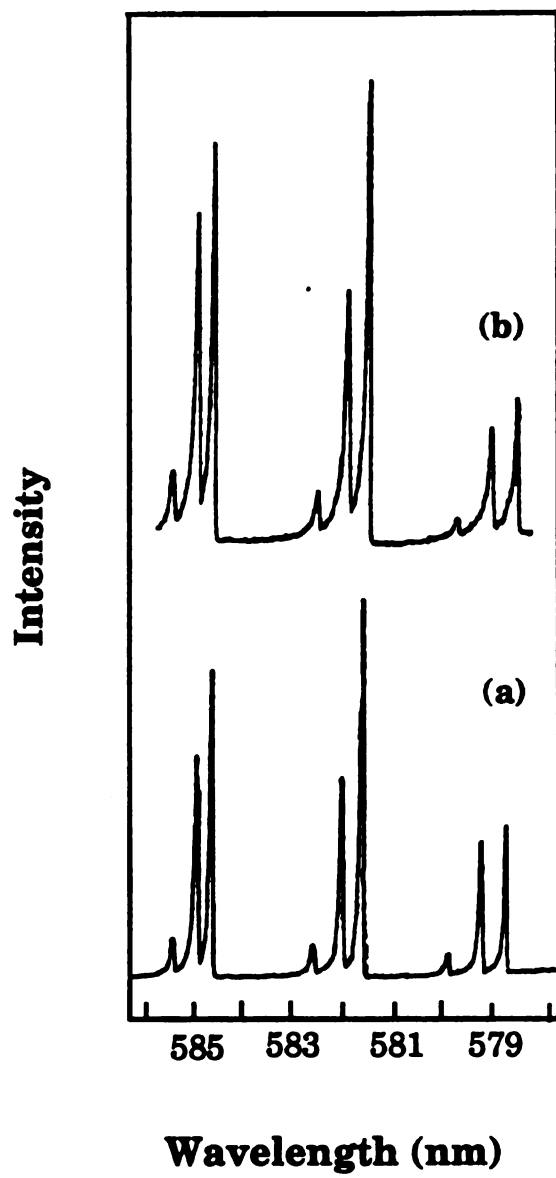
The number of collisions is proportional to the product of stagnation pressure  $P_0$  and the diameter of the nozzle  $D$ ,  $P_0 D$ . The effect of the nozzle size was measured by using various nozzle diameters (50 and 100  $\mu\text{m}$ ), under constant backing pressure  $P_0 = 0.5$  atm. Under otherwise identical experimental conditions, as the nozzle size is increased a better resolved spectrum is obtained (Figure 3-14).

### D. Sensitivity

As described above, the effect of the scattered laser light was serious for the desired quantitative measurements. However, the one-beam two-photon excitation measurement of jet-cooled perylene may be possible despite the scattered laser light, providing the two-photon cross-section is sufficiently high. Unlike the one-photon excitation of perylene, which involves resonance emission from the excited state, the fluorescence from the two-photon induced excited state has higher energy than the exciting laser beam. Thus the scattered laser light can be reduced by filtering methods (see Chapter II).

The number of perylene molecules entrainable in a jet is very low, even when a large nozzle diameter is employed; a nozzle diameter of 200  $\mu\text{m}$  (the maximum diameter for continuous expansion attainable with our pumping system in order to maintain a pressure of  $< 5 \times 10^{-4}$  Torr in a jet with 1 atm argon expansion pressure) at a sample temperature of 220  $^{\circ}\text{C}$  provides  $\sim 10^{12}$  molecules in the laser/jet interaction cross-section. The

**Figure 3-14.** The effect of nozzle size on the internal temperature cooling: iodine molecules expanded through nozzle diameter  $D = 100\ \mu\text{m}$  (a) and  $50\ \mu\text{m}$  (b), over the excitation region  $578 - 586\ \text{nm}$ .

**Figure 3-14**

number of perylene molecules in  $10^{-4}$  M solution within the laser cross-section under the experimental conditions of Chapter II is  $>10^{14}$  molecules; the number of molecules in the jet is thus at least two orders of magnitude lower.

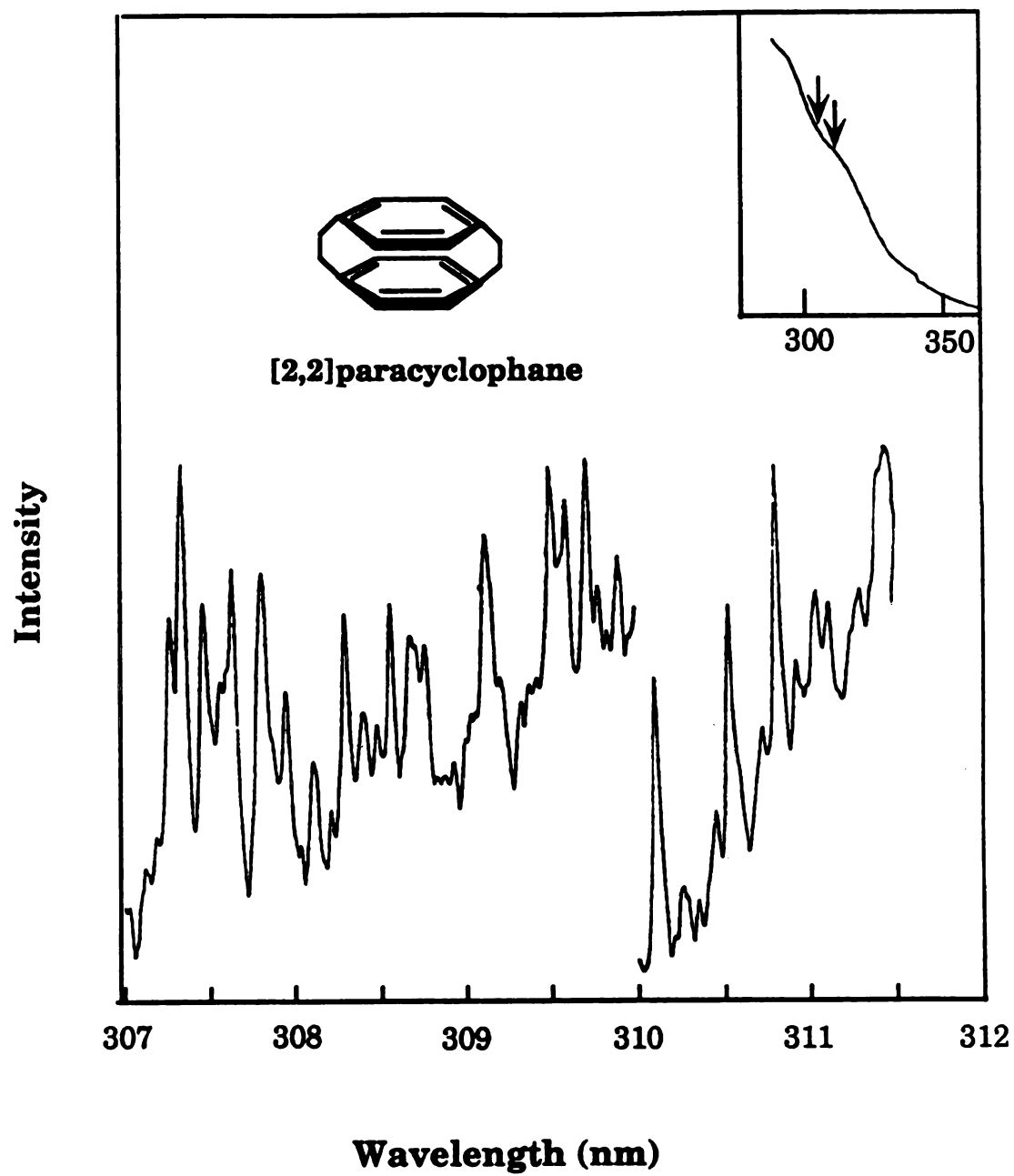
To test the sensitivity of our detection system, the one-photon excitation spectrum of [2,2]paracyclophane (PCP) was obtained over the excitation range 330 - 280 nm ( $A_g \rightarrow B_{1g}$ ). The oscillator strength of PCP is  $f = 0.001$  at 310 nm[134] and that of perylene is  $f = 0.332$  at 415.7 nm[50(a)]. A portion of the excitation spectrum for LIF from supersonic-jet expanded PCP is shown in Figure 3-15. (The inset is an absorption spectrum obtained at room temperature in isopentane solution; the arrows denote the spectral region reproduced in Figure 3-15 for the LIF of PCP in the jet.) PCP was heated to 150 °C (1 Torr, variac setting 50 V). The nozzle diameter was 200  $\mu\text{m}$ , the argon carrier pressure was 1 atm and the PMT power was 760 V. In the wavelength region above 300 nm in the jet spectrum, the baseline continues to rise, because of the increasing spectral response of the collecting glass lens and windows. Compared to the spectrum in reference [135], the cooling effect in our PCP LIF spectrum is poor, but the sensitivity of the detection system is comparable.

### E. Two-photon Excitation of Perylene

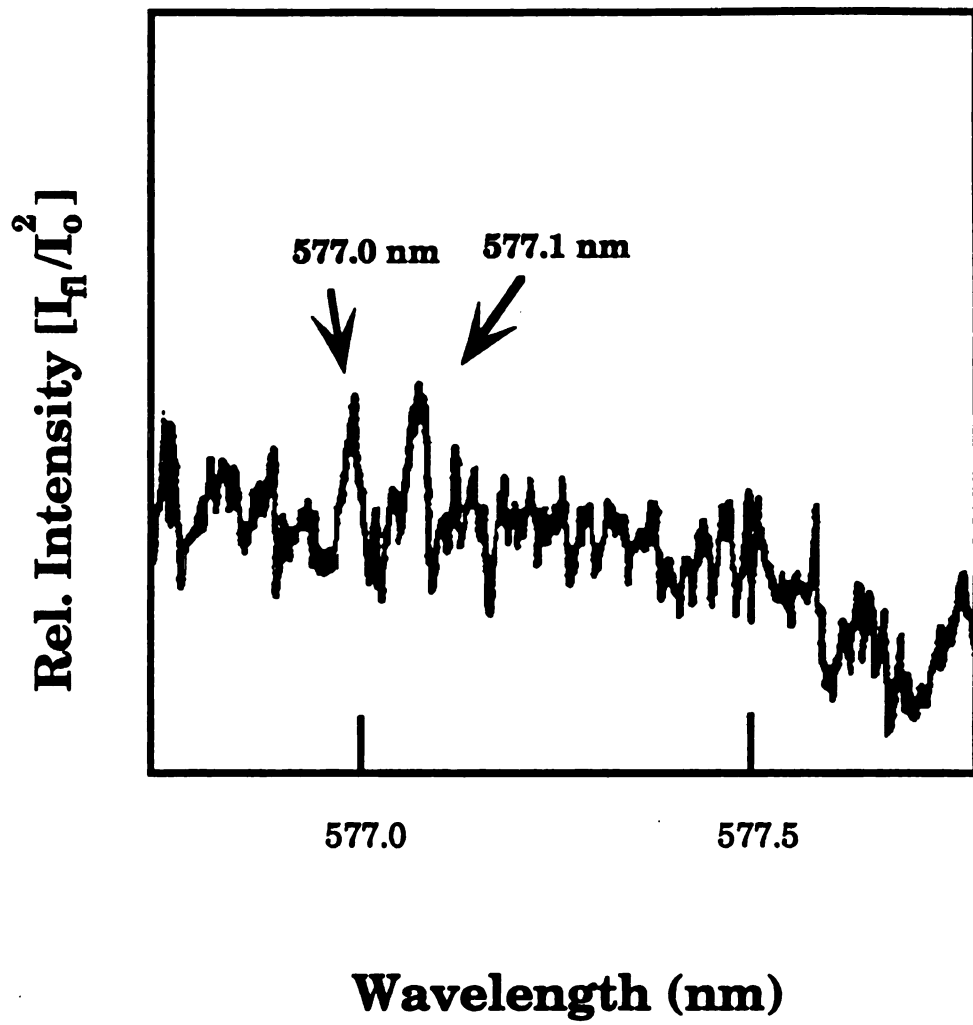
The preliminary result of the two-photon excitation of supersonic jet-cooled perylene over the region 576.8 - 577.8 nm (two-photon energy 34,670 - 34,610  $\text{cm}^{-1}$ , where the solution TPE spectrum shows strong enhancement; see Figure 2-14) is shown in Figure 3-16. This spectrum was obtained with

**Figure 3-15.** The laser induced fluorescence from [2,2]paracyclophane expanded through a supersonic jet, obtained over the excitation range 312 – 307 nm. The inset is a broader-range absorption spectrum obtained in isopentane solution at room temperature.



**Figure 3-15.**

**Figure 3-16.** Two-photon excitation spectrum of perylene in a supersonic jet over the dye laser wavelength 576.8 – 577.8 nm (two-photon energy 34,670 – 34,610  $\text{cm}^{-1}$ ).

**Figure 3-16.**

two-photons from same laser, and linear polarization of the excitation radiation. The nozzle diameter is 200  $\mu\text{m}$ , the argon carrier pressure is 0.5 atm, the distance  $X$  is 8 mm ( $X/D = 40$ ), and the PMT power is 1190 V. Much of the scattered laser light was removed by a Corning 5-57 filter in the detection optics. The one-photon spectrum of perylene in the jet was obtained before and between the measurements of the TPE, in order to check the alignment of the dye laser beam and of the detection system in relation to the molecular beam. Although the signal-to-noise level is low ( $\sim 1.5$ ), the peaks at about 577.0 and 577.1 nm from the two-photon induced excited state in the jet are reproducible and their intensity depends on the argon carrier pressure. Since both  $A_g$  and  $B_{1g}$  symmetry states are expected in this region according to the two-photon excitation spectrum of perylene in *n*-hexane solution, without a wider range spectrum and polarization analysis it is not possible to provide an assignment for these peaks.

Several reasons are suggested for the low signal-to-noise ratio in the TPE spectrum: 1) the number density of perylene molecules is low; 2) the alignments of the detection system and of the laser beam to the jet are not optimum; 3) glass windows in the detection system cut off emission in the wavelength region below 300 nm; and 4) unlike the relaxation in solution, following laser irradiation the contribution of collisions to the nonradiative relaxation process can be neglected in the jet. Thus the fluorescence from the two-photon induced electronic excited state could be one of transitions from the gerade excited state to vibronically ungerade ground state levels, or alternative radiative transitions could be involved in the decay processes (Figure 3-17). Therefore the cross-section for the emission from a two-photon induced excited state in a jet can be quite different from that in

**Figure 3-17.** The relaxation processes following two-photon excitation in solution (a), and in a jet, (b) and (c).

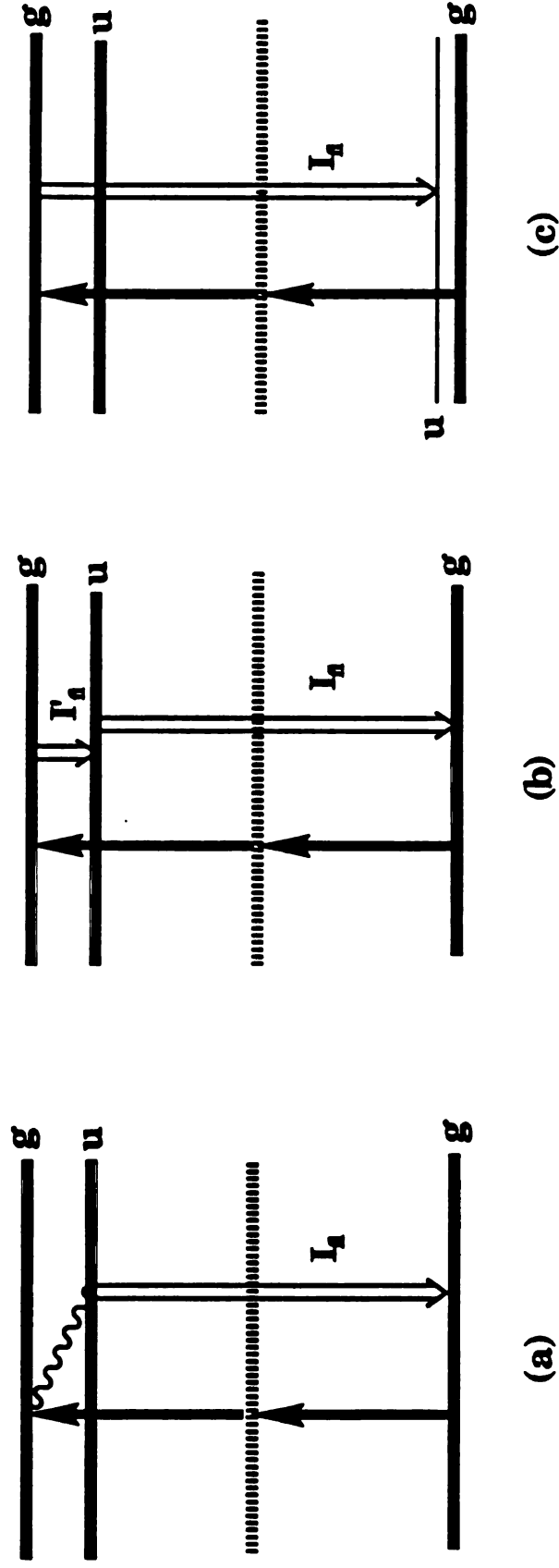


Figure 3-17.

solution. Nevertheless, it was promising that a signal from the two-photon induced electronic excited state of perylene could be detected with our home-built supersonic jet system.

To improve the signal-to-noise level, it is proposed that methods be utilized which can increase the number density of perylene [such as a slit nozzle, or a pulsed nozzle with large diameter ( $> 200 \mu\text{m}$ )], and that the measurements be systemized with one-photon excitation of supersonic jet-cooled perylene to optimize the alignment. With more carefully designed experiments, quartz optics and various filters, and time-resolved measurements with ultrashort ( $< 1 \text{ ns}$ ) laser pulses, it may be possible to understand the relaxation processes which follow the two-photon excitation of perylene excited states.

## REFERENCES



## REFERENCES

1. M. D. Levenson and S. S. Kano, "Introduction to Nonlinear Laser Spectroscopy", Boston, Academic Press, 1988.
2. a) R. C. Hilborn, *Am. J. Phys.*, **50**, 982-986 (1982).  
b) L. I. Schiff, "Quantum Mechanics", 3rd ed. McGraw-Hill, New York, 1968.
3. R. L. Kronig, *J. Opt. Soc. Amer.*, **12**, 547 (1926)
4. O. Howarth, "Theory of Spectroscopy" Halsted, New York, 1973.
5. A. Yariv, "Quantum Electronics", 2nd ed., p165, Wiley, New York, 1975.
6. A. Herzberg, "Infrared and Raman Spectra", Von Nostrand-Reihold, Princeton, New Jersey, 1945; D. A. Long, "Raman Spectroscopy", McGraw-Hill, New York, 1977.
7. H. O. Schrotter and H. W. Klockner, "Raman Spectroscopy of Gases and Liquids", C. A. Weber, ed. 1 (Topics in Current Physics), Springer-Verlag, Berlin, 1979.
8. F. Zernike and J. E. Midwinter, "Applied Nonlinear Optics", Wiley-Interscience, New York, 1973.
9. M.S. Feld and V. S. Letohov, eds. "Coherent Nonlinear Optics" (Topics on Current Physics 27). Springer-Verlag, Berlin, 1980.
10. N. Bloembergen, "Nonlinear Optics". Benjamin, New York, 1965, and references therein.
11. R. G. Brewer, Coherent Optical Spectroscopy, in "Nonlinear Spectroscopy" (Proc. Int. School Phys., Enrico Fermi, Course 64) (N. Bloembergen, ed.) North-Holland, publ., Amsterdam, 1977.
12. N. Bloembergen, in "Quantum Electronics; A Treatise", H. Robin and C. L. Tang, ed., Academic Press, New York, 1975.

13. T. H. Maiman, *Nature*, **187**, 493 (1960).
14. P. D. Maker and R. W. Terhune, *Phys. Rev.*, **137**, 801 (1965).
15. W. L. Peticolas, I. P. Goldsborough and K. E. Rieckhoff, *Phys. Rev. Lett.*, **10**, 43 (1963).
16. P. A. Franken, A. E. Hill, C. W. Peters and G. Weinreich, *Phys. Rev. Lett.*, **7**, 118 (1961).
17. M. Bass, P. A. Franken, A. E. Hill, C. W. Peters and G. Weinreich, *Phys. Rev. Lett.*, **8**, 18 (1962).
18. a) A. Szoke and A. Javan, *Phys. Rev. Lett.*, **10**, 521 (1963).  
b). R.A. McFarlane, W.R. Bennet, Jr. and W. E. Lamb, Jr., *Appl. Phys. Lett.*, **17**, 53 (1970)
19. a) A. M. Bonch-Bruerich and V. V. Khodovoi, *Sov. Phys-usp.*, **8**, 1 (1965).  
b) W. L. Peticolas, *Annu. Rev. Phys. Chem.*, **18**, 233 (1967).  
c) H. Mohr, in "Quantum Electronics: A Treatise" (H. Robin and C. L. Tang, eds.), Vol. 1, Academic Press, New York, 1975.
20. S. H. Lin, Y. Fujimura, H. J. Neusser and E. W. Schlag, "Multiphoton Spectroscopy of Molecules", Academic Press, Orlando Fla., 1984.
21. W. M. McClain and R. A. Harris, in "Excited States", Vol. 3, ed., E. C. Lim, Academic, New York, 1977.
22. T. R. Bader and A. Gold, *Phys. Rev.*, **171**, 997 (1968).
23. M. Inoue and Y. Toyozawa, *J. Phys. Soc. Japan*, **20**, 363 (1965).
24. P. R. Monson and W. M. McClain, *J. Chem. Phys.*, **53**, 29 (1970).
25. W. M. McClain, *J. Chem. Phys.*, **55**, 2789 (1971).
26. R. G. Bray and R. M. Hochstrasser, *Mol. Phys.*, **72**, 3999 (1976).
27. M. Goeppert-Mayer, *Naturwissenschaften*, **17**, 932 (1921).
28. W. Kaiser and C. G. B. Garrett, *Phys. Rev. Lett.*, **7**, 229 (1961)
29. D. Frohlich and M. Mahr, *Phys. Rev. Lett.*, **16**, 895 (1966).

30. a) R. A. Swofford and W. M. McClain, *J. Chem. Phys.*, **59**, 5740 (1973).  
b) R. A. Swofford and W. M. McClain, *Rev. Sci. Instr.*, **46**, 246 (1975).
31. L. Wunsch, H. Neusser and E. W. Schlag, *Z. Naturforsch.*, **36**, 1340 (1981).
32. a) A. Bergman and J. Jortner, *Chem. Phys. Lett.*, **15**, 309 (1972).  
b) A. Bergman and J. Jortner, *Chem. Phys. Lett.*, **26**, 323 (1974).
33. J. R. Whinney, *Acc. Chem. Res.*, **7**, 225 (1974).
34. W. C. Lineberger and T. A. Patterson, *Chem. Phys. Lett.*, **13**, 40 (1972).
35. a) P. M. Johnson, *J. Chem. Phys.*, **62**, 4562 (1975);  
b) P. M. Johnson, *J. Chem. Phys.*, **64**, 4638 (1976).
36. V. J. Kleinschmidt, W. Tottleben and S. Reutsh, *Exp. Tech. Physik*, **22**, 191 (1974).
37. W. M. McClain, *Acc. Chem. Res.*, **7**, 129 (1974).
38. U. Fritzer, Ph. Keller and G. Schaack, *J. Phys.*, **E8**, 530 (1975).
39. L. Zandee and R. B. Bernstein, *J. Chem. Phys.*, **71**, 1359 (1979).
40. U. Boesl, H. J. Neusser and E. W. Schlag, *J. Chem. Phys.*, **72**, 4327 (1980).
41. S. J. Cyvin, *J. Mol. Struc.*, **100**, 75 (1983).
42. N. L. Allinger and J. T. Sprague, *J. Am. Chem. Soc.*, **95**, 3893 (1973).
43. I. B. Berlman and M. Rokni, *Chem. Phys. Lett.*, **22**, 458, (1973); C. Rullier, A. Declémy, and Ph. Kottis, *Chem. Phys. Lett.*, **110**, 308, (1984).
44. R. G. Harvey, ed., "Polycyclic Hydrocarbons and Carcinogenesis", ACS Symposium Series 283, American Chemical Society, Washington D. C., 1985.
45. a) M. A. Koner and A. Yu. Slepukhin, *Teor. i Eksperim. Khim.*, **9**, 105 (1973).

- b) B. Fourmann, C. Jouvét, A. Tramer, J. M. LeBars and Ph. Millie, *Chem. Phys.*, **92**, 25 (1985).
46. C. T. Ryan and T. K. Gustafson, *Chem. Phys. Lett.*, **44**, 241 (1976).
47. a) C. Bouzou, C. Jouvét, J. B. LeBlond, P. Millie, A. Tramer and M. Sulkes, *Chem. Phys. Lett.*, **93**, 161 (1983).
- b) S. Schwartz and M. Topp, *Chem. Phys.*, **83**, 245 (1984)
- c) B. E. Forch, K. J. Chen and E. C. Lim, *Chem. Phys. Lett.*, **100**, 389 (1983).
48. a) H. Preeskamp, A. Laufer and M. Zander, *Chem. Phys. Lett.*, **112**, 479 (1984).
- b) R. M. Hochstrasser, *J. Chem. Phys.*, **40**, 2559 (1964).
49. a) V. L. Bofdanov and V. P. Klochkov, *Opt. Spectrosc.*, **45**, 51 (1978).
- b) T. V. Bolotnikova and O. F. Elnikova, *Opt. Spectrosc.*, **36**, 397 (1974).
- c) J. Tanaka, *Bull. Chem. Soc., Japan*, **36**, 1238 (1963).
50. a) Y. Tanizaki, T. Yoshinaga and H. Hiratsuka, *Spectrochim. Acta*, **34A**, 205 (1978). [See also references cited therein.]
- b) A. P. Blokhin, V. A. Povedailo and V. A. Tolkachev, *Opt. Spectrosc.*, **60**, 37 (1986).
- c) M. Mestechkin, L. Gutyrva and V. Poltavets, *Opt. Spectrosc.*, **28**, 244 (1970).
- d) S. Matsunuma, N. Akamatsu, T. Kamisuki, Y. Adachi, S. Maeda and C. Hirose, *J. Chem. Phys.*, **88**, 2956 (1988).
51. H. Zimmermann and N. Joop, *Z. Elektro. Chem.*, **65**, 138 (1961).
52. N. A. Borisevich, S. P. Pliska and V. A. Tolkachev, *Sov. Phys. Dokl.*, **26**, 1145 (1981).
53. E. Clar, *Spectrochim. Acta*, **4**, 116 (1950).

54. P. R. Callis, T. W. Scott and A. C. Albrecht, *J. Chem. Phys.*, **78**, 16 (1983).
55. M. Newsham, Ph. D. Dissertation, Michigan State University (1988).
56. B. Steven, *Chem. Rev.*, **57**, 439 (1975).
57. F. Bowen and S. Veljkovic, *Proc. Roy. Soc.(London)*, **A236** (1956).
58. R. Thiim, M. S. Thesis, Michigan State University (1982).
59. A. P. Aleksandrov, V. P. Bredikhin and V. N. Genkin, *JETP Lett.*, **10**, 117 (1969).
60. S. Speiser and S. Kimel, *J. Chem. Phys.*, **51**, 5614(1969).
61. R. P. Drucker and W. M. McClain, *J. Chem. Phys.*, **61**, 2609 (1974).
62. E. Clar and W. Schmidt, *Tetrahedron*, **33**, 2093 (1977).
63. R. M. Hochstrasser and C. A. Nyi, *J. Chem. Phys.*, **72**, 2591 (1980).
64. S. J. Cyvin, B. N. Cyvin and P. Klæboe, *Spectrosc. Lett.*, **16**, 239 (1983).
65. F. Ambrosino and S. Califano, *Spectrochim. Acta*, **21**, 1401 (1965).
66. C. Rulliere, A. Declémy and Ph. Kottis, *Chem. Phys. Lett.*, **110**, 308 (1984).
67. R. M. Hochstrasser, *J. Chem. Phys.*, **40**, 2559 (1964).
68. S. K. Chakrabarti, *J. Mol. Spectrosc.*, **37**, 571 (1971).
69. D. H. Levy, *Sci. Am.*, **250**, 96 (1984).
70. R.E. Smalley, B. L. Ramakrishna, D. H. Levy and L. Wharton, *J. Chem. Phys.*, **61**, 4363 (1974).
71. A. Kantrowitz and J. Grey, *Rev. Sci. Instrum.*, **22**, 328 (1951).
72. a) G. B. Kistiakowsky and W. P. Slichter, *Rev. Sci. Instrum.*, **22**, 333 (1951).
- b) E. W. Becker and K. Bier, *Z. Naturforsch. Teil A*, **9**, 975 (1954).
73. J. B. Anderson, R. P. Andres and J. B. Fenn, *Adv. Chem. Phys.*, **10**, 275 (1965).

74. R. Campargue and R. Lebehot, 9th Symp. *Rarefied Gas Dynamics*, ed. M. Becker, M. Fiebig. Porz-Wahn, DFVLR Press (1974).
75. J. P. Toennies and K. Winkelmann, *J. Chem. Phys.*, **66**, 3965 (1977).
76. H. W. Liepmann and A. Roshko, "Elements of Gas Dynamics", p.40 New York: Wiley (1957).
77. H. Ashkenhas and F. S. Sherman, *Rarefied Gas Dynamics*, 4th Symp., ed. J. H. de Leeuw, **2**, 84. New York: Academic Press (1966).
78. J. B. Anderson and J. B. Fenn, *Phys. Fluids*, **8**, 780 (1965).
79. D. R. Miller, J. P. Toennies and K. Winkelmann, 9th Symp. *Rarefied Gas Dynamics*, ed. M. Becker, M. Fiebig. Porz-Wahn, DFVLR Press (1974).
80. N. Abauf, J. B. Anderson, R. P. Andres, J. B. Fenn and D.R. Miller, *Rarefied Gas Dynamics*, 5th Symp, ed., C. L. Brundin, Academic Press, New York (1967).
81. R. A. Larsen, S. K. Neoh and D. R. Herschbach, *Rev. Sci. Instrum.*, **45**, 2511 (1974).
82. A. Amirav, U. Even and J. Jortner, *J. Chem. Phys.*, **51**, 31 (1980).
83. E. Kolodney and A. Amirav, *Chem. Phys.*, **76**, 5684 (1982).
84. U. Even, J. Magen and J. Jortner, *J. Chem. Phys.* **76**, 5684 (1982).
85. T. A. Milne and F. T. Greene, *Adv. in High Temp. Chem.* **2**, 107 (1969).
86. A. L. J. Burgmans, J. M. Farrar and Y. T. Lee, *J. Chem. Phys.*, **64**, 1345 (1976), and referenced cited therein.
87. A. P. J. von Deursen and J. Reuss, *J. Chem. Phys.*, **63**, 4559 (1975).
88. R. Campargue, *Rev. Sci Instrum.*, **35**, 111 (1964).
89. R. Campargue, Ph. D. thesis, Univ. Paris, France (1970).
90. R. Campargue, *J. Chem. Phys*, **52**, 1795 (1970).

91. J. B. Fenn and J. Deckers, *Rarefied Gas dynamics*, 3rd Symposium, vol. 1, J. A. Laurman, ed., Academic Press, New York (1963); J. B. Fenn and J. B. Anderson, *Rarefied Gas Dynamics*, 4th Symposium, vol. II, J. H. De Leeuw, ed., Academic Press, New York (1966); J. B. Fenn, J. B. Anderson, R. P. Andres and G. Maise, *Rarefied Gas Dynamics*, 4th Symposium, vol. II, J. H. De Leeuw, ed., Academic Press, New York (1966).
92. J. B. Anderson in "Molecular Beams and Low Density Gasdynamics", P. P. Wegener, ed., Marcel Dekker, New York (1974).
93. U. Even, J. Magen and J. Jortner, *J. Am. Chem. Soc.*, **103**, 4583 (1981); U. Even, J. Magen, J. Jortner, J. Friedman and H. Levanon, *J. Chem. Phys.*, **77**, 4374 (1982); U. Even, J. Magen, J. Jortner and J. Friedman, *J. Chem. Phys.*, **77**, 4384 (1982); U. Even, J. Magen and J. Jortner, *J. Chem. Phys.*, **77**, 4391 (1982).
94. D. K. Hsu, D. L. Monts and R. N. Zare, "Spectral Atlas of Nitrogen Dioxide", New York: Academic, 1978.
95. D. L. Monts, T. G. Dietyz, M. A. Duncan and R. E. Smalley, *Chem. Phys.*, **45**, 133 (1980).
96. C. H. Chen, S. D. Kramer, D. W. Clark and M. G. Payne, *Chem. Phys. Lett.*, **65**, 419 (1979).
97. D. R. Preuss, S. A. Pace and J. L. Gole, *J. Chem. Phys.*, **71**, 3553 (1979).
98. D. Eisel, D. Zevgolts and W. Demtroder, *J. Chem. Phys.*, **71**, 2005 (1979).
99. A. Herrmann, S. Leutwyler, E. Schumacher and L. Woste, *Chem. Phys. Lett.*, **52**, 418 (1977).
100. P. Huber-Walchli, D. M. Guthals and J.W. Nibler, *Chem. Phys. Lett.*, **67**, 233 (1979).
101. M. P. Sinha, A. Schultz and R. N. Zare, *J. Chem. Phys.*, **58**, 549 (1973).

102. T. D. Gaily, S. D. Rosner and R. I. Holt, *Rev. Sci. Instrum.*, **47**, 143 (1976).
103. a) W. Sharfin, K. E. Johnson, L. Wharton and D. H. Levy, *J. Chem. Phys.*, **71**, 1292 (1979).  
b) P. S. H. Fitch, L. Wharton and D. H. Levy, *Chem. Phys. Lett.*, **48**, 177 (1977).
104. R. Campargue and B. Soep, *Chem. Phys. Lett.*, **64**, 469 (1979).
105. T. Chaiken, T. Benson, M. Gurnick and J. D. McDonald, *Chem. Phys. Lett.*, **61**, 195 (1979).
106. a) J. B. Hopkins, D. E. Powers, S. Mukamel and R. E. Smalley, *J. Chem. Phys.*, **72**, 5049 (1980).  
b) T. G. Dietz, M. A. Duncan, A. C. Pulu and R. E. Smalley, *J. Phys. Chem.*, **86**, 4026 (1982).
107. T. Suzuki, N. Mikami and M. Ito, *J. Phys. Chem.*, **90**, 6432 (1986).
108. D. H. Semmes, J. S. Baskin and A. H. Zewail, *J. Am. Chem. Soc.*, **109**, 4104 (1987); J. L. Knee, L. R. Khundkar and A. H. Zewail, *J. Chem. Phys.*, **87**, 115 (1987).
109. H. G. Lohmannsroben, K. Luther and M. Stuke, *J. Phys. Chem.*, **91**, 3499 (1987).
110. E. Heller and R. C. Brown, *J. Chem. Phys.*, **79**, 3336 (1983).
111. C. E. Otis, J. L. Knee and P. M. Johnson, *J. Chem. Phys.*, **78**, 2091 (1983); C. E. Otis, J. L. Knee and P. M. Johnson, *J. Chem. Phys.*, **80**, 13 (1984).
112. C. A. Haynam, D. V. Brumbaugh and D. H. Levy, *J. Chem. Phys.*, **80**, 2256 (1984); C. A. Haynam, D. V. Brumbaugh and D. H. Levy, *J. Chem. Phys.*, **79**, 1581 (1983); C. A. Haynam, C. Morter, L. Young and D. H. Levy, *J. Phys. Chem.*, **91**, 2526 (1987); P. R. R. Langridge-Smith, C. A.



- Haynam, D. V. Brumbaugh and D. H. Levy, *J. Phys. Chem.*, **85**, 3739 (1981).
113. S. Leutwyler and J. Jortner, *J. Phys. Chem.*, **91**, 5558 (1987).
114. E. A. Mangle and M. R. Topp, *Chem. Phys.*, **112**, 427 (1987).
115. J. B. Hopkins, D. E. Power and R. E. Smalley, **85**, 3739 (1981).
116. K. D. Borsen, H. L. Seizle and E. W. Schlag, *J. Chem. Phys.*, **85**, 1726 (1986).
117. T. A. Stephenson and S. A. Rice, *J. Chem. Phys.*, **81**, 1083 (1984); S. A. Rice, *J. Phys. Chem.*, **90**, 3036 (1986).
118. H. Saigusa and M. Ito, *J. Chem. Phys.*, **81**, 5692 (1984); H. Abe, N. Mikami and M. Ito, *J. Phys. Chem.*, **86**, 1766 (1982); H. Abe, N. Mikami, M. Ito and Y. Udagawa, *J. Phys. Chem.*, **86**, 2567 (1982); Y. Tomioka, M. Ito and N. Mikami, *J. Phys. Chem.*, **87**, 4401 (1983).
119. K. Fuke, H. Yoshiuchi and K. Kaya, *J. Phys. Chem.*, **88**, 5840 (1984); K. Fuke, T. Yabe, N. Chiba, T. Kohida and K. Kaya, *J. Phys. Chem.*, **90**, 2309 (1986).
120. D. H. Levy, L. Wharton and R. Smalley, "Chem. Biochem. Appl. Lasers", **2**, 1, C. B. Moore, ed., New York, Academic Press (1977).
121. R. Tembreull and D. M. Lubman, *Anal. Chem.*, **58**, 1299 (1986); R. Tembreull and D. M. Lubman, *Anal. Chem.*, **59**, 1082 (1987); R. Tembreull and D. M. Lubman, *Anal. Chem.*, **59**, 1003 (1987).
122. A. Amirav, U. Even and J. Jortner, *Anal. Chem.*, **54**, 1666 (1982); M. Sonnenschein, A. Amirav and J. Jortner, *J. Phys. Chem.*, **88**, 4214 (1984); A. Amirav, M. Sonnenschein and J. Jortner, *Chem. Phys.*, **102**, 305 (1986).
123. V. Vaida, *Acc. Chem. Res.*, **19**, 114 (1986); D. G. Leopold, V. Vaida and M. F. Granville, *J. Chem. Phys.*, **81**, 4210 (1984).

124. T. S. Zwier, M. E. Carrasquillo and D. H. Levy, *J. Chem. Phys.*, **78**, 5493 (1983).
125. M. Ito, T. Ebata and N. Mikami, *Ann. Rev. Phys. Chem.*, **39**, 123 (1988).
126. H. Fukuoka, T. Imasaka and N. Ishibashi, *Anal. Chem.*, **58**, 375 (1986); T. Imasaka, N. Yamaga and N. Ishibashi, *Anal. Chem.*, **59**, 419 (1987).
127. C. H. Sin, H. M. Pang, D. M. Lubman and J. Zorn, *Anal. Chem.*, **58**, 487 (1986).
128. J. Grotemeyer, U. Boesel, K. Walter and E. W. Schlag, *J. Am. Chem. Soc.*, **108**, 4233 (1986).
129. J. M. Hayes and G. J. Small, *Anal. Chem.*, **54**, 1202 (1982).
130. B. V. Pepich, J. B. Callis, J. D. Sheldon Danielson and M. Gouterman, *Rev. Sci. Instrum.*, **57**, 878 (1986); B. V. Pepich, J. B. Callis, D.H. Burns, M. Gouterman and D. A. Kalman, *Anal. Chem.*, **58**, 2825 (1986).
131. R. E. Smalley, D. H. Levy and L. Wharton, *J. Chem. Phys.*, **64**, 3266 (1976).
132. J. C. Kettley, T. F. Palmer and J. P. Simons, *Chem. Phys. Lett.*, **115**, 40 (1985).
133. A. Amirav, U. Even and J. Jortner, *Chem. Phys.*, **51**, 31 (1980).
134. S. Iwata, K. Fuke, M. Sasaki, S. Nagakura, T. Otsubo and S. Misumi, *J. Mol. Spectrosc.*, **46**, 1 (1973).
135. A. Ron, M. Noble and E. K. Lee, *Chem. Phys.*, **83**, 215 (1984).